Fabrication and characterisation of electrospun polyvinylidene fluoride (PVDF) nanocomposites for energy harvesting applications

A thesis submitted to Brunel University London for the degree of Doctor of Philosophy

2016

Hang Song

Wolfson Centre of Material Processing
Brunel University London

Abstract

Three systems of electrospun composite membranes with piezoelectric polymer polyvinylidene fluoride (PVDF) as matrix incorporating:

1) Carbon based fillers: carbon nanotube (CNT) and graphene oxide (GO);

2) Ceramic based fillers-barium titanate (BT), zinc oxide (ZnO) and nanoclays (halloysite and bentonite);

3) Cellulosic fillers: microcrystalline cellulose (MCC) and nanocrystalline cellulose (NCC) at different loadings were prepared by electrospinning process.

Influence of filler type and loading on total PVDF crystallinity (X_c), relative fraction of β phase (piezoelectric phase) in total crystalline PVDF (F_β), volume fraction of β phase in the samples (v_β) and piezoelectric coefficient d_{33} were characterised and analysed.

Correlation between v_β and piezoelectric performance (d_{33}) will be focused by this work. A common situation was observed for the composites-d_{33} increased while v_β is reduced by the fillers, so it can be concluded that d_{33} of the composites is not totally up to their v_β, there are other factors that need to be taken into account. For example, for carbon based filler like CNT, it increased electric conductivity of sample during and after electrospinning process, making it easier for charges produced by β crystals from inside of sample to be transferred to surfaces of the sample, and possibly promoting orientation of β crystals in d_{33} direction, therefore enhanced d_{33} of the composites though β phase formation was significantly hindered by inclusion of CNT; For piezoelectric ceramic fillers like BT and ZnO, a possible combined piezoelectricity from filler and β phase PVDF might enhanced d_{33} though less β phase was formed; And for non-piezoelectric and non-conductive fillers, enhancement in orientation of β crystals might play a major role in promotion of d_{33}.

Keywords: electrospinning; polyvinylidene fluoride (PVDF); nanocomposites; piezoelectric coefficient d_{33}; energy harvesting

Acknowledgements

I wish to acknowledge my supervisor Prof. Jim Song for his unconditional support and guidance, encouragement, kindness and patience which helped me immensely in developing and advancing the research assembled in this thesis. I would also like to express my appreciation to my external supervisor Dr Wen-hui Song who provided valuable guidance and support to my research.

I wish to express gratitude to the staff and fellow students in Wolfson Centre for Material Processing, Experimental Techniques Centre and College of Engineering and Design for their technical and administrative assistances in relation to this research.

I also wish to thank all my friends I met in the UK for all the support and companion during this period.

Last but not least, I wish to thank my parents, grandparents and all my family members and relatives for their encouragement, love and support.

List of Contents

Chapter 1. Introduction to the project 9
1.1 The background 9
1.2 Aim and objectives 11
1.2.1 Aims 11
1.2.2 Objectives 11
1.3. Structure of this thesis 11
Chapter 2. Literature Review 12
2.1 Energy demand present and future 12
2.2 Non-renewable energies 13
2.2.1 Fossil fuels 13
2.2.2 Nuclear energy 13
2.3 Renewable energies 14
2.3.1 Solar energy 15
2.3.2 Hydropower 15
2.3.3 Wind 16
2.3.4 Geothermal 16
2.3.5 Biofuels 17
2.4 Energy harvesting (EH) 17
2.4.1. Definition and description of EH 17
2.4.2. Different technologies for energy harvesting 18
2.5. Piezoelectric energy harvesting 21
2.6 Piezoelectricity 22
2.6.1 History of piezoelectricity 22
2.6.2. Mechanism of piezoelectricity 23
2.7. Piezoelectric materials 24
2.7.1. Inorganic piezoelectric materials 24
2.7.2. Organic piezoelectric materials (polymers) 25
2.7.3. Piezoelectric composites 26
2.7.4. Applications 26
2.8. Piezoelectric polymers 28
2.8.1 Piezoelectric polymers 28

2.8.2. Polyvinylidene fluoride (PVDF) 30
2.9. Nanocomposites in general 33
2.9.1. Nanoparticles 33
2.9.2. Nanofibres 38
2.9.3. Nanocomposites 42
Ceramic-matrix nanocomposites 43
Metal-matrix nanocomposites 44
Polymer-matrix nanocomposites 44
2.10. PVDF-based nanocomposites 45
2.10.1. PVDF/cellulose systems 45
2.10.2. Polymer/carbon systems 47
2.10.3. PVDF/ceramic systems 51
2.11. Gaps of knowledge and needs of this work 56
Chapter 3. Experimental Detail 58
3.1 Materials 58
3.1.1. The common polymers, solvents and additives used in all suspension systems 58
3.1.2. The ceramic fillers 59
3.1.3. Carbon-based fillers 60
3.1.4. Cellulose fillers 62
3.2. Preparation of suspensions 64
3.2.1. The PVDF/ceramic systems 64
3.2.2. The PVDF/carbon systems 66
3.2.2. The PVDF/cellulose systems 68
3.3. Assessments of dispersion and sedimentation stability of suspensions 70
3.4. Electrospinning of the suspensions 70
3.5. Characterisations of the electrospun composite membranes 71
3.5.1. Microstructure of the electrospun composite membranes 71
3.5.2. Crystallinity 72
3.5.3. Piezoelectric properties 72
Chapter 4. Results and discussions – The PVDF/ceramic systems 74
4.1. Dispersion/sedimentation stability of the suspensions 74
4.2. Dispersion of particles in the composites 76
4.3. Morphology of the electrospun membranes 77
4.4. Crystalline properties 80

4.4.1. Total PVDF crystallinity analysis 80
4.4.2. Analysis for relative fraction of β phase, F_β, in crystalline PVDF 84
4.4.3. Volume fraction of β phase in the PVDF and PVDF/ceramic composites 87
4.5. Piezoelectric properties 90
4.6. Summary 93
Chapter 5. Results and discussions – The PVDF/carbon systems 96
5.1. State of dispersion and sedimentation stability of the suspensions 96
5.2. Dispersion of particles in the composites 97
5.3. Morphology of the electrospun membranes 98
5.5. Crystalline properties 99
5.5.1. Total PVDF crystallinity, Xc 99
5.5.2. Analysis for relative fraction of β phase, F_β, in crystalline PVDF 101
5.5.3. Volume fraction of β phase in PVDF and PVDF/carbon composites, v_β 102
5.6. Piezoelectric properties 104
5.7. Summary 106
Chapter 6. Results and discussions – The PVDF/cellulose systems 108
6.1. State of dispersion and sedimentation stability of the suspensions 108
6.2. Morphology of the electrospun membranes 110
6.3. Crystalline properties 113
6.3.1. Total PVDF crystallinity analysis, X_c 113
6.3.2. Analysis for relative fraction of β phase, F_β, in total crystalline PVDF 114
6.3.3. Volume fraction of β phase in the PVDF and PVDF/cellulose composites, v_β 116
6.4. Piezoelectric properties 117
6.5. Summary 120
Chapter 7. Comparison across the three systems 122
Chapter 8. Conclusions and proposed further work 125
List of references 128
Appendix I 143
Appendix II 145

Nomenclature

ACS	- American Chemical Society
AFM	-Atomic force microscopes
ATR	-Attenuated total reflectance
BC	-Bacterial cellulose
BET	-Brunauer, Emmett and Teller
BT	-Barium titanate
CNT	-Carbon nanotube
PVDF	-Polyvinylidene fluoride
CT	-Chemo Therapy
CVD	-Chemical vapour deposition
DARPA	-Defence Advanced Research Projects Agency
DC	-Direct current
DI	-Deionised
DLS	-Dynamic light scattering
DMAc	-Dimethylacetamide
DMF	-Dimethylformamide
DMSO	-Dimethyl sulfoxide
DNA	-Deoxyribo Nucleic Acid
DSC	-Differential scanning calorimetry
EH	-Energy harvesting
EIA	-Energy Information Administration
ESD	-Electrospray deposition
FEG	-Field emission gun
FESEM	-Field emission scanning electron microscope
FGO	-Functionalised graphene oxide
FTIR	-Fourier transform infrared spectroscopy
GNs	-Graphite nanosheets
GO	-Graphene oxide
GPC	-Gel permeation chromatography
GPS	-Global Positioning System
HPC	-Hydroxypropyl cellulose

INS	-“Islands-in-the-sea”
MALDI-TOF	-Matrix-assisted laser desorption/ionization time-of-flight mass spectrometry
MAP	-Manifold absolute pressure
MCC	-Microcrystalline cellulose
MRI	-Magnetic Resonance Imaging
MWCNT	-Multi-walled carbon nanotube
NCC	-Nanocrystalline cellulose
NDT	-Non-destructive testing
NFC	-Nanofibrillar cellulose
NFES	-Near-field electrospinning
NMR	-Nuclear magnetic resonance
NTA	-Nanoparticle Tracking Analysis
OECD	-Organization for Economic Co-operation and Development
P(VDF-TrFE)	-Poly(vinylidene-trifluoroethylene)
PEG	-Polyethylene glycol
PHB	-Poly(3-hydroxybutyrate)
PLA	-Polylactic acid
PLLA	-Poly-L-lactide
PLZT	-Lead lanthanum zirconate titanate
PMMA	-Poly(methyl methacrylate)
PMN	-Lead magnesium niobate
PT	-Lead titanate
PV	-Photovoltaic
PVD	-Physical vapour deposition
PVDF	-Polyvinylidene fluoride
PVF	-Polyvinyl fluoride
PVP	-Polyvinylpyrrolidone
PZT	-Lead zirconate titanate
RFID	-Radio Frequency Identification
RNA	-Ribonucleic Acid
RPM	-Revolutions per minute
SAW	-Surface acoustic wave devices
SD	-Standard deviation
SEM	-Scanning electron microscope

SWCNT	-Single-walled carbon nanotube
ST	-Strontium titanate
STM	-Scanning tunnelling microscopes
TA	-Thermal Analysis
TEM	-Transmission electron microscope
TEMPO	-2,2,6,6-tetramethylpiperidine-1-oxyl radical-mediated oxidation
UV	-UltraViolet
UVS	-Ultraviolet-visible spectroscopy
VGCF	-Vapour grown carbon fibre
XPS	-X-ray photoelectron spectroscopy
ZnO	-Zinc oxide

Chapter 1. Introduction to the project

This thesis reports work on modification of polyvinylidene fluoride, PVDF, a polymeric piezoelectric material via incorporation of a range of nanofillers including ceramics, carbon and cellulose aimed at enhancement of piezoelectric performance of the nanocomposites. Nonwoven fibrous membranes of the PVDF/nanofiller composites were deposited by electrospinning process to produce flexible membranes for energy harvesting applications where strain/stress in structures due to mechanical movement can be converted to electric charge and thus a source of energy.

Background of the project is briefly reviewed. Aim and objectives of the project are then described and followed by a few brief words on structure of the thesis.

1.1 The background

Polyvinylidene fluoride, PVDF as a polymeric piezoelectric materials in form of electrospun nanofibre have been studied (Chanunpanich et al., 2007; Pu et al., 2010; Ribeiroa et al., 2010; Sundaray et al., 2013) as a non-woven flexible membranes for components in energy harvesting devices and demonstrated that piezoelectric and mechanical properties of pure PVDF membranes are low for practical applications. In particular, degree of crystallinity of PVDF is a crucial factor to the piezoelectric properties (Goncalves et al., 2013) and tensile strength of the membranes is important to the robustness of the devices. There is thus a need for performance enhancement of the membranes. A potential approach is incorporation of nanofillers to produce PVDF nanocomposites for structural and performance manipulation.

Three systems of such nano-enhancers are considered in this project:

a) Bio-based cellulose fillers;

b) Carbon-based fillers including carbon nanotube and graphene oxide;

c) Ceramic-based fillers including piezoelectric ceramics (barium titanate and zinc oxide) and non-piezoelectric nanoclays.

The inclusion of such fillers are expected to modify structure and properties of the PVDF nanocomposites in several ways. Depending on characteristics of the fillers, they may act as:

1) A nucleation agent to promote crystallinity of the PVDF matrix;

2) A reinforcement for gains in mechanical property;

3) A functional filler to offer additional enhancement in piezoelectricity.

Inclusion of ceramic fine piezoelectric ceramic fillers makes use of the inherent piezoelectric property of the fillers as a functional phase for additional gains in piezoelectric property while non-piezoelectric nanoclays widely used in polymer composites, are cost-effective candidates for effective nucleation and enhancement in mechanical properties.

Carbon-based fillers including carbon nanotubes (CNTs) and graphene oxide (GO) have been shown to have positive influence on polymorphs and crystallisation of PVDF and electric conductivity of the composites.

Cellulose is from natural and renewable resources and thus potentially more sustainable and cost effective. It can be produced as nano-fibrils and has been extensively studied in many polymer systems for enhancement of mechanical, thermal and electrical properties. The inclusion of cellulose is therefore expected to reinforce the PVDF electrospun fibres and contribute to mechanical and crystalline properties of the membrane.

Addition of such nano-sized fillers to PVDF solutions for electrospinning brings new challenges such as difficulties in filler dispersion and stability of the heterogeneous suspension systems. Which have to be carefully studied and formulated. Poor dispersion would affect the homogeneity of the suspension and potential blockage of the system while poor suspension stability would lead to variation of filler concentration during electrospinning.

1.2 Aim and objectives

1.2.1 Aims

This work is to investigate the effect of inclusion of three different types of fine fillers in PVDF on structure and properties of the electrospun composite nanofibre membranes for energy harvesting applications.

1.2.2 Objectives

Using pure PVDF solution as a bench mark, the influences of the three nanofiller systems will be investigated and compared to understand the following:

I. Formulation of PVDF/filler suspensions to achieve appropriate filler dispersion and suspension stability for electrospinning;

II. Effect of type, concentration and status of dispersion of the fillers in the suspension systems on structure and morphologies of the nano-composites, crystallisation behaviour of the PVDF matrix and piezoelectric property of the nano-composites;

III. Correlation between crystallinity (β phase volume fraction) and piezoelectric property of the electrospun composite membranes.

1.3. Structure of this thesis

Following the introduction of the project identifying aims and objectives, Chapter 1 gave a review on literature associated with this research work and identified gaps of knowledge to fulfill. Chapter 2 provided detailed information on experimental details covering materials, formulation designs, suspension preparations, fabrication of electrospun membranes and characterizations. It is followed by Chapters 3, 4, and 5 to present and discuss the results in the three PVDF composite systems, each with a section of summary. Brief comparisons were then made across the three systems in Chapter 6. Chapter 7 summarised the key conclusions of this work and proposed further work.

Chapter 2. Literature Review

In this chapter, energy harvesting is generally described in the context of supplementary measures to meet our energy demands. Then focus will be given to those using piezoelectric materials in the energy harvesting devices. Following a brief review of piezoelectric materials, attention is given to PVDF. Electrospinning, the most used process for producing flexible PVDF membrane is then described and extended to work on PVDF matrix composites incorporating different types of filler.

2.1 Energy demand: present and future

Energy is ubiquitous in our daily lives and we are depending on energies in various forms. We make use of all types of energy to generate electricity and heat, and to supply power for manufacture, transportation and many other living necessities.

The U.S. Energy Information Administration (EIA) released a report in 2011, which predicts that world energy needs will increase 53% from 2008 to 2035 (Atabani et al., 2012). The increasing demands for energy and depletion of fossil energy sources drives the developments in more sustainable and renewable energy supplies.

Between 2007 and 2030, fossil fuels is expected (OECD, 2009) to remain the dominant energy sources, occupying 77% of the total increase of energy demand. Coal is the largest increase in demand followed by gas and oil (Figure 2.1). The fossil fuels are not renewable and will eventually run out. They also cause the main causes of air pollution and global warming, so the development of more renewable and environmentally friendly energy supplies is increasingly important.

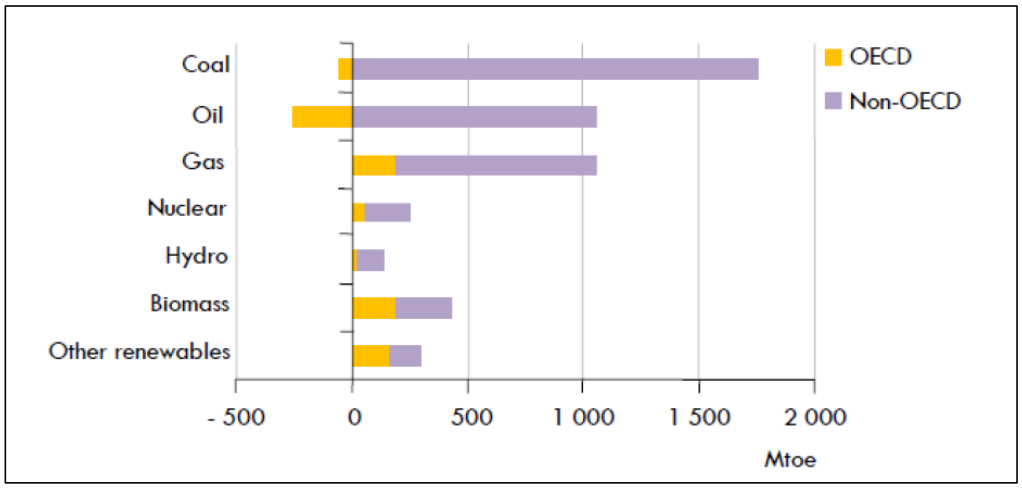

Figure 2.1: Change in primary energy demand, 2007 – 2030 (OECD, 2009)

2.2 Non-renewable energies

2.2.1 Fossil fuels

Human beings burn fossil fuels including coal, oil and gas to get energy. The result of fossil fuel combustion is the generation of heat and the emission of water, carbon dioxide (CO_2) which is the major greenhouse gas, toxic pollutants like methane (CH_4) and nitrous oxide (N_xO). This means the consumptions of fossil fuels cause serious problems of air pollutions and global warming.

Fossil fuels are known as non-renewable energy resources because of time for their formation takes millions of years, but they are consumed much quicker than being reproduced. The world population is growing with the speed of more than 2% per year, driving further increase of energy demand. So meeting energy demand and protecting environment simultaneous is one of the main challenges we are facing.

2.2.2 Nuclear energy

Nuclear energy is generated by non-explosive nuclear reactions, and nuclear power plants use nuclear fission to heat water into steam to generate electricity. Identified world resources of uranium are around 5.5 million tonnes and at current rate of consumption, these resources

correspond to about 100 years of use (Commission of the European Communities, 2008). Nuclear fuel provides considerable amount of energy with low carbon (CO_2) emission but has potential threat to human safety and environment.

2.3 Renewable energies

Renewable energy is derived from naturally and continuously replenished resources, and there are a variety of forms including solar energy, hydropower, wind, geothermal and biofuels. According to EU statistics of primary energy consumption in 2008, share of renewables is currently low, as shown in Figure 2.2 and shares of renewable energy from different sources is shown in Figure 2.3.

In recent years, governments all over the world have paid much more attention to the development of renewable energies. European commission proposed the '20-20-20' target initiative which including reducing greenhouse gas emissions by at least 20 % (compared with 1990 levels) by 2020, improving energy efficiency by 20 % by 2020, raising the share of renewable energy to 20 % by 2020 and increasing use of biofuels in transport fuel sector to 10 % by 2020) (Cialani & Perman, 2014).

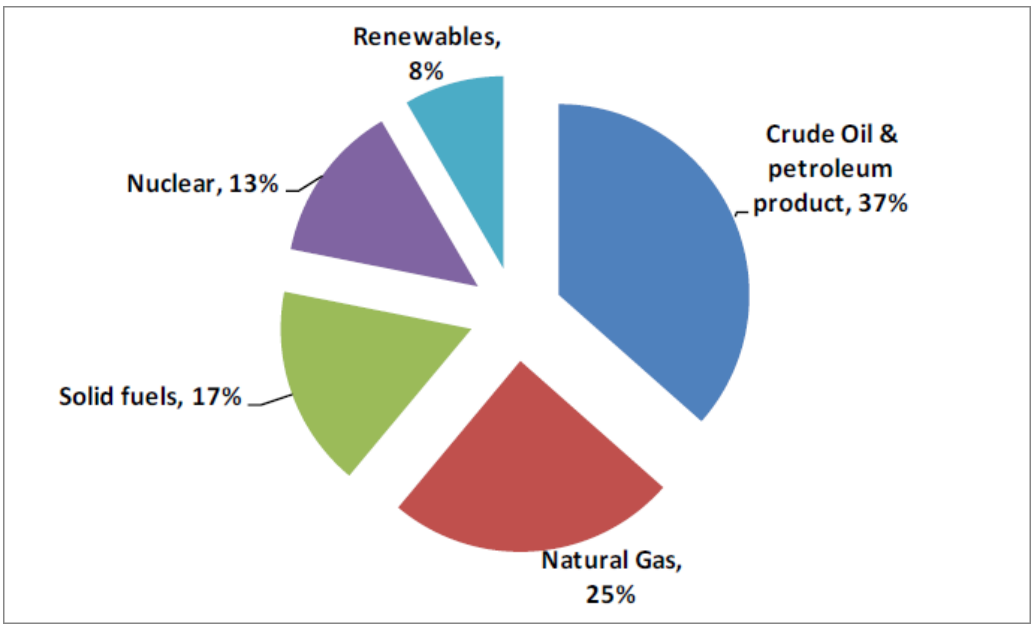

Figure 2.2: Comparison of primary production of energy from different fuels in EU27 based on Gross Inland Consumption (Eurostat, 2010)

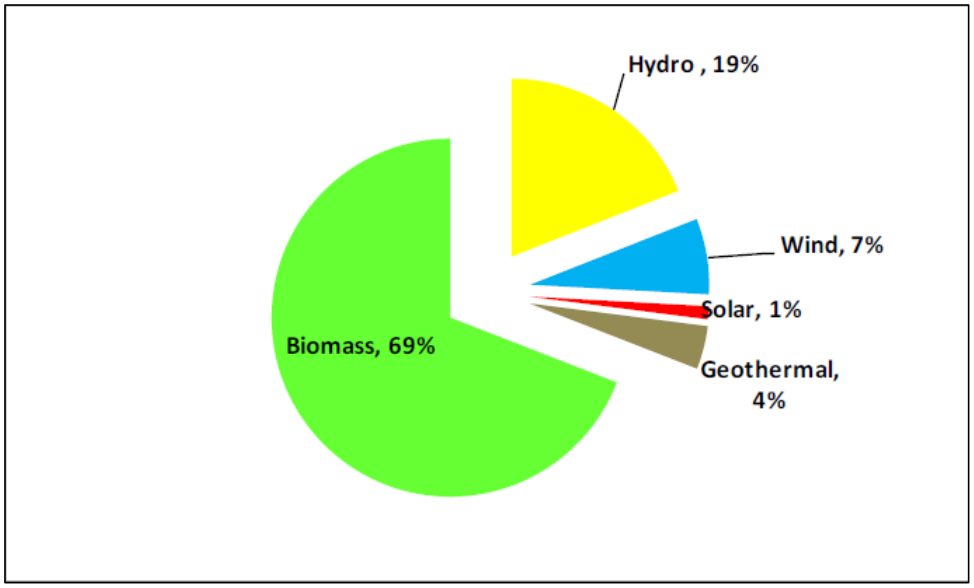

Figure2.3: Share of primary production of renewable energy in EU27 showing primary production of renewable energy from different sources (Eurostat, 2010)

2.3.1 Solar energy

Solar energy includes heat and radiation from the sun. We rely on solar energy to gain heat, light to grow foods and to generate electricity by using, for instance, solar water heaters, solar-cell panels and photovoltaic power plants. Solar energy technologies include solar heating, solar photovoltaics, solar thermal electricity, solar architecture and artificial photosynthesis (Crabtree & Lewis, 2007).

2.3.2 Hydropower

Hydropower energy uses kinetic or potential energy of water to generate electricity. Hydropower is renewable because the global water is reproduced automatically, continuously and naturally by water cycle on the earth. The types of hydropower include waterwheels, hydroelectricity, damless hydro, vortex power, tidal power, tidal stream power, wave power, osmotic power, marine current power and ocean thermal energy conversion (Frenger et al., 2014).

2.3.3 Wind

Wind energy system harness the kinetic energy of the wind using wind turbines to generate electricity, wind mills to drive machines, wind pumps to pump water or drainage, or wind sails to propel ships (Righter, 1996). Wind energy has many advantages: renewable, environmentally friendly and widely available geographically. Disadvantages are, producing noise, occupying lands and affecting natural beauty.

2.3.4 Geothermal

Geothermal energy is the heat stored under the ground generated during the process of globe formation and development because of radioactive decay of minerals and solar energy absorbed by the earth (Kalogirou, 2013). It has no emission of greenhouse gas or pollutant but is not widely, geographically available.

Figure 2.4: Carbon cycle of plant-based biomass (Canadian Biofuel, 2010)

2.3.5 Biofuels

Biofuels utilises energy stored in biomass, including wood and forestry residues, plants, by-products or residues from horticultural/agricultural/animal farming. Biomass is more sustainable than fossil fuels, as shown by the carbon cycle in Figure 2.4.

2.4 Energy harvesting (EH)

Energy is "lost" in form of heat or vibrations in our daily life and industrial processes but it can be recaptured and made use of by different kinds of energy harvesting devices. For instance, heat can be harvested by using thermoelectric or pyroelectric materials to generate electric power, vibrations (sounds) and movements can be harvested by using piezoelectric materials to produce electric power. Different types of energy harvesting techniques are reviewed in this section.

2.4.1. Definition and description of EH

Energy harvesting, also known as power harvesting or energy scavenging, capture and store energy derived from ambient sources including kinetic energy, solar power, wind energy, thermal energy and so on. The history of energy harvesting can be dated back to waterwheels and windmills, and humans have been exploring ways to capture and store energy from ambient sources for more than 50 years. In comparison with large-scale energy sources mentioned above, much smaller scale "wasted" energy is harvested. It can replace batteries to power for small, self-powered and wireless devices such as mobile phone, small sized computer, GPS, radio communication devices and wearable electronics, etc.

Energy can also be harvested to power small scale self-powered smart sensor systems which only need little amount of energy and depend on power of batteries previously, energy harvesters who capture energy from any possible sources can make these sensors functional for a much longer period of time. Energy can be stored in capacitors, batteries and super capacitors. Capacitors are used for applications who needing high energy spikes while,

batteries are used for those applications who needing stable energy flow, and super capacitors acts as the bridge between capacitors and batteries. An energy harvesting scheme puts power stored into a capacitor then boosted/regulated to a second storage capacitor or battery for the use in the microprocessor In terms of power density, for motion powered devices, typical values are a few $\mu W/cm^3$ for human body powered applications and hundreds of $\mu W/cm^3$ for generators powered from machinery (Mitcheson et al., 2004). The researches on energy harvesting is mainly driven by the desire to achieve wireless smart sensor networks and wearable/portable electronics or other devices, and is also driven by the willingness to tackle environmental problems including global warming and climate change.

There are many types of energy harvesting techniques including that used in auto-rewinding mechanical wristwatches, micro wind turbines, photovoltaic, thermoelectric and piezoelectric generators as described briefly below.

2.4.2. Different technologies for energy harvesting

2.4.2.1. Ambient radiation harvesting

This kind of energy source comes from radio transmitters such as radio frequency broadcasting which can be used to power remote devices such as Radio Frequency Identification (RFID) systems and individual nodes in wireless sensor network. (Percy et al., 2012).

2.4.2.2. Biomechanical harvesting

Biomechanical energy harvesters capture mechanical energy from biological tissues, for instance, "Max Donelan™" which straps around the knee allow the generation of 2.5 watts of power per knee, enough to power about 5 mobile phones (Sun, 2008). Another one called "The Socket™" used in football games can generate and store 6 watts (Megan Treacy, 2012).

2.4.2.3. Photovoltaic energy harvesting

Photovoltaic (PV) materials can be used in large-scale as in solar panels and small-scale in PV harvesting such as solar calculators powered by specially tuned amorphous silicon (Prasad & Snow, 2014).

2.4.2.4. Pyroelectric energy harvesting

This kind of technology generates electric power by making use of temperature change in pyroelectric materials such as polyvinylidene fluoride trifluoroethylene, P(VDF-TrFE) (Olsen et al., 1985) to generate electricity. More recently, lead lanthanum zirconate titanate (PLZT) ceramics was found promising because of its high energy densities at low temperatures (Navid & Pilon, 2011). Pyroelectric materials are often stable at high temperature, making it possible for them to be used to harvest energy from high temperature energy sources with higher thermodynamic efficiency. Pyroelectric energy harvesting has some disadvantages: low operating frequencies, requirement of time changing input, and limitations of small amount of power output.

2.4.2.5. Thermoelectric energy harvesting

Unlike pyroelectric, thermoelectric materials interconvert thermal gradients and electric fields for power generation or for refrigeration (Boukai et al., 2008). They can be used as generators, heaters and coolers. Ideally, they should have high electrical conductivity, low thermal conductivity and high Seebeck coefficient. In small scale, micro thermocouples can convert body heat into electricity, and in large scale, large thermocouples are used in nuclear radioisotope thermo-electric generator batteries. Current standard thermoelectric modules are made up with P-doped and N-doped bismuth-telluride semiconductors (connected electrically in series and thermally in parallel) sandwiched between wo metallised ceramic plates. Practical applications include the finger-heart rate meter (e.g. Fraunhofer Thermogenerator) by the Holst Centre (Micropelt, 2009) and the 15 mW thermogenerators by the Fraunhofer Gesellschaft (Reuters, 2008). Thermoelectric energy harvesting has many advantages: no moving parts (allow continuous operation for very long time), no materials must be refilled and heating/cooling can be reversed.

2.4.2.6. Magnetostatic energy harvesting

Based on Faraday's law, magnets can generate small amount of currents by moving relative to conductors because when they are sensitive to vibrations including small ones when shaking on a cantilever. Sensors in inaccessible places can now generate their own power and transmit data to outside receivers (Queiroz & Domingues, 2011).

2.4.2.7. Blood sugar energy harvesting

Blood sugar energy harvesting capture energy from the oxidation of blood sugars, and this kind of energy harvesters are known as biofuel cells which are used to power implanted electronic devices such as pacemakers, biosensors and RFID devices (Olivo et al., 2011).

2.4.2.8. Electromechanical energy harvesting

Mechanical motion such as vibration, noise, human motions etc., can be captured and converted to electric energy by three types of electromechanical transducers: electrostatic, electromagnetic and piezoelectric (Wang, 2008).

Electrostatic energy harvesting is based on the changing capacitance of capacitors by relative motion of capacitor plates to turn mechanical energy into electrical energy. The resulting devices are self-biasing, and can directly charge batteries, or can produce exponentially growing voltages on storage capacitors, from which energy can be periodically extracted by DC/DC converters (Tikalon, 2011).

Piezoelectric energy harvesting converts mechanical energy (strain) into electric energy. Most piezoelectric energy harvesters can only produce milliwatts of electric power and thus suitable for small scale electronic devices.

Numerous case studies can be found in application of piezoelectric harvesting. For instance piezoelectric materials are embedded in walkway flour to capture footstep energy of humans (Treehugger, 2006). Physical movements of trees are captured to power remote sensors and mesh networks to monitor forest fires and weather (Holmes, 2007).

2.5. Piezoelectric energy harvesting

As one of electromechanical technique in EH, piezoelectric energy harvesting has been briefly described in section 2.4.2.8. Since this work focus on development of polymeric piezoelectric composites for energy harvesting, this section covers further relevant details in the potentials of piezoelectric EH including: its current status, applications and market prediction.

Piezoelectric energy harvesting is recently attracting rapidly growing interest mainly due to its energy efficiency and environmental benefits. In comparison with other types of EH methods, some piezoelectric components can provide the highest efficiency and power output by size and cost, enabling replacement of batteries that brings environmental benefits and cost effectiveness.

There are many innovative ideas of energy harvesting using piezoelectric materials. These include powering battle field equipment by piezoelectric generators embedded in soldiers' boots and harvesting energy from human movements in train stations or other public places (Richard & Graham, 2006; Wright, 2007); using dance floors to produce electricity (Kannampilly, 2008) and harvesting vibrations from industrial machinery to charge batteries for backup supplies or to power microprocessors and wireless radios (Barbehenn, 2010).

Since 1990's, the power output of piezoelectric harvesters has jumped from μW to mW scales. This enables it to be used in a wide range of applications such as remote controls, switches, wireless sensor networks, condition monitoring sensors (e.g. tire pressure, rotor blades in helicopters), industrial asset tracking GPS/GPRS, etc. There are many ideas for energy harvesting by using piezoelectric materials like powering battle field equipment by piezoelectric generators embedded in soldiers' boots being researched by DARPA in the United States, harvesting energy from human movements in train stations or other public places, (Richard & Graham, 2006; Wright, 2007) using dance floors to produce electricity, (Kannampilly, 2008) and harvesting vibrations from industrial machinery to charge batteries for backup supplies or to power microprocessors and wireless radios (Barbehenn, 2010).

Furthermore, piezoelectric micro/nano-generators would be able to power muscle-driven elements and self-powered body implantable devices (Li et al., 2010; Yang et al., 2009), etc.

The energy harvesting market is predicted to grow from £450 million in 2012 to more than £950 million by 2017, and that investments in piezoelectric energy harvesting will grow to $145 million in 2018creating a $667 million market by 2022 (IDTechEx report, 2012).

2.6 Piezoelectricity

As the basis for this work, history and fundamental scientific understanding of piezoelectricity are reviewed in this section.

2.6.1 History of piezoelectricity

Piezoelectricity is electric charge that accumulates in response to applied mechanical strain in some specific materials such as crystals, ceramics, and biological substance such as bone, DNA and proteins (Holleret al., 2007). The word piezoelectricity means electricity coming from stress (strain) and originated from the Greek word *piezo/pieze* meaning electric/electron by pressing (Ueberschlag, 2001).

Piezoelectric effect is the linear electromechanical interaction between mechanical and electrical state in crystalline materials without inversion symmetry (Gautschi, 2002), and it is a reversible process: the generation of electricity resulted from applied mechanical strain (in generators or transducers) and the generation of mechanical strain resulted from applied electric field (in actuators) Piezoelectricity is thus versatile and can be used in many applications from production of ultrasonic waves detection of sound, to microbalances, ultrafine focusing of optical assemblies in scientific instruments and electronic devices for everyday uses.

Piezoelectric effect was first discovered by the brothers Pierre and Jacques Curie in 1880 (Manbachi & Cobbold, 2011). They found that Quartz and Rochelle salt showed piezoelectricity, but did not predict the reverse piezoelectric effect which was mathematically deduced from basic thermodynamic principles by Lippmann (1881). The Curies affirmed the existence of the converse effect immediately in 1881 and continued to prove the complete reversibility of electro-elasto-mechanical deformations in piezoelectric crystals quantitatively. Woldemar Voigt (1910) published a textbook, Crystal Physics, in which 20 piezoelectric

natural crystal classes were described the piezoelectric constants using tensor analysis was defined.

Piezoelectric devices were first used as sonar (ultrasonic submarine detector) to calculate distances to objects during World War I in France. In the next few decades, new piezoelectric devices were created and developed such as ceramic phonograph cartridges, ultrasonic transducer for measurement of elasticity and viscosity and ultrasonic time-domain reflectometers (Porcel, 2011).

During World War II, research groups from the USA, Russia and Japan discovered ferroelectrics which had much higher piezoelectricity than natural materials, and then research on barium titanate, BT, and lead zirconate titanate, PZT, took place. Quartz crystals were the first commercially used piezoelectric material in the USA, but scientists kept searching for materials with better performances. In Japan, piezoelectric ceramic materials were developed for piezoelectric filters, buzzers, audio transducers, igniters, gas-grill lighters, and ultrasonic transducers which was first used in early television remote controls and now used as echolocation device for cars (Porcel, 2011).

2.6.2. Mechanism of piezoelectricity

Piezoelectricity in solid materials is closely related to their electric dipole which possibly be carried by molecular groups or be induced by ions on crystal lattice sites with asymmetric charge environments. The dipole density can be calculated by summing up the dipole moments per volume of the crystallographic unit cell (Birkholz, 1995). The dipole density P is a vector field because every dipole is a vector. Dipoles close to each other are likely to be aligned in Weiss domains which are usually randomly oriented but can be aligned by poling by which a strong electric field is applied through the material usually at increased temperatures. However, not all materials can be poled (McKinstry, 2008).

The dipole density P will change when mechanical stress is applied and this may be caused by re-configuration of the environment induced by dipole or re-orientation of molecular dipole moments. Piezoelectricity will then appear in various polarisation strength and their directions, or both of them, are decided by orientation of P, symmetry of crystal and mechanical stress applied. P will change when a change of electric field is extending between

the crystal faces and the units of surface charge density equal to the ones of polarisation. Piezoelectricity is caused by dipole density change in a bulk material.

2.7. Piezoelectric materials

More than two hundred piezoelectric materials that can be used for energy harvesting, and some typical ones include quartz, barium titanate (BT), lead titanate (PT), cadmium sulphide (CdS), lead zirconate titanate (PZT), lead lanthanum zirconate titanate (PLZT), lead magnesium niobate ($MgNb_2O_9Pb_3$), polyvinylidene fluoride (PVDF), polyvinyl fluoride (PVF), etc. For piezoelectric ceramics, BT was first discovered and PZT is mostly used for piezoelectric energy harvesting. Piezoelectric ceramics are brittle but have better electromechanical properties than piezoelectric polymers (Konka, 2010). Some newly emerged requirements in properties like good flexibility, lightweight and low toxicity are attracting increasing attention to alternatives to PZT. Sodium potassium niobate, for instance, has similar properties to PZT without lead. Piezoelectric materials can be classified into three categories: inorganic, organic and composites as described below in more details.

2.7.1. Inorganic piezoelectric materials

Ceramic single crystal materials are generally anisotropic in properties (Schwartz, 2009; Konka, 2010). Many of them have piezoelectricity such as quartz (SiO_2), lithium nibonate ($LiNbO_3$), lithium tantalite ($LiTaO_3$), ammonium dihydrogen sulfate, lithium sulfate monohydrate, and Rochelle salt. They have advantages in some applications like frequency-stabilized oscillators in watches and radars, and surface acoustic wave devices in television filters and analogue signal correlators (Akdogan et al., 2005).

The largest class of piezoelectric ceramics is the Perovskite family (piezoelectric ceramics with the Perovskite structure) including barium titanate or BT ($BaTiO_3$), lead titanate or PT ($PbTiO_3$), lead zirconate titanate or PZT ($Pb(Zr_xTi_{1-x})O_3$), lead lanthanum zirconate titanate or PLZT ($Pb_{1-x}La_x(ZryT_{1-y})_{1-x/4}O_3$) and lead magnesium niobate or PMN ($Pb(Mg_{1/3}Nb_{2/3})O_3$) (Akdogan et al, 2005).

Perovskite structure consists of a simple cubic cell (with a big cation at the corner, a small cation in the body-centre position and oxygen O in the face-centre positions) and is a corner-

linked oxygen octahedral surroundings cations network.

The piezoelectric properties of materials with the Perovskite structure can be tailored by merging various cations in the Perovskite structure, for example, by substituting Ba with Pb, or vice versa, using Barium Titanate ($BaTiO_3$) and Lead Titanate ($PbTiO_3$) (Konka, 2010; Moheimani & Fleming, 2006; Schwartz., 2009).

Piezoelectric ceramics have strong piezoelectricity and high dielectric constant, but they have low mechanical quality factor, power loss and stability, therefore are suitable for power transducers and broadband filters but not suitable for applications that require high frequency and high stability. Quartz crystal on the other hand, has weak piezoelectricity and low dielectric constant and yet high mechanical quality factor and high stability, so they can be used for high frequency applications like frequency control standard vibrator, narrow band filters, high temperature ultrasonic transducer, etc. But they have cutting type restriction and limit in available size.

2.7.2. Organic piezoelectric materials (polymers)

The piezoelectric behaviour in polymers was first reported in 1969 (Kawai, 1969), and attributed to certain crystalline structure in the polymers during solidification from the melt.

Piezoelectric polymers fill niche fields where single crystals and ceramics cannot perform well. Generally, piezoelectric strain constant (d_{31}) of piezoelectric polymers is lower than that of piezoelectric ceramics, but piezoelectric stress constants (g_{31}) of piezoelectric polymers is much higher than that of piezoelectric ceramics.

Piezoelectric polymers possess high strength, high impact resistance, low elastic stiffness, low density, low dielectric constant, high voltage sensitivity and low acoustic and mechanical impedance, high dielectric breakdown and high operating field strength, making them useful in sensor, medical and underwater applications. In addition, they provide greater processing flexibility than ceramic counterparts and can be made into film of large areas, cut and formed into any shape and enable patterning electrodes on film surface and poling selected areas (Harrison & Ounaies, 2001).

Polymers such as polypropylene, polystyrene, poly (methyl methacrylate), polyvinyl acetate and odd number nylons such as Nylon-11 have piezoelectric properties, but strong piezoelectricity have only been observed in polyvinylidene fluoride (PVDF) and its copolymers like polyvinylidene fluoride-trifluoroethylene copolymer or P(VDF-TrFE).

PVDF consists of a carbon chain with alternating hydrogen and fluorine units attached to the carbon backbones to form repetitive units (-CH2-CF2-). PVDF has four different crystalline phases depending on chain conformation linkages: α or δ (TGTG'), β (TTTT), and γ (TTTGTTTG') (T-trans, G-gauche+, G'-gauche–). The β-phase possesses piezoelectricity because it shows spontaneous polarisation. The non-piezoelectric α-phase and γ-phase, may be converted to β-phase (with a pure dipole moment) by poling under high electric fields or by mechanical stretching, respectively (Akdogan et al., 2005), and δ phase is a polar polymorph of α phase (Erdtman, et al., 2012).

Piezoelectricity in PVDF is caused by attraction and repulsion between intertwined long-chain molecules under an electric field. The perpetual dipole polarisation of PVDF is enhanced by stretching and poling of extruded thin polymer sheets to induced formation of β-phase in PVDF. The piezoelectric polymers are mostly used for applications like ultrasonic hydrophones and directional microphones (Konka, 2010 & Schwartz, 2009). They will be described in further details in section 2.8.

2.7.3. Piezoelectric composites

Piezoelectric composites based on piezoelectric ceramics and polymers are promising as properties can tailored to achieve e.g. high coupling factors, low acoustic impedance, good mechanical flexibility, broader transducer bandwidth and low mechanical quality factor. These make them useful for e.g. underwater sonar and medical diagnostic ultrasonic transducers (Konka, 2010; Schwartz, 2009). PVDF based composites will be discussed further in section 2.8.

2.7.4. Applications

Piezoelectric technology is used in high-end technology markets including medical, mechanical, automotive and semiconductor technology and in devices for daily life. The

global demand for piezoelectric products was valued at approximately US$14.8 billion in 2010 (Lusiola, 2012). Manufacturing and automotive industries are currently biggest markets for application of piezoelectric products. Medical instruments, information and telecommunications also create strong demands. In piezoelectric devices, piezoelectric ceramics are mostly used, but market share of piezoelectric polymers are growing rapidly (Acmite Market Intelligence, 2011).

Applications of piezoelectric materials can be categorised into sensors, actuators and transducers.

Sensors

The working principle of piezoelectric sensors is to link electric surface change to the dimensional change or force acting on piezoelectric components. Detection of sound or air pressure change (particularly high frequency sound) is the most common application of sensors. Other examples of piezoelectric sensors include sensors for detection of vibration, shock, and knock for e.g. detection of sonar waves, ultrasonic acoustic emission testing, electric guitars and drum pads.

Actuator

Piezoelectric actuators receive electric signal (e.g. voltage change) and convert to mechanical action (e.g. a stroke) and hence work as reversed sensors. As very high electric voltage can cause only small changes in the dimension of piezoelectric elements, such actuator can be used for positioning with extreme accuracy. Multilayer piezoelectric ceramics actuators using layers thinner than 100 μm can achieve high mechanical response to voltage lower than 150 V.

Piezoelectric actuators are used in applications such as micro-positioning, multi-span beam controller, active vibration damping, piezoelectric motors (or other special-purpose motors), inkjet printers, hydraulic valve controller, dental scalers, ultrasonic welding, small-volume pumps and ultrasonic cleaning. Atomic force microscopes, AFM, and scanning tunnelling microscopes, STM, use converse piezoelectricity to keep sensing needle close to the probe (Le Letty et al., 2001). Piezoelectric actuators are used in XY stages for microscanning in

infrared cameras and for moving patients accurately inside active CT or MRI scanners in which strong radiation or magnetism interrupts electric motors (Simonsen, 2010).

Transducers

Transducers convert electrical signals to vibrational mechanical motion or vice versa, and thus have the ability of both sensors and actuators.

Piezoelectric transducers are used in applications such as flow measurement, level measurement, distance measurement, underwater sonar, medical scanners or imaging (e.g. checking unborn babies by ultrasound), ultrasonic non-destructive testing (NDT) transducers, automotive engine management systems, telephone speakers, sonar arrays, manifold absolute pressure (MAP) measurement and seismic investigations (Arnau, 2008).

2.8. Piezoelectric polymers

This work is on development of PVDF based nanocomposites for energy harvesting, further review on their structure, processing and properties will be given.

2.8.1 Piezoelectric polymers

Kawai discovered that stretched and electrically poled polyvinylidene fluoride (PVDF) showed outstanding piezoelectricity (Kawai, 1969). PVDF Since then, PVDF copolymers such as P[VDF-TrFE], P[VDF-TFE] and P[VDF-HFP] and PVDF/PMMA blends have been studied. Other polymers showing piezoelectricity include polyvinylidene cyanide and its copolymers, aromatic and aliphatic polyureas, polyvinyl chloride, aromatic polyamides/odd nylons, polyvinyl fluoride, polyvinyl acetate and ferroelectric liquid crystal polymers. (Brown et al., 1994; Green et al., 1986; Ibos et al., 1999; Ikeda & Suzuki, 1992; Kim et al., 1994; Le Grand, 1989; Nalwa, 1991; Nalwa, 1995; Pelrine et al., 1998; Wang et al., 1988).

In comparison with the most popular ceramic PZT, piezoelectric polymers have relatively lower piezoelectricity as shown in Table 2.1 (Ohigashi et al., 1984).

Table 2.1. Piezoelectric and related properties of P(VDF-TrFE), PVDF and PZT

Properties	P(VDF-TrFE)	PVDF	PZT-4A
e_{33} (C/m^2)	-0.23	-0.23	15.1
h_{33} (10^9 V/m)	-4.3	-4.3	2.7
g_{33} (Vm/N)	-0.38	-0.38	0.025
d_{31} (PC/N)	12.5	12.5	-123
density ($l0^3$ kg/m^2)	1.88	1.88	7.5
acoustic velocity u (km/s)	2.40	2.40	4.60
acoustic impedance (10^6 kg/m^2s)	4.51	4.51	34.8
elastic constant cD ($l0^9$ N/m)	11.3	11.3	159
coupling factor k,	0.30	0.30	0.51
dielectric constant	6.0	6.0	635
mechanical loss tangent	0.05	0.05	0.004
dielectric loss tangent	0.15	0.15	0.02

However, piezoelectric polymers have many other advantages including nontoxic (lead-free), flexible (low elastic constant), light weight (much lower density) and higher in certain piezoelectric constant and easy to process and thus have received increasing interests.

Piezoelectric polymers can be categorised into two classes. Class I material such as PVDF mainly consists of the materials that are poled by high electric field which typically show a symmetry of $C_{\infty v}$ group. Class II materials are those composed of uniaxially oriented chiral molecules which are most commonly biopolymers macroscopically aligned by mechanical stretching or by magnetic field. The structure of class II material has the symmetry of $D_{\infty h}$. The representative material for class II is α-helical poly(amino acid) (e.g. PBLG) and polyesters with chiral repeat units (Furukawa, 1989; Nakiri et al., 2004).

PVDF and P(VDF-TrFE) copolymers show greatest piezoelectricity among piezoelectric polymers in temperature range of -40℃ to 100℃. P(VDF-TrFE) copolymers however, are expensive (>$250/lb resin) and extremely difficult to produce, and thus occupy quite a small percentage of commercial piezoelectric polymer. In comparison, PVDF is inexpensive ($8/lb

resin) and dominated all important commercial piezoelectric polymer applications which is an important reason to be chosen as the base materials for this work.

2.8.2. Polyvinylidene fluoride (PVDF)

Polyvinylidene fluoride (or polyvinylidene difluoride, PVDF) is a pure non-reactive thermoplastic fluoropolymer and is produced by the polymerisation of vinylidene fluoride (or vinylidene difluoride). It is generally used in applications with requirement of high purity, strength, resistance to solvents, acids, bases and heat and low smoke generation. PVDF has a relatively low melting point of approximately 177 °C, a low density, and low cost comparing to other fluoropolymers. It is available as sheets, films, panels, tubing, piping products, crosslinked closed-cell foams and premium wire insulators. It can be extruded, injection moulded or welded and is commonly used in chemical, medical, defence, semiconductor industries and in lithium ion batteries (Ueberschlag, 2001).

There are three major brands of PVDF being sold in market: Hylar (Solvay), Kynar (Arkema) and Solef (Solvay).

PVDF has a chemical composition of $(CH_2\text{-}CF_2)_n$ and is a semi crystalline polymer. It achieves a spherocrystal structure and a non-polar phase with a helical (TGTG') configuration after melting processing, then strong mechanical orientation of PVDF is needed to induce solid state phase transition from α phase to highly polar β phase with a two dimensional zigzag all trans (TTTT) chain configuration as shown in Fig 2.5. Subsequent poling of the film is proceeded under controlled temperatures at field strength exceeding 100 V/μm (Bloomfield PE, 1988). The films are then thermally annealed to realise the controlled mechanical relaxation necessary to produce commercially stable materials. The properties of piezoelectric PVDF are thus made more anisotropic due to the processing method.

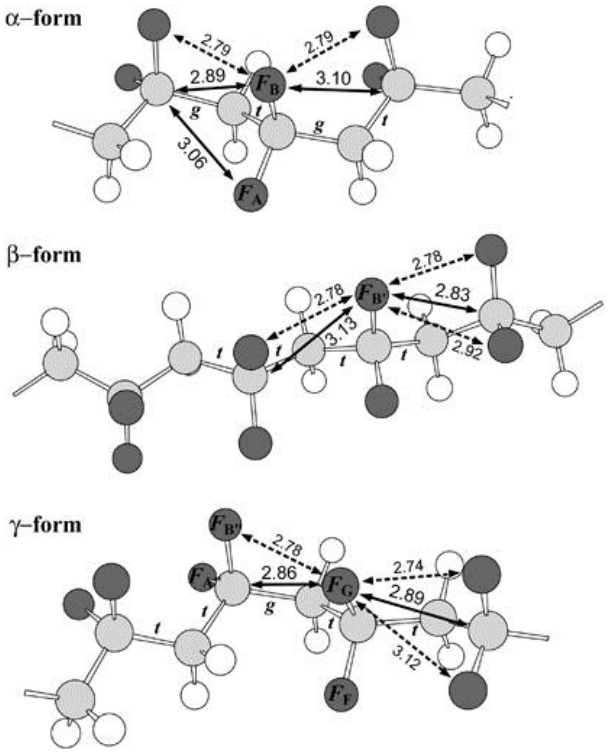

Figure 2.5: Schematic structures of 3 forms of chain configuration in PVDF

2.8.2.1. Properties

Strong piezoelectricity of PVDF was observed in 1969, and poled PVDF thin films were found to have much stronger piezoelectric coefficient (6–7 pC/N) than any other polymeric counterparts (Kawai & Heiji, 1969).

The glass transition temperature (T_g) of PVDF is approximately −35 °C and the crystallinity is about 50 to 60%. It has a negative d_{33} value, which means that it will contract instead of expand (or vice versa), unlike other piezoelectric materials under the same electric field. PVDF has four forms of crystalline phases depending on chain conformations as trans (T) or gauche (G) linkages: α or δ (TGTG'), β (TTTT), and γ (TTTGTTTG'). Generally speaking, the α phase is kinetically favourable. Therefore, normal crystallisation from the melt and solution-casting from non-polar solvents typically result in the α phase. The β phase in PVDF is thermodynamically more stable. Therefore, the β phase can be obtained by high-pressure crystallisation from the melt or mechanical stretching and/or electric poling of the original α phase. In addition, the γ phase can be obtained by either solution-casting from strongly polar solvents such as N, N-dimethyl formamide (DMF), N, N-dimethyl acetamide (DMAc), and dimethyl sulfoxide (DMSO), or crystallisation at high temperatures (Gregorio & Cestari,

1994; Tashiro, 1995). When chains of PVDF are packed into crystalline lattices, a net dipole will be created in β, γ and δ phases making them polar crystalline phases and no net dipole in α phase making it non-polar. Among three polar phases, β phase has the greatest spontaneous polarisation per unit cell thus shows the best piezoelectric and ferroelectric properties (Tashiro, 1995).

2.8.2.2. Processing

PVDF can be synthesised through a free radical or controlled radical polymerisation process from gaseous VDF monomer, this can be followed by processes like melt casting, solution casting, film casting and spin coating.

Solvents like dimethyl formamide and more volatile butanone are used for solution based processing. Fluoro surfactant perfluorononanoic acid is used in an ion form for aqueous emulsion polymerization (Prevedouros et al., 2006). Solvents like dimethyl sulfoxide or tetrahydrofuran are used for molecular weight characterisation through gel permeation chromatography, GPC.

PVDF after are typically in α phase without piezoelectricity, in order to achieve piezoelectric β phase, PVDF materials (except thin films) need to be stretched or annealed, and they must be poled under strong electric field (above 30 MV/m) first to gain piezoelectric response. Thick films (more than 100 μm) are usually heated to 70–100 °C during poling to obtain higher piezoelectric response.

2.8.2.3. Applications

The piezoelectric property of PVDF has been explored in sensors, actuator and transducers and described in section 2.7.4. For conventional applications, PVDF is commonly used as insulation for electrical cables and printed circuit board due to its flexibility, light weight, low thermal conductivity, heat resistance and high chemical corrosion resistance. In electronic industry, PVDF is used to produce low-cost strain gauges, tactile sensor arrays, lightweight audio transducers and as a standard binder material used in the manufacture of composite electrodes for lithium ion batteries. In addition, PVDF is used for monofilament fishing lines

with lower optical density, harder surface and higher density comparing to nylon ones (Ueberschlag, 2001).

2.9. Nanocomposites in general

In this section, fundamental aspects in nanocomposites will be reviewed. It starts with a review in nanoparticles and nanofibres, the dispersed phases in common nanocomposites. Then the concept of nanocomposites with the key features in comparison with conventional composites and their classifications will be described.

2.9.1. Nanoparticles

2.9.1.1. The Definition

Nanoparticle refers to the smallest unit (as single particle, clusters of particles or relics of agglomerate) with regard to its motion within the matrix of composites as in reality, complete separation of clusters/agglomerates into single particle are rarely achieved. Particles are further classified according to their diameters (or equivalent) (Wadell, 1935). The ranges of diameters of coarse, fine and ultrafine particles (nanoparticles) are suggested as 2,500 to 10,000 *nm*, 100 to 2,500 *nm* and 1 to 100 *nm*, respectively (Buzea et al., 2007). Nanoparticles are not necessarily equiaxial, they should have at least one dimension in the 1 to 10 *nm* range and a narrow size distribution. Nanopowders are usually agglomerated nanoparticles, or nanoclusters (Fahlman, 2007).

2.9.1.2. The key features

Nanoparticles attracts great scientific interest because they are a bridge between bulk materials and atomic/molecular structures. A bulk material have invariable physical properties despite its size, but size-dependent properties are often observed in nano-scale, therefore the properties of materials change when their sizes are close to nano-scale and when the percentage of atoms on the material surface becomes important. For bulk materials larger than one micron the atom percentage on the surface is insignificant with regard to the atom number in the bulk of the material. Some unexpected properties of nanoparticles are mainly caused by the large surface area of the materials. Nanoparticles have unexpected optical

properties because they are small enough to limit their electrons and produce quantum effects. For instance, absorption of solar radiation in photovoltaic cells is much higher in materials consist of nanoparticles than it is in thin films of continuous material and the smaller the particles, the higher the solar absorption. Other size-dependent property changes include quantum confinement in semiconductor particles, surface plasmon resonance in metal particles and superparamagnetism in magnetic materials. However, these changes of physical properties are not always desirable. For example, ferromagnetic materials smaller than 10 nm can change their magnetisation direction by using room temperature thermal energy, but this makes them inadaptable for memory storage (Evans & Davidge, 1969).

2.9.1.3. Different types and applications

Large range of different types of nanoparticles have been produced and studied for different benefits in biomedical, optical, electronic and mechanical applications. These include metal, dielectric and semiconductor nanoparticles, semi-solid and soft nanoparticles and hybrid structures like core–shell nanoparticles. Semiconducting nanoparticles are known as "quantum dots" when they are small enough (<10nm) so as to enable quantisation of electronic energy levels (Roduner, 2006). Such nanoparticles are used in biomedical applications as drug carriers or imaging agents. A typical nanoparticle of semi-solid nature is liposome. Various kinds of liposome nanoparticles are currently used clinically as delivery systems for anticancer medicines and vaccines (Zhang et al., 2008). Janus nanoparticles with one half hydrophilic and another hydrophobic and are especially effective for stabilising emulsions. They can self-assemble at water/oil interfaces and act as solid surfactants (Srinivas et al., 2006). The high specific surface area of nanoparticles offers a huge driving force for diffusion particularly at elevated temperatures and thus sintering (e.g. of ceramics) can be proceeded at lower temperatures, over shorter time scales than for coarse particles. In addition, nanoparticles have shown some useful properties for everyday products such as "self-cleaning surfaces" in materials containing titanium dioxide nanoparticles; "enhanced UV blocking" properties by zinc oxide nanoparticles in sunscreen lotion preparation (Lange & Metcalf, 1983; Mat, 1970) and "smart and functional clothing" coated with nanoparticles (Evans, 1987).

Nanoparticles come in different shape and surface morphologies, a subject in the field of micromeritics. Spheres, rods, fibres and cups are just a few of the shapes that have been

grown. Nanospheres, nanoreefs, nanoboxes and so on sometimes appear spontaneously as an effect of a templating or directing agent present in the synthesis like miscellar emulsions or anodised alumina pores, or from the inherent crystallographic growth patterns of the materials themselves (Niedermeyer, 2016). Some of these morphologies may serve a purpose like long carbon nanotubes being used to connect an electrical junction. Amorphous particles usually adopt a spherical shape because of their microstructural isotropy, and the shape of anisotropic microcrystalline whiskers corresponds to their special crystal habit.

2.9.1.4. Surface coating and functionalities

The surface coating of nanoparticles have significant effect on their functionalities. The surface coating can adjust their stability, solubility and targeting. A coating that is multivalent or polymeric gives high stability (Duan et al., 2010). Functionalised nanoparticles based catalysts can be used for catalysis of many organic reactions. For biological applications, the surface coating should be polar to give high aqueous solubility and avoid nanoparticle aggregation. In serum or on the cell surface, highly charged coatings enhance ambiguous binding, while polyethylene glycol linked to terminal hydroxyl or methoxy groups repel undefined interactions (Mitchnick et al., 1999). Nanoparticles can be linked to biological molecules which can act as address tags to direct the nanoparticles to specific sites within the body (Taylor et al., 2013), specific organelles within the cell, (Belloni et al., 1998) or to follow specifically the movement of individual protein or RNA molecules in living cells (Brinker & Scherer, 1990). Common address tags are monoclonal antibodies, aptamers, streptavidin or peptides. These targeting agents should be covalently linked to the nanoparticle and be present in a controlled number per nanoparticle. Multivalent nanoparticles bearing multiple targeting groups can cluster receptors, which can activate cellular signalling pathways and give stronger anchoring. Monovalent nanoparticles bearing a single binding site (Corriu & Anh, 2009; Hench et al., 1990; Klein, 1994), avoid clustering and thus are preferable for tracking the behaviour of individual proteins. Red blood cell coatings can help nanoparticles evade the immune system (Pais, 2005).

2.9.1.4. Synthesis or preparation

There are many techniques for synthesis/preparation of nanoparticles. Among them, attrition and pyrolysis are two methods for high output production. In attrition, macro or micro scale

particles are ground in a ball mill or other size reducing equipment. The resulting particles are then air classified to recover nanoparticles. In pyrolysis, a vaporous precursor is forced through an orifice at high pressure and burned. The resulting solid is air classified to recover oxide particles from the by-product gases. Pyrolysis often lead to aggregates and agglomerates rather than single particles.

The thermal plasma temperatures are in the order of 10,000 K at which solid powder in micrometres evaporates easily. The major types of the thermal plasma torches used to produce nanoparticles are DC plasma jet, DC arc plasma and radio frequency (RF) induction plasmas (Fauchais et al., 2008). Laboratory units are operated at power levels between 30 and 50 kW while the industrial scale units can reach levels up to 1 MW. The plasma methods have been used for synthesis of different oxides, carbides and nitrides of Ti and Si nanoparticles (Hahn, 1997).

Inert gas condensation is frequently used to make nanoparticles from metals with low melting points. The metal is vaporised in a vacuum chamber and then super-cooled with an inert gas stream. The super-cooled metal vapour condenses into nanometre size particles which can be carried in the inert gas stream and deposited on a substrate (Gandhi et al., 2010).

Nanoparticles can also be produced by radiation chemistry. Radiolysis from γ rays can create strongly active free radicals in solution. This technique uses water, a soluble metallic salt, a radical scavenger (a secondary alcohol) and a surfactant (organic capping agent). High γ doses in the order of 104 *Gray* are is required. During the process, reducing radicals will decline metallic ions down to the zero-valence state. A scavenger chemical will preferentially interact with oxidising radicals to avoid the re-oxidation of the metal. Metal atoms begin to combine into particles once in the zero-valence state. Chemical surfactant surrounds the particle during formation and regulates its growth. The surfactant molecules stayed on the particle in sufficient concentrations to prevent it from dissociating or forming clusters with other particles. This method allows for tailoring particle size and shape by adjusting precursor concentrations and gamma dose (Whitesides et al., 1991).

The sol-gel is a wet chemical technique (also known as chemical solution deposition) widely used in the fields of materials science and ceramic engineering. This process are mainly used for the manufacture of materials like metal oxide starting from a chemical solution(sol, short for solution) which acts as the precursor for an comprehensive network (or gel) of discrete particles or network polymers (Dabbs & Aksay, 2000). Typical precursors are metal

alkoxides and metal chlorides, which experience hydrolysis and polycondensation reactions to form either a network "elastic solid" or a colloidal suspension, which is a system consist of discrete submicrometre particles dispersed to various degrees in a host fluid. Formation of a metal oxide includes connecting the metal centres with oxo (M-O-M) or hydroxo (M-OH-M) bridges producing metal-oxo or metal-hydroxo polymers in solution. The sol develops towards the formation of a gel-like two-phase (liquid and solid phase) system whose morphologies range from discrete particles to continuous polymer networks (Hewakuruppu et al., 2013). A significant amount of fluid may need to be removed at first for the recognition of the gel-like properties because the particle density of colloid may be too low. Centrifugal separation can be used to accelerate the phase separation process. Removal of the remaining liquid requires a drying process which is typically accompanied by shrinkage and densification. Then a thermal treatment is usually necessary to favour further polycondensation and improve mechanical properties and structural stability through final sintering, densification and grain growth. The precursor sol can be either deposited on a substrate to form a film by dip-coating/spin-coating or used to produce powders like microspheres and nanospheres. The sol-gel method is a cheap and low-temperature technique that allows for the fine control of chemical composition of the product. Even small amount of dopants like organic dyes and rare earth metals can be introduced in the sol and dispersed in the final product evenly. Sol-gel derived materials have various applications in optics, electronics, energy, space, sensors, medicine and separation technology like chromatography (Buffat & Borel, 1976; Taylor et al., 2012).

To avoid flocculation or agglomeration of nanoparticles, preparation of them are generally carried out in colloids where the solid particles are sufficiently small to show Brownian motion to prevent sedimentation and precipitation (Taylor et al., 2011). Alternatively, physical or chemical vapour deposition (PVD or CVD) may be used to form nano-sized single crystal particles (Granqvist et al., 1976; Hayashi et al., 1997). But their non-aggregated depositions have lognormal size distribution because of the combination of diffusion and drift (Hayashi et al., 1997; Kiss et al., 1999). Monodisperse nanoparticles and colloids are often preferred as they offer the potential of total control over interparticle forces required by the containment of a uniformly dispersed assembly of strongly interacting particles in suspension (Turner, 1908).

2.9.1.5. Characterisation

Characterisation of nanoparticle is essential to understand synthesis, functions, and applications of different nanoparticles. Various techniques can be used for analysing specific characteristics. These include electron microscopy (TEM, SEM AFM); spectroscopy (X-ray photoelectron spectroscopy, XPS, X-ray diffraction, XRD, Fourier transform infrared spectroscopy, FTIR, matrix-assisted laser desorption/ionization time-of-flight mass spectrometry, MALDI-TOF and ultraviolet-visible spectroscopy, UVS); dynamic light scattering (DLS), dual polarisation interferometry and nuclear magnetic resonance (NMR). The technology for Nanoparticle Tracking Analysis (NTA) allows direct tracking of the Brownian motion and allows the sizing of individual nanoparticles in solution (Filipe et al., 2010).

It should be noted that not all types of the nanoparticles mentioned above have been used as dispersion phases in solid nanocomposites. In many cases they are used in coatings or in colloid suspension of liquids and so on.

2.9.2. Nanofibres

2.9.2.1. Definition

Following the definition of nanoparticles in section 2.9.1, nanofibres refer to fibres that are below 100 *nm* in diameter. For instance, the average diameter of electrospun fibres ranges from 100 nm to 500 nm (Subbiah et al., 2004). Similar to nanoparticles, nanofibres have high specific surface area (around a thousand times greater than that of a human hair) and therefore have similar potential as nanoparticles in nanocatalysis, tissue scaffolds, protective clothing, filtration and nano-electronics (Teo & Ramakrishna, 2006). The additional characteristic of almost infinite aspect ratio for continuous makes it particularly attractive for mechanical reinforcement in nanocomposites.

2.9.2.2. Key features

High specific surface area, high strength and stiffness, "defect-free" and the possibility of producing three dimensional structures have increased the interest in nanofibres (Subbiah et al., 2004). For instance, polymer nanofibres of diameters 100 *nm* possess extraordinary high specific surface area of around 1000 m^2/g. Nanofibres and nanofibre mats have many potential applications such as in filtration, protective clothing, aerospace, electronic devices, tissue engineering, sensors, and biomedical uses (Nasir et al., 2005). Nanofibre mats, for instance, has found application as drug carriers for the drug delivery system (Kenawy et al., 2002).

2.9.2.3. Methods of processing

Electrospray deposition (ESD)

Electrospray deposition (ESD) is an electric field induced spray process and a versatile method for preparation of nano-micro scaled fibre (Nasir et al., 2006). The ESD process is composed of the following steps: (1) a strong electric field is applied between a polymer solution contained in a nozzle and a conductive substrate; (2) when the voltage reaches a critical value, electrostatic forces overcome the surface tension of the solution;(3) charged droplets or jets are sprayed from the tip of the nozzle in a dry environment; and (4) the dried droplets or jets are finally collected on the substrate to form a thin film. In the ESD process, some parameters including concentrations of polymer and additives, viscosity, surface tension and feeding rate of the polymer solution, environment humidity, applied voltage and nozzle-to-ground collector distance will affect the fibre diameter and morphology (Zhou & Gong, 2008). In ESD processed PVDF, the total crystallinity and melting point were decreased while oriented β crystalline structure was induced (Nasir et al., 2005).

Bicomponent spinning

The production of nanofibres by bicomponent spinning process has two steps: spinning "islands-in-the-sea" (INS) or "segmented pie" bicomponent fibres, and then removal of one of the component. INS fibres, first created by Toray Industries, typically consist of a mass of individual 'islands' of one polymer surrounded by a 'sea' or matrix of another polymer. The sea polymer has to be removed by dissolving it with a solvent or by melting to leave ultrafine filaments. Splittable bicomponent fibres by melt-spinning process, known as "segmented pie" fibres, provide a method to produce nanofibres with noncircular cross-sections. Splittable

fibres with 16 segments using polyester and nylon have been produced by the spun bond process. The methods used to split bicomponent fibres in spun bonded webs include physical, chemical and mechanical methods (Zhou & Gong, 2008).

Melt-blowing

Melt-blowing developed in the 1950s at the Naval Research Laboratory is currently one of the main sources for fibres with small diameters, it is a non-woven manufacturing process, in which a polymer melt is extruded through dies, attenuated by heated, high-velocity air streams and spun into the fibres. The fibres are then deposited on to a collector randomly and form a non-woven web. Many methods have been tried to reduce the diameter of conventional melt-blown fibres. The most direct method is to reduce the feed rate of polymer melt for producing finer melt-blown fibres, which can only reduce the fibre size to a limited extent at the cost of the fibre production rate. Another improved melt-blowing process includes producing INS fibres and then dissolving the sea component of the melt-blown fibres, which requires a time-consuming dissolving step to produce finer fibres. Splittable fibres by melt-blowing is another method which may not be suitable to split mechanically the melt-blown segmented pie fibres because of weak strength and inter-fibre bonding. Non-woven webs were produced in a melt-blowing process using different combinations of primary plates and secondary plates in a modular die plate assembly. Polypropylene nanofibres were melt-blown using a special die. Bodaghi and Sinangil (2009) extended the conventional melt-blowing technology to manufacture non-woven webs containing nanofibres by a specific spin-pack assembly, which allows changing the rheology of the polymer melts by an amount sufficient to produce phase separation between the first and second polymer jets. Ellison et al. (2007) demonstrated that there is no basic theoretical limitation for the melt-blowing technique to produce polymeric fibres with diameters of several hundred nanometres. Melt-blowing may be used to produce INS fibres that contain more than 600 island fibrils with diameters as low as 50 nm (Zhou & Gong, 2008).

Flash spinning

Flash spinning is a modified version of spun bonded technology in which a polymer like polypropylene is dissolved and extruded. As the solvent rapidly evaporates at the spinneret, individual filaments break into a highly fibrillar form and are collected on a moving screen

forming a web. Flash spinning has been used to produce plexifilamentary film-fibril strands consisting of ultrafine fibres from a spin fluid as a further development of the melt-blowing process. It is easier to produce discrete fibres from high molecular weight polymers by flash spinning than other conventional processes. However, flash spinning technique developed so far do not produce fibrous webs consisting of solely nanofibres, micrometre fibres and sub-micrometre fibres can also be found (Zhou & Gong, 2008).

Electrospinning

Under the influence of electric field, a flowing dielectric polymer solution stretches as it emerges from a needle or a spinneret to form a cone, commonly referred to as Taylor cone, from the tip of which tiny droplets lift off. If the applied voltage is sufficiently high, the droplets lifting off coalesce to form thin jet of liquid. The formation of the Taylor cone and the thin jet of liquid are dependent on the viscosity and electrical resistivity of the polymer solution. For low viscosity solutions, the jet breaks up into droplets, while for high viscosity solutions it travels to the collector as fibre jets (Deitzel et al., 2001). Provided that the solvent containing the polymer evaporates fast enough, the thin jets will form fibres. After the initiation from the cone, the jets undergoes a chaotic motion or bending instability and are field directed towards the oppositively charged grounded collector, which collects the charged fibres (Yarin et al., 2001). The configuration of the collector can vary from a flat plate to rotating drum to obtain different fibre sizes, orientation and the resulting electrospun 3D structures (Reneker et al., 2000; Shin et al., 2001; Teo & Ramakrishna, 2006).

Electrospinning has attracted great attention as a technique to manufacture various ultrafine polymeric fibres that are difficult to be achieved by other methods. It has been proved to be an easy and feasible method to produce fibres with diameters in nanometre to sub-micrometre range from polymers, ceramics, composites and metals in form of solution or melt. Electrospinning was created in the 1930s, and the production of ultrafine fibres with diameter less than 1 μm was reported in 1971. The great potential of the process in nanofibre production attracted rapid increase of interests in mid-1990s. Recent research reported has been focused on exploring various materials that are electrospinnable, characterisations of the fibres and finding new applications for them.

Only non-woven nanofibre materials have been commercially feasible to produce so far, and manufacture of nanofibre yarns with controlled orientation of the nanofibres is still one of the

most serious challenges (Zhou & Gong, 2008). Electrospun biomaterials have been tested as scaffolds for tissue engineering of blood vessel, skin, bone, cartilage, skeletal muscle, neural and many other soft tissues (Pham et al., 2006; Sill & von Recum, 2008; Szentivanyi, et al., 2011).

2.9.3. Nanocomposites

2.9.3.1 Definition and key features

A nanocomposite is a multiphase solid material where one of the phases has 1, 2 or 3 dimensions of below 100 *nm* or structures with nano-scale repeating distances between different phases (Ajayan et al., 2003). The mechanical, optical, electrical, thermal, electrochemical, and catalytic properties of nanocomposites differ significantly from that of component materials as the results of high specific surface area which enhances chemical reactivity and strengthening/stiffening and quantum effects which gives rise to new optical, electrical and magnetic properties (Zeng et al., 2014).

The influence of nano-scale dimension of phases have been summarised by Kamigaito (1994) as the dimension decrease: <100 nm for getting superparamagnetism, mechanical strengthening or limiting matrix dislocation movement; <50 nm for changing refractive index; <20 nm for softening a hard magnetic material; and <5 nm for catalytic activity.

Although nanocomposites is based on the capability to produce and manipulate nano-dimensional phases in materials using modern technologies, use of nanocomposites can be traced back to earlier civilisation of mankind. Jose-Yacaman et al. (Jose-Yacaman et al., 1996) studied the origin of colour depth and the resistance to acids and bio-corrosion of Maya blue paint and attributed to mechanisms due to the nanoparticles in it. Nano-scale organo-clays had been used to control flow of polymer solutions or constitution of gels from the mid-1950s, and polymer/clay composites became topics of textbooks by the 1970s (Theng, 1979).

Nanocomposites differ from conventional composites because of the extraordinarily high surface area to volume ratio of the dispersed phase(s) and/or their singularly high aspect ratio. The dispersed phase(s) can be nano-sized minerals, fibres/whiskers (e.g. carbon nanotubes or electrospun fibres or nanocellulose) or sheets like exfoliated clay stacks. Specific interfacial

area between the matrix and dispersed phase in nanocomposites can be a few orders of magnitude higher than that of conventional composites, leading to drastic changes in properties. In polymer nanocomposites, properties related to interfacial chemistry, degree of cure in thermosets, chain mobility chain configuration or crystallinity can all change significantly (Ajayan et al., 2003). The specific interfacial area means that a relatively small quantity of nano-scale reinforcement can have a remarkable improvement in properties of the composites such as optical properties, dielectric properties, heat resistance and mechanical properties.

Although nano-scale dispersed phases can be precipitated *in–situ* during processing stages such as in metal solidification, generally though, the nano-scale reinforcement is added and dispersed into the matrix during processing. The weight percentage of the nanoparticles is typically kept very low (e.g. 0.5 to 5 wt%) because of the low percolation threshold of fillers especially for non-spherical, high aspect ratio fillers such as nanometre-thin platelets like clays or nanometre-diameter fibres like carbon nanotubes.

2.9.3.2 Classification

Nanocomposites may be classified into categories based on the matrix which give rise to ceramic-, metal- and polymer-matrix nanocomposites. A brief review is given below.

Ceramic-matrix nanocomposites

Ceramics are non-metal, inorganic compounds and engineering ceramics consist of oxides, nitrides, borides, silicides, etc. As ceramics are inherently brittle, one the most attractive enhancement is their toughness and hence more ductile metal phases is typically dispersed in a ceramic matrix for this purpose. Ideally both the metallic and ceramic components are well dispersed in each other to achieve special nanoscopic properties (Kruis et al., 1998). In addition, there have been reports on enhanced properties such as optical, electrical/magnetic, tribological, corrosion resistance, as reviewed by Zhang et al. (2003).

Measures must be taken to prevent chemical reaction between two components since metallic component may easily react with ceramic and lose its metallic features. One of such measures

is to choose metal immiscible with the ceramic matrix, for example, Cu is immiscible with TiO_2 in the Gibbs' triangle of Cu-O-Ti over big areas (Effenberg et al., 2001).

In thin-film (thicknesses from a few *nm* to tens of μm deposited on an underlying substrate), gas flow sputtering using hollow cathode technique is proved to be effective for preparation ceramic-matrix nanocomposites films. It is a vacuum-based deposition technique and is related to high deposition rates and the growth of nanoparticles in gas phase. Nanocomposite layers prepared using this technique from TiO_2 and Cu demonstrated high mechanical hardness, small friction coefficients and high corrosion resistance (Birkholz et al., 2004).

Metal-matrix nanocomposites

Metal-matrix nanocomposites can incorporate different types of dispersed materials such as boron nitride and carbon nitride nanoparticles (Bakshi et al., 2010) or metal oxides and nano-scale Al powder hybrid sol–gel with a silica base to form a superthermite "energetic" nanocomposite (Gash, 2008; Ryan et al., 2008). Carbon nanotube has also been extensively studied in metal-matrix nanocomposites (Bakshi et al., 2010), designed to utilise the high tensile strength and electrical conductivity of carbon nanotubes. Homogeneous dispersion of carbon nanotubes into metallic matrix and formation of strong interfacial adhesion between the matrix and the nanotubes proved to be vital.

Polymer-matrix nanocomposites

Polymermatrix nanocomposites can incorporate a wide range of second materials including ceramics, clays, or carbon nanotubes and nanoparticles (Mai & Yu, 2006; Pinnavaia & Beall, 2001) as well as inorganic nanowires and nanorods (Zeng et al., 2014).

Not only mechanical properties such as strength and stiffness (Rafiee et. al, 2009) but also time-dependent properties such as crystallisation behaviour (Patil et al., 2010), flame retardancy (Morgan & Wilkie, 2007), biodegradability of the matrix (Manias, 2007) and biocompatibility for implants (Subbiah et al., 2004).

As particle size decrease, nano-fillers tend to form stronger agglomerates which must be disrupted to achieve homogeneous and stable dispersion within the matrix so as to utilise the

high aspect ratio and/or the high specific surface area of the fillers (Usuki et al., 1993). Dispersibility of nanoparticles is a complex matter and influenced by a many factors including inter-particle attraction and fusion, surface chemistry and treatment as well as processing conditions such as viscosity and intensity of shear mixing, (Song & Evans, 1993) etc.

2.10. PVDF-based nanocomposites

Considerable research has been published on PVDF-based composites. This section reviews literature in this area which is directly relevant to this work on electrospinning of PVDF/nanofiller composites membrane. Focus will be given to the three systems of filler in PVDF matrix: PVDF/cellulose, PVDF/ceramics and PVDF/carbon.

2.10.1. PVDF/cellulose systems

Cellulose is from natural and renewable resources and thus potentially more sustainable and cost effective. It can be produced as nano-fibrils (Abraham et al., 2011; Wu et al., 2013; Bendi & Imae, 2013; Cai & Yang, 2011; Khalil et al., 2012; Wang et al., 2012), and has been extensively studied in many polymer systems (e.g. PLA/nanocrystalline cellulose system (Pirani et al., 2013), polyvinyl alcohol/cellulose nanocrystals/silver nanoparticles system (Xu et al., 2013),poly(3-hydroxybutyrate-co-4-hydroxybutyrate/surface modified nanocrystalline cellulose system (Zhang et al., 2013), cellulose/polyvinyl alcohol system (Abdulkhani et al., 2013), polylactide/cellulose nanowhiskers (Lee et al., 2013), bacterial cellulose nanofibrils/poly(3-hydroxybutyrate) system (Cai & Yang, 2010), PMMA/Cellulose system (Banerjee et al., 2013)) for enhancement of mechanical properties (Bentchikou et al., ?(http://congress.cimne.upc.es/rilem04/admin/Files/FilePaper/p223.pdf); Bermany et al., 2013; Orts et al., 2005; Sawai et al., 2011), thermal properties (Banerjee et al., 2013; Low & Alamri, 2012; Sawai et al., 2011), crystallinity (Meyabadi & Tayebeh, 2013; Song et al., 2013), electrical properties (Kalidindi et al., 2010) including piezoelectric properties (Kalidindi et al., 2010). Inclusion of cellulose is therefore expected to reinforce the PVDF electrospun fibres and contribute to mechanical and crystalline properties of the membrane.

Meanwhile, inclusion of nanoparticles such as nanoclay, inorganic salts, carbon nanotubes (CNTs), graphene oxide (GO), and other polymers in PVDF matrix can effectively affect polymorphs and crystallisation of PVDF (He et al., 2013).

Cellulose is a highly crystallised natural carbohydrate polymer comprising repeated anhydroglucose units linked by b-1,4-glycosidic bonds (C–O–C) (Klemm et al., 1999), it is one of the most abundant natural macromolecule existing in various forestry resources such as wood, and straw of agricultural plants or synthesised by biomass such as tunicates and bacteria (Khalil et al., 2012). Cellulose has a series of advantages as a renewable biomass material including abundance (or low cost), biodegradability, recyclability, friendly to environment (i.e. non-polluting) and renewability (Hua et al., 2009), making it an inexpensive filler system particularly in polymers, friendly and a potential replacement for conventional fillers/reinforcement materials (Klemm et al., 2005).

Inclusion of cellulose in polymers matrix is of great interest in the development of nanocomposites as cellulose nanocomposites showed outstanding properties (Moon et al., 2011). In addition, it can be incorporated into bio-based polymers or bioplastics to produce biocomposites or biodegradable composites

Depending on their dimension, cellulose filler can be categorised into micro- and nano-scale celluloses. Microcrystalline cellulose (MCC) are single or of cellulose fibre bundle within particle size range of 20–80 μm and can be produced by diluted acid hydrolysis (Bondeson et al., 2006). MCC is of low-cost and has large specific surface area, high reactivity, and biodegradability and therefore has been widely used in medicine, food, and cosmetics (Bai & Li, 2009).

The nano-scale cellulose can be further categorised into or nanoparticles known as nanocrystalline cellulose (NCC -needle-like whiskers) and nanofibrillar cellulose (NFC - high aspect ratio nanofibrils) (Khalil et al., 2012; Samir et al., 2005). NCC and NFC are normally produced by size reduction or deconstruction of cellulose using hydrolysis and ultrasonication (Ranby, 1951; Yousefi et al., 2013).

The attractive properties including high tensile strength (Eichhorn & Davies, 2006), high elastic modulus (Rusli & Eichhorn, 2008; Šturcová et al., 2005), low thermal expansion coefficient (Nishino, 2004) and specific optical properties such as birefringence (Hermans, 1963; Marchessault et al., 1959; Revol et al., 1992), enable NCC to find applications in paints, security papers, foods, emulsions/dispersions, hygiene/absorbent, packaging, pharmaceutical and nanocomposites (Eichhorn, 2011; Habibi et al., 2010).

Cellulose had been included in polymers to form polymer/cellulose composites to obtain enhanced properties.

Cellulose fibres has been used in PMMA/cellulose composites to enhance tensile, moisture uptake and thermal properties (Banerjee et al., 2014), in starch/cellulose films to enhance mechanical and moisture barrier properties (Müller et al., 2009); Bacterial cellulose (BC) has been used in poly(3-hydroxybutyrate), PHB, to obtain PHB/BC nanocomposite with improved biocompatibility, biodegradability and mechanical properties (Barud et al., 2011). Fibrillated 2,2,6,6-tetramethylpiperidine-1-oxyl radical-mediated oxidation (TEMPO) oxidized cellulose was included in hydroxypropylcellulose matrix to form a bio-based nanocomposite (Rattaz et al., 2011).

Nanofibrillar cellulose (NFC) has been incorporated in hydroxypropyl cellulose (HPC) (Zimmermann et al., 2010) and in polymer gels to enhance mechanical properties (Orts et al., 2005).

Only very limited attempts have been made to use cellulose nanowhiskers (NCC) in PVDF (Rajesh et al., 2014) to induce β-phase formation, or in PVDF co-polymers (e.g. poly(vinylidenefluoride-hexafluoropropylene)) (Lalia et al., 2014) for electrospinning membranes used in lithium-ion batteries.

2.10.2. Polymer/carbon systems

Carbon based fillers/reinforcement used in polymers include conventional carbon fibre and carbon black and carbon nanofillers such as graphene (or graphene derived e.g. graphene oxide), carbon nano-tubes, (CNT) and carbon nanofiber. The nano-carbon fillers become increasingly attractive due to their low density and superior functional (e.g. thermal and

electrical conductivities) and specific mechanical properties (Kuilla et al., 2010; Potts et al., 2011; Ramanathan et al., 2008).

Numerous polymer/carbon nanocomposite systems have been studied (e.g. Gojny et al., 2003; Grunlan et al., 2004; Maksimenko et al., 2007, etc.). Performance enhancement of the nanocomposites depends mainly on the types of matrix and filler (Park et al., 2006; Yuen et al., 2007), concentration, morphology and dispersion of the carbon nano-fillers and the matrix-filler interaction (Al-Saleh & Sundararaj, 2009; Panwar et al., 2009). This section will focus PVDF/carbon nanocomposites incorporating two types of carbon nano-fillers: carbon nano-tubes (CNT) and graphene oxide (GO).

2.10.2.1. PVDF/CNT systems

CNTs can be considered as a result of folding graphite layers into carbon cylinders and may be of a single-walled (SWCNTs) or multi-walled carbon nanotubes (MWCNTs). CNTs can be metallic or semiconducting depending on folding angle and diameter (Martel et al., 1998). Owning to their low density, high electrical/thermal conductivity and specific strength and modulus, CNTs are the most widely used nanofillers to produce conducting polymer nanocomposites with excellent electromagnetic (Pande et al., 2009) and optoelectronic properties (Choi et al., 1999) and/or mechanical properties (Qian et al., 2000). Enhancement in mechanical strength and electrical conductivity require good control of alignment of CNTs interfacial bonding with the polymer matrix (Breuer & Sundararaj, 2004; Giordani et al., 2006; Mathur et al., 2008). At present, CNTs are relatively high in costs which to some extent limit their volume industrial applications.

Using different processing methods, different types of CNTs have been studied in PVDF/CNT nanocomposites with attempt to promote crystallisation in PVDF and enhance piezoelectric properties and/or increase mechanical properties. The outcomes are summarised in Table 2.2. While there is considerable discrepancies in their effect on total crystallinity of PVDF matrix, there appear to be a general agreement that CNTs promote β phase formation regardless the processing methods.

2.10.2.2. PVDF/GO systems

Graphene Oxide (GO) is of much lower cost than CNTs. It may consists of exfoliated monolayers or layered stacks depending on extent of dispersion. It has have very high aspect ratios with length ranging from 400 to 500 *nm* and thicknesses down to about 1 *nm*.
GO has many advantages including 2D-lamellar structure, high specific surface area, good dispersibility in water and various organic solvents (Dreyer et al., 2010) and possession of various reactive groups (Paredes et al., 2008) making it a cost-effective nanofiller for polymer nanocomposites. Incorporation of GO can enhance mechanical and functional properties including tensile strength (Hua et al., 2007; Liu et al., 2011), elastic modulus, thermal stability, gas barrier, and electrical conductivity of polymer nanocomposite.

Table 2.2: Summary of influences of CNTs on properties PVDF/CNT nanocomposites

Type of CNT	Processing methods	Optimal concentration of CNT*	Impact on crystalline or piezoelectric properties	References
MWCNT	Solution casting (with subsequent drawing and poling)	0.05 wt%	More β phase was produced with CNT addition and achieved highest voltage output at 0.05 wt% CNT	Levi et al., 2004
MWCNT	Immersion precipitation	-	Crystallisation of β phase was enhanced using MWCNTs. Crystal size of PVDF was reduced while crystallinity and crystallisation temperature were increased	Tao et al., 2013
Unzipped multi-walled CNTs (µCNTs)	Solution coagulation	0.3 wt%	µCNTs promoted PVDF crystallisation and facilitated β phase formation; decreased α phase content, leading to a maximum d_{33} of 38.4 *pC/N*	He et al., 2013
MWCNT	Solution blending	-	MWCNTs increased on-set of crystallisation temperature & reduced	Li et al., 2013

			crystallisation rates of PVDF. Nucleation and growth rate of spherolite decreased with increase of MWCNTs wt%.	
SWCNTs & MWCNTs	Electrospinning (using modified rotating disk collector)	0.01wt% (SWCNT)	SWCNTs and extensional force can work synergistically to induce highly oriented β phase; MWCNTs could not be well aligned along fibre axis, which causes poor crystal orientation.	Yee et al., 2012
MWCNT and vapour grown carbon fibre (VGCF)	solution casting stretched uniaxially and poled in silicon oil	0.05 wt%	Fillers did not significantly affect crystallinity of β-phase but play a role in β-phase nucleation during stretching.	Wu et al., 2013
CNTs	near-field electrospinning (NFES) on a rotating glass tube collector	0.03 wt%	CNTs interact with PVDF leading to apparent β-phase increase. Maximum voltage and current output were 43.6 mVp-p and 240 nIp-p at 15 Hz, respectively.	Liu et al., 2013
MWCNT	shear flow	above 2 vol%,	While increasing MWCNT wt% reduced PVDF crystal size, crystallisation rate increased together with an increase in β phase crystallisation. Crystallisation temperature increased due to heterogeneous nucleation of PVDF. Inclusion of MWCNTs and shearing possibly enhanced β-phase formation.	Mago et al., 2008
MWCNT	solution	-	MWCNT promoted β	Fernando et

compound		**phase formation in solution compounded PVDF films. Amino-double-walled CNT can affect β to α polymorphic balance.**	**al., 2004**

*wet basis

With regards to PVDF/GO nanocomposites prepared using different processing methods, the influence of different types of GOs on crystalline and/or piezoelectric properties are summarised in Table 2.3. GO appeared to be a remarkable nucleation agent and induced β- or γ- transformation from the non-piezoelectric α-phase, particularly in that prepared by sol-gel method. However, piezoelectric information was scares and no attempt was made to correlate to the crystallinity data.

2.10.3. PVDF/ceramic systems

A large number of piezoelectric (e.g. lead zirconate titanate, PZT, barium titanate, BT, strontium titanate ST, quartz, and zinc oxide, ZnO) and non-piezoelectric ceramic fillers have been studied in PVDF/ceramic composites. This section will review the former types focusing on barium titanate (BT) and zinc oxide (ZnO) and the latter focusing on nanoclays.

2.10.3.1. PVDF/BT and PVDF/ZnO systems

Barium titanate (BT) and zinc oxide (ZnO) are piezoelectric and/or ferroelectric ceramics (Dang et al., 2005; Hong et al., 2005) and many efforts have been made to develop polymeric matrix composites which combine good flexibility and ease of processing of polymers with good piezoelectric properties of the ceramics (Dang et al., 2002; Gregorio Jr et al., 1996).

Table 2.3: Summary of influences of GOs on properties PVDF/GO nanocomposites

Type of Graphene	Processing method	Optimal concentration of GO (Wet basis)	Impact on crystalline or piezoelectric properties	References
GO	**Sol-gel method & spin-coating**	**1 wt%**	**Significantly enhanced β-phase crystallisation and claimed a complete**	**Hu et al., 2014**

			transformation to β at 1 wt% GO	
Graphite nanosheets (GNs)	**Solution casting**	**2.5 wt%**	**Both conductivity and dielectric constant are significantly enhanced near percolation threshold, and high dielectric constant of 173 C/(Vm) is obtained at 1 kHz.**	**Li, et al., 2010**
Graphene	**Non-solvent vapour adsorption, ageing, dipping in fresh water & freeze-drying**	**1 wt%**	**Clear promotion of PVDF crystallisation; changes PVDF from α phase to γ phase**	**Li et al., 2013**
Functionalised graphene oxide (FGO)	**Spin cast on Si-wafer**	**-**	**Restrained growth of α-phase and facilitated formation of β- and γ-phases**	**Thangavel et al., 2014**

BT was chosen to be used as a filler to form an electrospun PVDF composites for following reasons:

1) A combined piezoelectricity from both PVDF and BT can possibly take place in the composites, whose piezoelectric performance will then be enhanced;
2) BT may play a role of nucleating agent during electrospinning process, which will promote crystallisation of PVDF which is a vital factor for piezoelectric performance of the composites;
3) BT may be able to increase electric conductivity of sample during electrospinning, which can possibly lead to facilitation of β crystalline phase (piezoelectric phase) formation and crystal orientation enhancement of the β phase.

ZnO is widely used in liquid crystal displays, window coatings, gas sensors, optoelectronic devices, solar cells, surface acoustic wave devices (SAW) and ultrasonic transducers because

of its unique combination of electrical (Schropp & Madan, 1989), optical (Purica et al., 2000), and piezoelectric properties (Emanetoglu et al., 1999).

PVDF/BT and PVDF/ZnO nanocomposites prepared using different processing methods are listed in Table 2.4 and Table 2.5, in which the influence of different types of BTs or ZnO on crystalline and/or piezoelectric properties of the nanocomposites are summarised.

Table 2.4: Summary of influences of BTs on properties PVDF/BT nanocomposites

Type of BT	Processing method	Optimal concentration of BT	Impact on crystalline or piezoelectric properties	References
Surface treated particles	Solution casting	20 vol %	Improved dielectric permittivity, reduced loss tangent, decreased crystallite size, increased crystallinity and shifted crystallisation temperature of PVDF enhanced dielectric displacement, and increased energy density.	Yu et al., 2013
Self-prepared	Solution casting	-	Dielectric constant =7 C/(Vm) dissipation factors = 0.03	Upadhyay & Deshmukh, 2013
Sol–gel & electrospinning	Two-step electrospinning process	30 wt % of total PVDF	Co-contribution to piezoelectricity from BT and PVDF confirmed (d_{33} = 50 *pm/V*)	Baji et al., 2011
mean size of 200 nm	High-energy ball cryomilling	≤ 5 wt%	β phase increased while α- and γ phase reduced after milling.	Olmos et al., 2013

			Lowered crystallisation rate	
Prepared with metallic barium & tetraethyl Orthotitanate	Spin-coating	30 vol %	Dielectric constant of composite increased with BT particle size and vol % and peaked to 31.8 V/m & capacitance density of 0.63 nF/mm^2 at a BT size of 27.3 nm.	Jung et al., 2009
Powder	Solution casting	2 wt%	Activated BT facilitate crystallisation of β-phase while non-activated BT facilitate crystallisation of α-phase	Chanmal & Jog, 2008
Prepare by microwave assisted hydrothermal method	Spin-coating &electrospinning	Weight ratio BT : PVDF = 1:10	β phase fraction in PVDF was increased	Corral-Flores & Bueno-Baqués, 2011
Powder	Mixing, fusing & pressing	up to 30 wt%	PVDF remained α-phase regardless of BT content; Hindrance to PVDF crystallisation growth with BT content increasing; PVDF crystallisation prohibited by BT; Melting temperature of composite & heat of fusion of PVDF decreased with increased BT content	Mao et al., 2010
Surface functionalised with dopamine	Refluxing	50 wt%	Dielectric constant of composite enhanced to 56.8 V/m at 103 *Hz*	KumaráThakur et al., 2011
Particle sizes 25 -	Two-step mixing	80 wt% (on	Dielectric constant of	Fu et al., 2015

500 *nm* by a solvothermal method		**total solid weight)**	**composite remained constant as BT was >250 *nm* while it increases with decreasing particle sizes and peaked at BT particle size 80–100 *nm***	
Nanoparticles	**Electrospinning**	**5 wt%**	**Increased β phase fraction**	**Song et al., 2012**

Table 2.5: Summary of influences of ZnO on properties PVDF/ZnO nanocomposites

Type of ZnO	Processing method	Optimal concentration	Impact on crystalline or piezoelectric properties	References
nanoparticles (>100 *nm*)	**Spray coating**	**-**	**PVDF crystallised predominantly in β-phase without ZnO**	**Mohamed et al., 2014**
Self-prepared	**Dip-coating**	**-**	**Reduces β phase content and PVDF exists predominantly in α phase**	**Lee et al., 2012**

2.10.3.2. PVDF/Nanoclay systems

Nanoclay have been widely utilised to enhance thermal and mechanical properties of polymeric nanocomposite resulting good dispersibility and processability. They has a high aspect ratio and is easily obtainable and relatively cheap (Tjong & Jiang, 1999). Nanoclay also shows good flame retardant property and nontoxicity and gas barrier properties, making it suitable for high-temperature-resistant and food packaging materials (Chen et al., 2013; Gabr et al., 2013; Gilman, 1999).

Filler impacts of different types of nanoclay on crystalline and mechanical properties of PVDF by using different processing method are summarised in Table 2.6:

Table 2.6: Summary of influences of nano-clays on properties PVDF/nanoclay nanocomposites

Type of nanoclay	Processing method	Optimal concentration of nanoclay	Impact on crystalline or piezoelectric properties	References
Organically modified Lucentite	Electrospinning	1.5 wt%	Facilitated an α to β crystalline phase transformation	Yoon & Kelarakis, 2014
Lucentite™ SWN and STN	Electrospinning	1.0% for SWN and 0.2% for STN	Both increased β and γ phase while decreasing α phase	Yu & Cebe, 2009
Cloisite 20A and 30B	Cast extrusion	3%	Produced PVDF films with dominant β phase crystalline structure	Sadeghi & Ajji, 2009
Cloisite 30B	Melt mixing	7%	Promoted a α to β phase transition & β phase content increased with nanoclay content	Rahmani et al., 2014
Cloisite 20A	Electrospinning & solvent casting	3%	Nanoclay and electrospinning process facilitate formation of β phase	Neppalli et al., 2013

2.11. Gaps of knowledge and needs of this work

Through reviewing of literatures, gaps of knowledge and needs of this work were identified. There are three major gaps in knowledge:

1) Lack of direct correlation of change in volume faction of β crystalline PVDF with piezoelectric performance (d_{33}) of electrospun PVDF composites;
2) Lack of comparison for electrospun PVDF composites containing different fillers (different composite systems);
3) Influence of various processing method on PVDF composite piezoelectric properties is unclear.

Therefore this work:

a) Use a systematic approach and three systems: PVDF/inorganic fillers (carbon nanotube and graphene oxide), PVDF/ceramics (including piezoelectric and non-piezoelectric ones) and PVDF/cellulose, to evaluate effects of filler type and loading on composite properties;
b) Conduct a series of characterisations for the composite to correlate volume faction of β crystalline PVDF to piezoelectric performance (d_{33}) of the composites;
c) Use a single processing method-electrospinning (which is able to produce flexible piezoelectric membrane with facilitation of β phase formation) for all systems to eliminate effect of processing method while use film casting for comparison with electrospinning.

Chapter 3. Experimental Detail

3.1 Materials

All materials, unless specified, were supplied by Sigma-Aldrich.

3.1.1. The common polymers, solvents and additives used in all suspension systems

Morphology of the as-received polyvinylidene fluoride, PVDF, powder is shown in Figure 3.1 and the technical data are shown in Table 3.1.

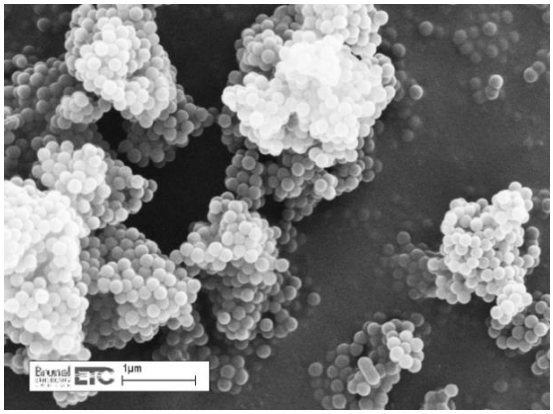

Figure 3.1: SEM pictures of the as-received PVDF powder showing nano-particles in agglomerates

Table 3.1 Data sheet of the as-received polyvinylidene fluoride (PVDF) powder

Vapour pressure	**15 *mm* Hg (32 °*C*)**
Molecular weight average M_w	**~534,000 by GPC**
Glass transition temperatures T_g	**−38 °*C***
Melting transition temperatures T_m	**171 °*C***
Density (at 25 °*C*)	**1.74 *g/ml***
Loss on drying	**≤ 2.00 %**

Polyethylene glycol (PEG) in form of a powder, was used as dispersion stabiliser for some electrospinning suspensions. The solvent used were N,N-Dimethylacetamide (DMAc), N,N-Dimethylformamide (DMF) and a laboratory reagent grade acetone.

3.1.2. The ceramic fillers

Technical data of the as-received ceramic fillers (two piezoelectric ceramic powders: barium titanate (BT) and zinc oxide (ZnO) and two non-piezoelectric nano-clays) are summarised in Table 3.2a and 3.2b and morphologies of them are shown in Figure 3.2.

Table 3.2a Technical data of the barium titanate (BT).

Form	**nanopowder (cubic crystalline)**
Assay	**≥99% trace metals basis**
Dielectric constant	**150**
Particle size	**<100 *nm* (BET)**
Density (at 25 °*C*)	**6.08 *g/ml***

Table 3.2b Technical data of the zinc oxide (ZnO).

Grade	**ACS reagent (puriss. p.a.)**
Assay	**≥99.0% (KT)**
Impurities	**≤0.0005% total nitrogen (N)**
Anion traces	**Chloride (Cl-): ≤10 *mg/kg***
Density (at 25 °*C*)	**1.74 *g/ml***
Loss on drying	**≤ 2.00 %**

Information of two non-piezoelectric nanoclays: halloysite and bentonite are summarised in Table 3.2c and 3.2.d and shown in Figure 3.2d and 3.2e.

Table 3.2c Technical data of the halloysite nanoclay

Form	**Nanopowder**
Diameter × L	**30-70 *nm* × 1-3 *μm*, nanotube**
Refractive index	**n20/D 1.54**
Surface area	**64 m^2/g**
Capacity	**8.0 m_{eq}/g cation exch. cap.**
Density	**2.53 *g/ml* (true specific gravity)**

Table 3.2d Technical data of the bentonite nanoclay

Form	**Powder**
Loss on Drying	**<18%**
Average Particle Size	**<25 μm**
Bulk Density	**600 - 1100 kg/m^3**

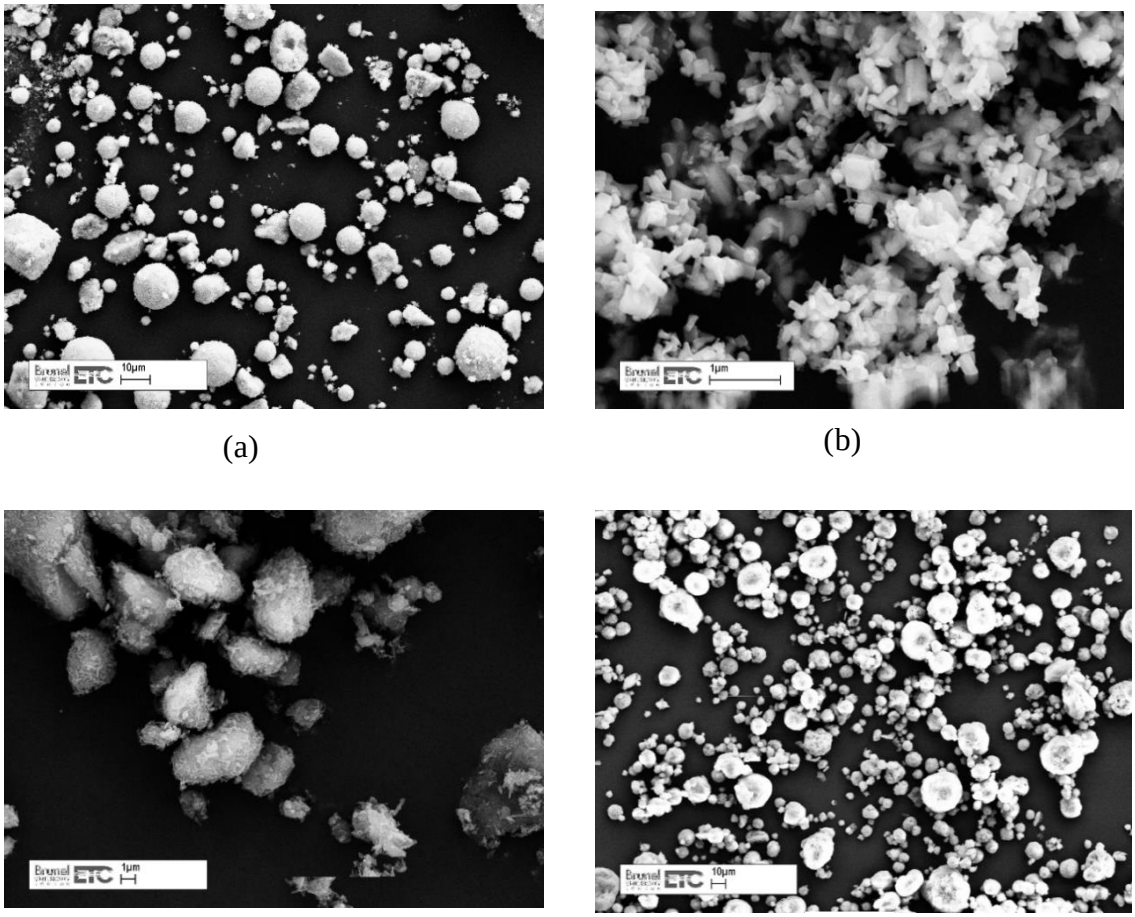

(a) (b)

(c) (d)

Figure 3.2: SEM images of the ceramic powders showing morphologies of particles and/or agglomeration: a) BT; b) ZnO; c) halloysite and d) bentonite.

3.1.3. Carbon-based fillers

Information of a multi-walled carbon nanotube (MWCNT) and graphene oxide (GO) are as in Table 3.3a and 3.3b and morphology of the MWCNT and GO is shown in Figure 3.3a and 3.3b.

Table 3.3a Information of the as-received MWCNT powder

Supplier	Cambridge Nanosystems, UK
Average Diameter	60 ±20 *nm*
Average Length	100 -3,000 *μm*
Purity	>95%
Catalyst Impurities:	<5%
Surface Area (BET)	>40 m^2/g

Table3.3b. Information of the as-received GO powder

Form	powder (15-20 sheets, 4-10% edge-oxidised)
Dispersibility	water and polar solvents dispersible
Bulk density	~1.8 g/cm^3

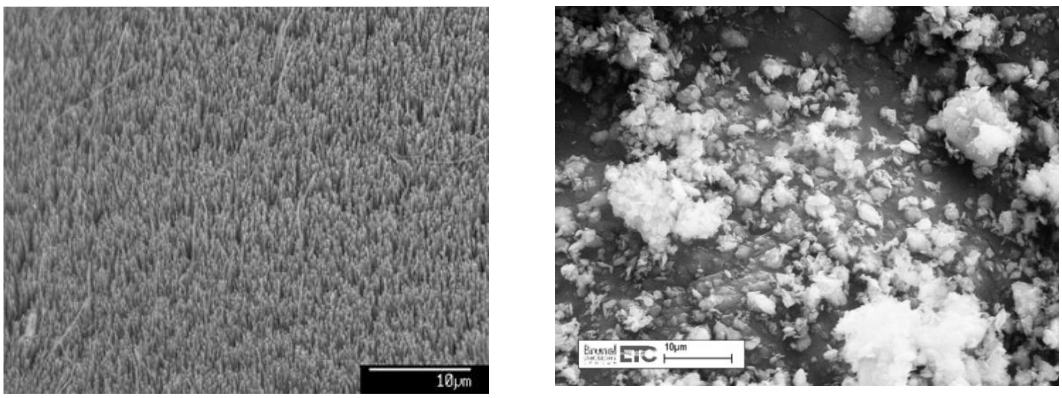

(a) **(b)**

Figure 3.3: SEM image of a) MWCNT fibres grown on a template and b) as-received GO powders showing status of agglomeration.

3.1.4. Cellulose fillers

Technical data of three as-received micro-crystalline cellulose, MCC, powders (MCC20, MCC50 and MCC90) are listed in Table 3.4 and Figure 3.4a-c show morphologies of them.

Table 3.4: Technical data of MCCs

ID	Particle Size *(μm)*	Crystallinity (%)	pH	Density *(g/ml)*
MCC20	**20**	**81.5**	**5-7**	**0.5**
MCC50	**50**	**78.0**	**-**	**0.6**
MCC90	**90**	**83.1**	**5-7**	**0.6**

Nanocrystalline cellulose (NCC) was produced from the three MCCs using acid hydrolysis method (Bondeson et al., 2006). A concentration of 10.2 *g* MCC per 100 *ml* of aqueous sulphuric acid solution (64 wt%). This was done in an ice bath with the acid being added drop by drop whilst stirring to avoid overheating until the concentration was reached. The mixture was then heated to 44 *°C* a hot plate while magnetically stirred for 10 minutes and then allowed extra 130 minutes for hydrolysis. The mixture was allowed to cool to room temperature before 200 *ml* of deionised (DI) water was added whilst stirring to dilute the acid. The suspension was then centrifuged at 12,000 RPM for 15 minute with the supernatant being decanted and replaced with DI water. The process was repeated 4 times. After 4th cycle, diluted sodium hydroxide (NaOH) solution (~10 wt%) was added whilst stirring to neutralise the suspension to pH7 monitored with a pH probe. The suspension was then rinsed by centrifuging and decanting processed described earlier to remove salt and ultrasonically treated at 120 *W* in a Grant ultrasonic bath for two 10-minute intervals and surrounded in ice to avoid overheating. The resulting concentrated NCC suspensions were thick white gel-like substances known as hydro-gels.

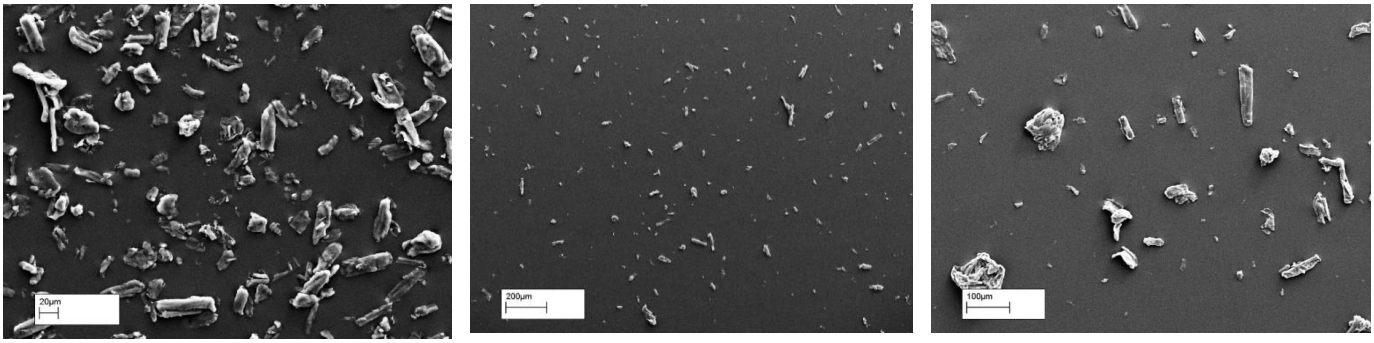

(a) (b) (c)

Figure 3.4: SEM microscopy showing size and morphologies of a) MCC20; b) MCC50 and c) MCC90, noting the different scales.

Cellulose contents of the NCCs produced were assessed using drying method. A small amount of each NCC was weighed before and after being dried for ~2 hours in a dish on a hot plate set at 120℃. The results are summarised in Table 3.5 and yield of NCCs produced was then calculated as shown in Table 3.6.

Table 3.5 Cellulose contents in the NCC gels from mass change during drying.

NCC ID*	Mass before drying (*g*)	Mass after drying (*g*)	Cellulose content (*wt%*)
NCC20	**0.038**	**0.005**	**13.3**
NCC50	**0.069**	**0.010**	**14.4**
NCC90	**0.142**	**0.025**	**17.7**

*Named after the MCC used.

Table 3.6. Yield of NCCs

NCC ID	NCC gels produced (*g*)	Cellulose content (*wt%*)	Cellulose produced (*g*)	MCC used (*g*)	Yield (*wt%*)
NCC20	**22.42**	**13.3**	**2.99**	**10.2**	**29.3**
NCC50	**26.63**	**14.4**	**3.84**	**10.2**	**37.7**
NCC90	**24.72**	**17.7**	**4.39**	**10.2**	**43.0**

The cellulose content was used in calculation of formulation described later. As the hydrolysis is essentially a size reduction process, the relatively higher yield for NCC from coarse MCC (e.g. comparing NCC20 with NCC90) is likely due to the loss of finest cellulose particles during decanting indicating relative average larger particle size in the resulted NCC. No attempt has been made to assess the particle size is the NCC gels using SEM due to technical difficulties and absence of alternative techniques (e.g. laser diffraction particle sizing for nanoparticles). Judges from the fact of gel formation of the resulted NCCs and observations in literature using the same hydrolysis method (Bondeson et al., 2006), size of cellulose crystalline particles in the NCC hydro-gels should have been significantly lower (by order of at least two orders of magnitude) than that of the MCCs as will be confirmed later in optical microscopy.

3.2. Preparation of suspensions

3.2.1. The PVDF/ceramic systems

The density of the as-received ceramic fillers are listed in Table 3.7 and used to calculate the *vol%* of fillers on dry basis.

Table 3.7: Density of the PVDF and ceramic fillers

Materials	Density (*g/ml*)
The as-received PVDF	**1.74**
BT	**6.08**
ZnO	**5.61**
halloysite	**2.53**
bentonite	**0.85**

3.2.1.1. The PVDF/BT system

Formulation of the PVDF/BT suspensions is shown in Table 3.8. Each batch of suspension prepared was approximately 5 *ml*.

Table 3.8: Formulation of the PVDF/BT suspensions

Sample ID	Wet basis (*wt%*)				Dry basis (*wt%/vol%*)	
	PVDF	Acetone	DMF	BT	PVDF	BT
BT-12.5%	9.5	51.9	33.9	4.8	66.7/87.5	33.3/12.5
BT-17.6%	9.3	50.7	33.1	7.0	57.2/82.3	57.2/17.6
BT-22.2%	9.1	49.5	32.3	9.1	50.1/77.6	49.9/22.2

The BT powder was dispersed into DMF to obtain a suspension which was magnetically stirred for 1 hour and then ultrasonically agitated for 10 minutes by using Branson Sonifier 250. PVDF solution (approximately 18 wt% in acetone) was then mixed with the BT/DMF suspension to obtain a final suspension for assessment of BT dispersion, sedimentation stability and electrospinning.

3.2.1.2. The PVDF/ZnO system

Formulation of the PVDF/ZnO suspensions is shown in Table 3.9 below. Each batch of suspension prepared was approximately 4.6 *ml*.

Table 3.9: Formulation of the PVDF/ZnO suspensions

Sample ID	wt% (wet basis)				vol% (dry basis)	
	PVDF	Acetone	DMF	ZnO	PVDF	ZnO
ZnO-13.4%	9.5	51.9	33.9	4.8	66.7/86.6	33.3/13.4
ZnO-23.6%	9.1	49.5	32.3	9.1	50.1/76.4	49.9/23.6
ZnO-31.7%	8.7	47.4	30.9	13.0	40.1/68.3	59.9/31.7

The same procedure as production of PVDF/BT suspensions for electrospinning was used to produce PVDF/ZnO suspensions.

3.2.1.3. The PVDF/nanoclay system

Formulation of the PVDF/nanoclay suspensions is shown in Table 3.10. Each batch of suspension prepared was approximately 5 *ml*.

Table 3.10: Formulation of the PVDF/nanoclay suspensions

Sample ID*	Wet basis (*wt%*)				Dry basis (*wt%/vol%*)	
	PVDF	Acetone	DMF	Nanoclay	PVDF	Nanoclay
Halloysite-1.4%	10.0	54.3	35.5	0.2	98.0/98.7	2.0/1.4
Halloysite-3.3%	10.0	54.2	35.4	0.5	95.3/96.7	4.8/3.3
Halloysite-6.4%	9.9	53.9	35.2	1.0	90.9/93.6	9.1/6.4
Halloysite-9.3%	9.9	53.6	35.0	1.5	87.0/90.7	13.0/9.3
Bentonite-2.0%	10.0	54.3	35.5	0.2	98.0/98.0	2.0/2.0
Bentonite-4.9%	10.0	54.2	35.4	0.5	95.3/95.1	4.8/4.9
Bentonite-9.3%	9.9	53.9	35.2	1.0	90.9/90.7	9.1/9.3
Bentonite-13.3%	9.9	53.6	35.0	1.5	87.0/86.7	13.0/13.3

*Based on *vol%* dry basis

A solvent mixture was prepared from DMF and acetone. The nanoclays (halloysite and bentonite) were dispersed in the DMF/acetone solvent mixture. Then the PVDF powders was dissolved into the nanoclays/DMF/acetone suspension and was stirred magnetically for 2 days at 40–50℃ (Yu & Cebe, 2009) and subsequently ultrasonically agitated for 30 minutes (Yoon & Kelarakis, 2014) sealed in glass containers to avoid solvent loss by using Grant ultrasonic bath.

3.2.2. The PVDF/carbon systems

3.2.2.1. The PVDF/CNT system

Formulation of the PVDF/CNT suspensions is shown in Table 3.11. Each batch of suspensions prepared was approximately 5 *ml*.

Table 3.11: Formulation of the PVDF/CNT suspensions

Sample ID*	Wet basis (*wt%*)					Dry basis (*wt%/vol%*)		
	PVDF	Acetone	DMF	CNT	PVP	PVDF	CNT	PVP
CNT-0.05%	9.5	51.9	33.9	0.01	4.75	66.7/58.0	0.07/0.05	33.3/42.0

CNT-0.15%	**9.5**	**51.8**	**33.9**	**0.03**	**4.75**	**66.6/57.9**	**0.21/0.15**	**33.2/41.9**
CNT-0.25%	**9.5**	**51.8**	**33.9**	**0.05**	**4.75**	**66.5/57.9**	**0.35/0.25**	**33.2/41.9**

*Based on *vol%* dry basis where density information used for calculation of *vol%* is given in Table 3.12.

Table 3.12: Theoretical density of the polymers, carbon fillers and solvents.

Materials	Density (*g/ml*)
acetone	**0.79**
DMF	**0.94**
PVDF	**1.74**
PVP	**1.20**
CNT	**2.10***
GO	**1.85**$^{\xi}$

* (Lehman et al., 2011); $^{\xi}$ (Hudson et al., 2014)

A co-solvent to dissolve PVDF was prepared from DMF and acetone. CNT was first dispersed in DMF/acetone by sonicating the suspension with an ultrasonic probe (Branson Sonifier 250, UK) for 10 minutes to facilitate uniform dispersion of MWCNT. PVDF and PVP were then dissolved in the CNT/DMF/acetone suspension and magnetically stirred for 20 minutes.

3.2.2.2. The PVDF/GO system

Formulation of the PVDF/GO suspensions is shown in Table 3.13. Each batch of suspensions prepared was approximately 5 *ml*. No PVP was used to stabilise these suspensions.

Table 3.13: Formulation of the PVDF/GO suspensions

Sample	Wet basis (*wt%)*				Dry basis (*wt%/vol%)*	
ID*	**PVDF**	**Acetone**	**DMF**	**GO**	**PVDF**	**GO**
GO-4.6%	**10.0**	**54.2**	**35.4**	**0.5**	**95.3/95.4**	**4.8/4.6**
GO-12.6%	**9.9**	**53.6**	**35.0**	**1.5**	**87.0/87.4**	**13.0/12.6**

GO-19.4%	**9.7**	**53.1**	**34.7**	**2.5**	**80.0/80.6**	**20.0/19.4**

***Based on *vol%* dry basis

The PVDF powder was dissolved in a mixed solvent of DMF and acetone. The GO powder was dispersed in DMF as described earlier. Then PVDF/DMF/acetone solution was mixed with the GO/DMF suspension and magnetically stirred for 20 minutes.

3.2.2. The PVDF/cellulose systems

3.2.2.1 The PVDF/MCC systems

Formulation of the PVDF/MCC suspensions is shown in Table 3.14 using the density data in Table 3.15. Each batch of suspension prepared was approximately 5 *ml*. For some suspensions, polyethylene glycol (PEG) was added as a suspension stabiliser (Hsu & Viscio, 1997; Ryan, 1980).

Table 3.14: Formulation of the PVDF/MCC suspensions

Sample ID*	Wet basis (*wt%*)					Dry basis (*wt%*/*vol%*)		
	PVDF	Acetone	DMAc	MCC	PEG	PVDF	MCC	PEG
MCC20-1.1%	**10.3**	**55.8**	**33.9**	**0.1**	**-**	**99.0/98.9**	**0.9/1.1**	**-**
MCC50-1.1%	**10.3**	**55.8**	**33.9**	**0.1**	**-**	**99.0/98.9**	**0.9/1.1**	**-**
MCC20-10.2%	**10.2**	**55.3**	**33.6**	**1.0**	**-**	**91.0/89.8**	**9.0/10.2**	**-**
MCC50-10.2%	**10.2**	**55.3**	**33.6**	**1.0**	**-**	**91.0/89.8**	**9.0/10.2**	**-**
MCC90-10.2%	**10.2**	**55.3**	**33.6**	**1.0**	**-**	**91.0/89.8**	**9.0/10.2**	**-**
MCC20-9.2% (PEG)	**10.1**	**54.7**	**33.2**	**1.0**	**1.0**	**83.4/79.4**	**8.3/9.2**	**8.30/11.4**
MCC50-9.2% (PEG)	**10.1**	**54.7**	**33.2**	**1.0**	**1.0**	**83.4/79.4**	**8.3/9.2**	**8.30/11.4**
MCC90-9.2% (PEG)	**10.1**	**54.7**	**33.2**	**1.0**	**1.0**	**83.4/79.4**	**8.3/9.2**	**8.30/11.4**
MCC20-37.3%	**9.8**	**53.1**	**32.2**	**5.0**	**-**	**66.1/62.7**	**33.9/37.3**	**-**
MCC50-37.3%	**9.8**	**53.1**	**32.2**	**5.0**	**-**	**66.1/62.7**	**33.9/37.3**	**-**
MCC90-37.3%	**9.8**	**53.1**	**32.2**	**5.0**	**-**	**66.1/62.7**	**33.9/37.3**	**-**

* Based on *vol%* dry basis

Table 3.15. Density data

Materials	Density (*g/ml*)
The as-received PVDF	1.7
PEG	1.1
MCCs and NCCs	1.5*

***** (Dufresne, 2013; Sun, 2008)

PVDF was first dissolved in acetone. Then DMAc was divided into two portions to produce PVDF/acetone/DMAc and MCC/DMAc suspensions respectively. If PEG was incorporated, DMAc was divided into three portions to produce PVDF/acetone/DMAc, MCC/DMAc and PEG/DMAc solutions/suspensions, respectively. The PVDF/acetone solution was ultrasonificated using a Grant ultrasonic bath till fully dissolved and was then added into the MCC/DMAc suspension drop-by-drop using a syringe while being magnetically stirred. If PEG was included, the PEG/DMAc solution was mixed with the MCC/DMAc suspension and then the PVDF/acetone solution. The suspensions were then assessed for dispersion of MCC particles, sedimentation stability before electrospinning.

3.2.2.2 The PVDF/NCC systems

Formulation of the PVDF/NCC suspensions is shown in Table 3.16. Each batch of suspension prepared was approximately 5 *ml*. The same procedure described earlier for

Table 3.16: Formulation of the PVDF/NCC suspensions

Sample ID*	Wet basis (*wt%*)					Dry basis (*wt%/vol%*)	
	PVDF	Acetone	DMAc	NCC$^{\xi}$	water$^{\xi}$	PVDF	NCC$^{\xi}$
NCC20-1.1%	10.2	55.4	33.6	0.1	0.6	99.0/98.9	1.0/1.1
NCC50-1.1%	10.2	55.5	33.7	0.1	0.6	99.0/98.9	1.0/1.1
NCC90-1.1%	10.2	55.5	33.7	0.1	0.5	99.0/98.9	1.0/1.1

NCC20-5.4%	**9.9**	**53.8**	**32.7**	**0.5**	**3.2**	**95.3/94.6**	**4.7/5.4**
NCC50-5.4%	**9.9**	**54.0**	**32.7**	**0.5**	**2.9**	**95.3/94.6**	**4.7/5.4**
NCC90-5.4%	**10.0**	**54.3**	**33.0**	**0.5**	**2.3**	**95.3/94.6**	**4.7/5.4**

* Based on *vol%* dry basis; $^{\xi}$NCC or water in the NCC hydro-gels.

PVDF/MCC suspensions was used to produce the PVDF/NCC suspensions. High concentration suspensions at 1 *wt%* of NCC was also prepared but as it tend out to be too viscous for subsequent electro-spinning process, no attempt was made in further assessment.

3.3. Assessments of dispersion and sedimentation stability of suspensions

Degree of dispersion (or destruction of agglomerates) of fillers was assessed using optical microscopy and transmission electron microscope (TEM). For optical microscopic observation, a drop of suspension was squeezed into a membrane between two thin cleaned glass slides and observed with transmission light on a Zeiss Axioskop 2 MAT Incident Light Microscope for relics of agglomerates. And for TEM observation, casting membranes made from the suspensions were embedded in epoxy resin and were then sectioned into layers with thickness of about 100 nm by using RMC Boeckeler PT-PC PowerTome Ultramicrotomes, the sectioned samples were then placed on copper grids for TEM observation by using a JEOL2100 field emission gun transmission electron microscope (FEG TEM).

Sedimentation test was conducted to check if the stability of the suspensions was sufficient during electrospinning process. The suspensions placed in test tubes were checked each hour after preparation for signs of sedimentation (or phase separation) up to 6-8 hours. Absence of obvious sedimentation over this length of time was considered sufficiently stable for the duration of electrospinning process which typically last for less than an hour.

3.4. Electrospinning of the suspensions

A purpose-built device shown in Figure 3.5 was used for electrospinning of the suspensions. It contains a Luer Lock syringe pump system fitted with a 14-gauge metal needle (1.70 mm

inside diameter and 2.11 mm outside diameter) for dosing/delivering of the suspensions at a flow rate of 1.0-1.6 *ml/h*. A voltage of 15-20 *kV* was applied between the tip of the needle and the flat-bed collecting plate separated by a distance of 150 *mm*. The collector plate was covered with an aluminium foil for easy separation of membranes from the plate. These electrospinning conditions are based on an experimental study for optimisation of parameters for electrospinning of neat PVDF solutions.

In addition, casting membranes made from neat PVDF solution and PVDF/filler suspensions were prepared: a small amount of the solution or the suspensions were poured into evaporating dish once they were prepared. Then the evaporating dishes were covered with a piece of filter paper, allowing evaporation of the solvents in a fume cupboard overnight to obtain dry films.

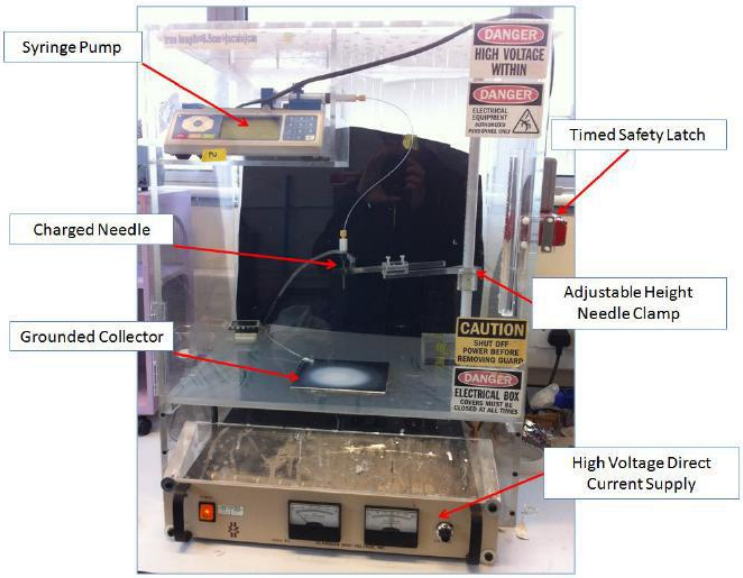

Figure 3.5: A purpose-built electrospinning device

3.5. Characterisations of the electrospun composite membranes

3.5.1. Microstructure of the electrospun composite membranes

The electrospun membranes were sputter-coated with gold and the morphology of them was analysed using a field emission scanning electron microscope (FESEM, Zeiss Supra 35VP) at 5 *kV*.

3.5.2. Crystalline properties

A differential scanning calorimeter (DSC, TA Instruments, QSeries 2000) was used to determine total crystallinity of PVDF in the nanocomposites. Temperature during test was ramped at 10 *°C/min* in a nitrogen atmosphere. Fourier transform infrared spectroscopy (FTIR) spectra of the nanocomposites were collected using a Perkin Elmer Spectrum One spectrometer. The as-received PVDF powder, the electrospun membranes and cast films were scanned from 4000 to 650 cm^{-1} in attenuated total reflectance mode (ATR) to obtain relative fraction of β phase F_β of the samples based on Equation 4.2.

3.5.3. Piezoelectric property

Piezoelectric charge constant d_{33} of electrospun nanocomposite membranes (with the aluminium foil on one side) was measured by using ZJ-6B d_{33}/d_{31} meter (Institute of Acoustics, Chinese Academy of Sciences). A 5×5 points matrix for the d_{33} measurements was used, as shown in Figure 3.6. This matrix was designed to assess the variation of d_{33} over an area of measurement and to confirm if it is affected by the distance from edge of the sample. As variation from the required horizontal positioning of samples may give rise in additional stress, the influence on d_{33} from such was assessed for a selection of samples bended to several different angles (12, 24, 36, 48, 60°) during the d_{33} measurements.

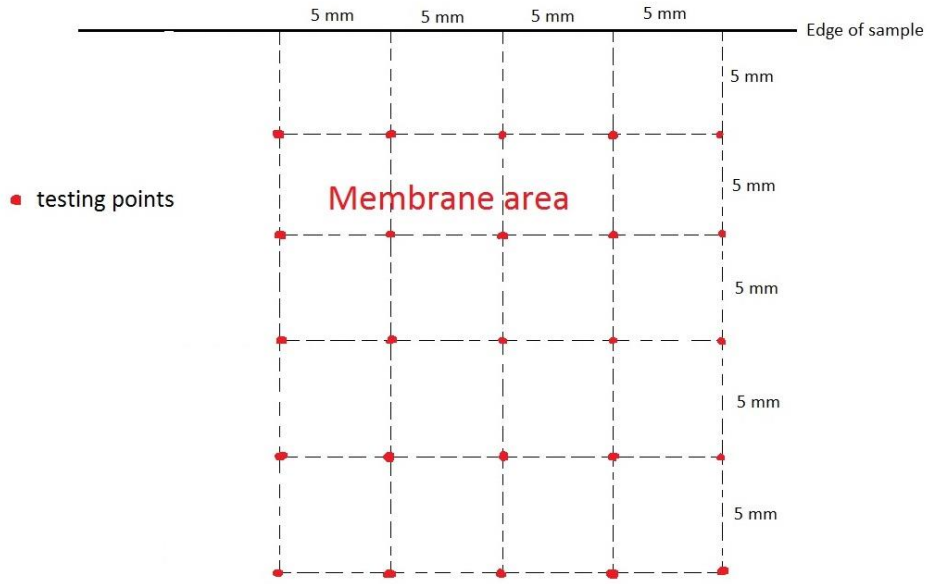

Figure 3.6: 5×5 points matrix for the d_{33} measurements

Chapter 4. Results and discussions – The PVDF/ceramic systems

4.1. Dispersion/sedimentation stability of the suspensions

Optical microscopy showing state of dispersion in the PVDF/BT suspensions are shown in Figure 1.1a & b. Find particles were well dispersed and there was only a low degree of agglomeration in BT-12.5% (Figure 4.1a).

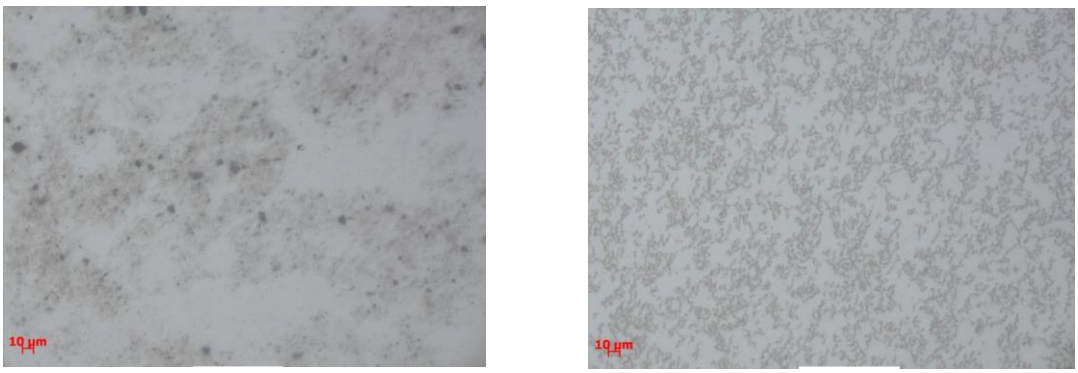

(a) (b)

Figure 4.1: Optical microscopy of the suspensions showing good dispersion: a) BT-12.5%; b) BT-22.2%.

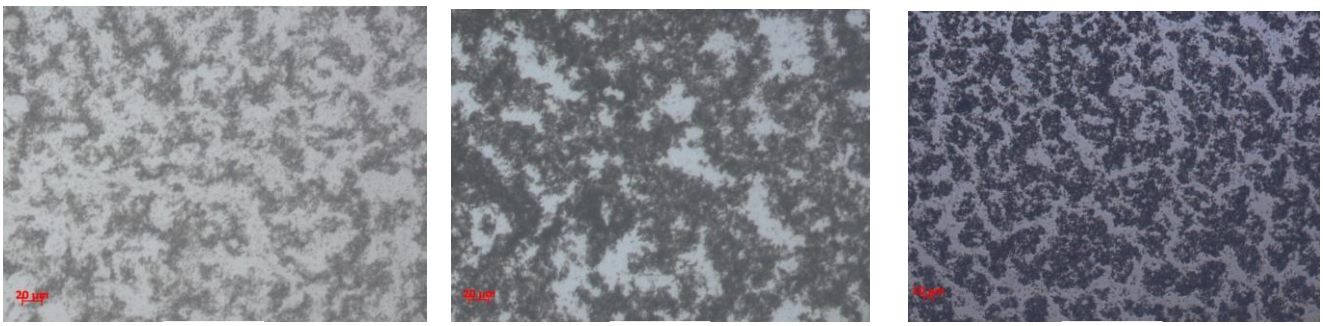

(a) (b) (c)

Figure 4.2. Optical microscopy of the suspensions showing different degrees of flocculation: a) ZnO-13.4%; b) ZnO-23.6%; and c) ZnO-31.7%.

Optical microscopy showing state of dispersion in the PVDF/ZnO suspensions are in Figure 4.2a-c. Different degrees of flocculation of particles could be observed in all suspensions, suggesting that the ultrasonication process was sufficient to break up the loosely bonded

particles (or clusters) as evidenced from that of the as-received powder but there is lack of inter-particle repulsion , indicating that a dispersant or stabiliser may need to be used to prevent their flocculation.

Optical microscopy showing state of dispersion in the PVDF/halloysite suspensions are shown in Figure 4.3a-d. Despite dispersion of fine particles or small clusters, there were clearly undispersed agglomerates in all suspensions.

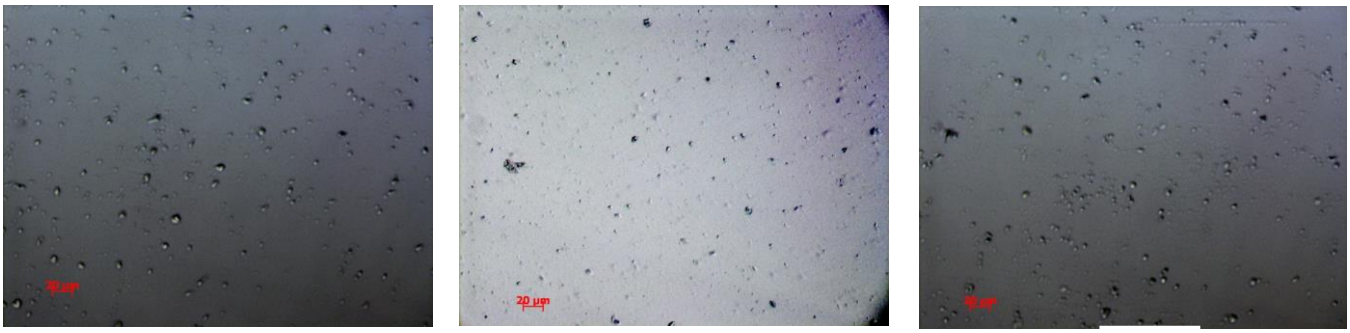

(a) (b) (c)

Figure 4.3. Optical microscopy of suspensions showing different degrees of agglomerate residues: a) Halloysite-1.4%; b) Halloysite-3.3% and c) Halloysite-9.3% suspension

Optical microscopy showing state of dispersion in the PVDF/bentonite suspensions are shown in Figure 4.4a & b. Similar state of dispersion can be observed as in the PVDF/halloysite suspensions.

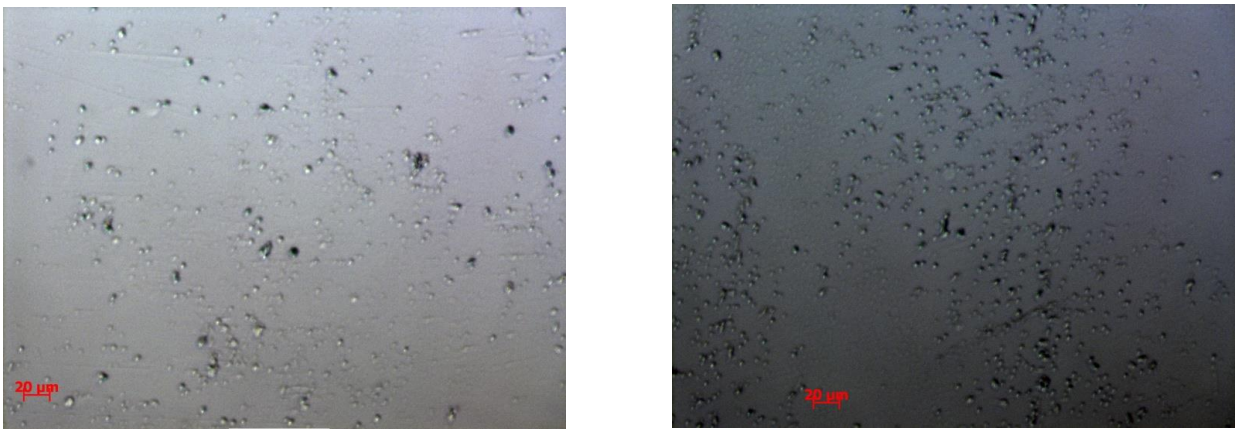

(a) (b)

Figure 4.4: Optical microscopy of suspensions showing un-dispersed agglomerates: a) Bentonite-2.0% and b) Bentonite-13.3%

Obvious sedimentation or phase separation was not observed for any of the suspensions over 6-8 hours after preparation, indicating that the suspensions were sufficiently stable for the duration of electrospinning process.

4.2. Dispersion of particles in the composites

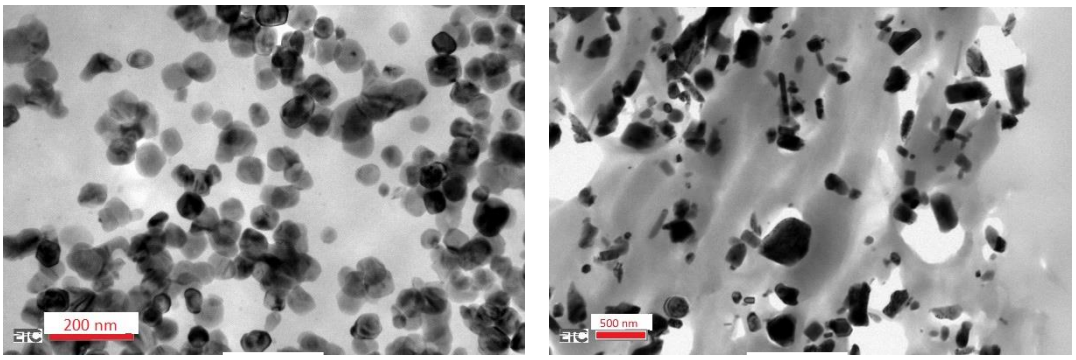

(a) (b)

Figure 4.5: TEM images of cast films made from a) BT-12.5% and b) ZnO-23.6% composites confirming well dispersed individual particles.

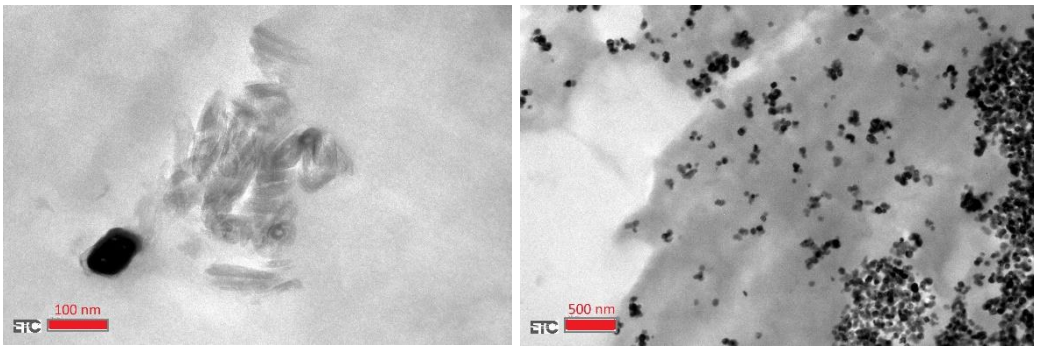

(a) (b)

Figure 4.6. TEM images of cast films made from: a) Halloysite-3.3% confirming intercalated halloysite clusters and b) both dispersed individual particles and residue agglomerates.

TEM images from a selective cast films are shown for BT-12.5% in Figure 4.5a and ZnO-23.6% in Figure 4.5b. They confirmed well separated particles in the composites for the two piezoelectric ceramics.

TEM images of the Halloysite-3.3% suspension (Figure 4.6a) shows layered structure of the halloysite in a small intercalated cluster while in Figure 4.6b, both individual bentonite particle and agglomerate can be observed.

4.3. Morphology of the electrospun membranes

Nanofibres of all the electrospun membranes have random orientations, and the nanofibres can be aligned by using a rotating drum (disk) collector (Wang et al., 2014; Yee et al., 2008).

Uniform and beadless fibres are desired for electrospun membranes, however during electrospinning sometimes some fibres are not produced and only beads are formed because of jet breaking up into droplets (Chanunpanich et al., 2008). Increase in surface tension of electrospinning suspension may be major cause of bead formation and uniformity loss on electrospun fibres (Ribeiro et al., 2010). Formation of beaded structure is also related to rapid increase of spinning current, which results in reduction of surface area (Subbiah et al., 2005).

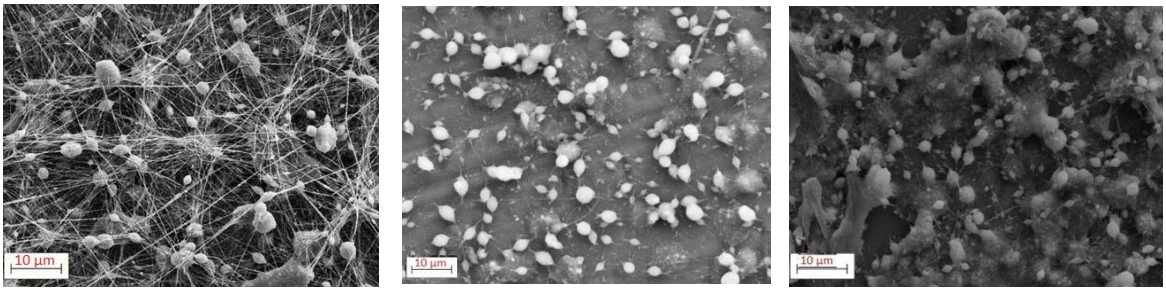

(a) (b) (c)

Figure 4.7: SEM microscopy of a) the BT-12.5% electrospun membranes showing considerable beads; b) the BT-17.6% and c) BT-22.2% composites showing domination of beads and lack of nanofibres.

For the PVDF/BT system, as shown in Figure 4.6 a-c, only BT-12.5% (Figure 4.6a) was spun into significant amount of nanofibres. Those of higher BT concentrations (Figure 4.6b and c) were dominated by a large amount of beads and very few fibres. At higher filler concentrations, the residue agglomerates may have contributed to more frequent jet breakage during the electrospinning process.

For the PVDF/ZnO system, as shown in Figure 4.7 a-c, the lower ZnO concentration suspensions produced relatively lower fibre contents (Figure 4.7a and 14.7b for ZnO-13.4% and ZnO-23.6%, respectively) while higher ZnO suspension ZnO-31.7% (Figure 4.7c) produced decent non-woven structure of fibre. Since the suspensions are flocculated as described previously, they behaved differently in comparison with the PVDF/BT system. The flocculation clearly did not seem to have negative impact on jet formation.

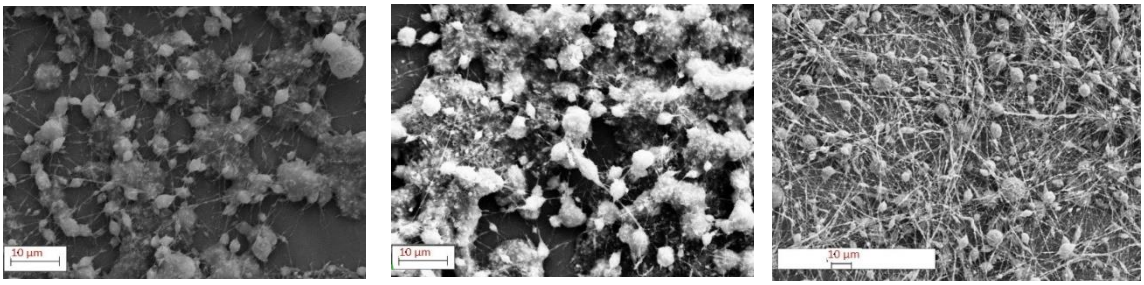

(a) (b) (c)

Figure 4.8. SEM microscopy of a) ZnO-13.4%; b) ZnO-23.6% and ZnO-31.7% electrospun membranes showing influence of ZnO loading on the structure.

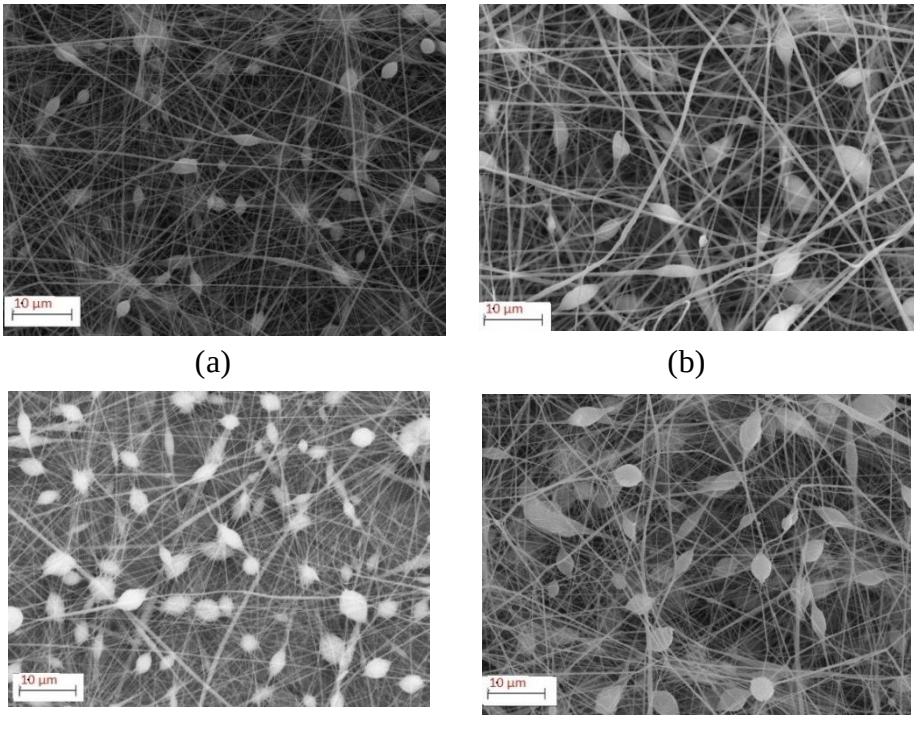

(a) (b)

(c) (d)

Figure 4.9: SEM microscopy of a) halloysite-1.4%; b) Halloysite-3.3%; c) Halloysite-6.4% and d) Halloysite-9.3% electrospun membranes.

For the PVDF/halloysite system, as shown in Figure 4.8a-d, good quality membranes with beads were achieved at all halloysite concentrations. The beads having a narrow size distribution can be attributed to the agglomerates in the suspensions.

For PVDF/bentonite system, as shown in Figure 4.9 a-d, good fibre architect structure for all levels of bentonite concentrations (Figure 4.9 a, c and d) except for Bentonite-4.9%; (Figure 4.9 b). Similar to that in the PVDF/halloysite system, beads formation could be attributed to the agglomerates.

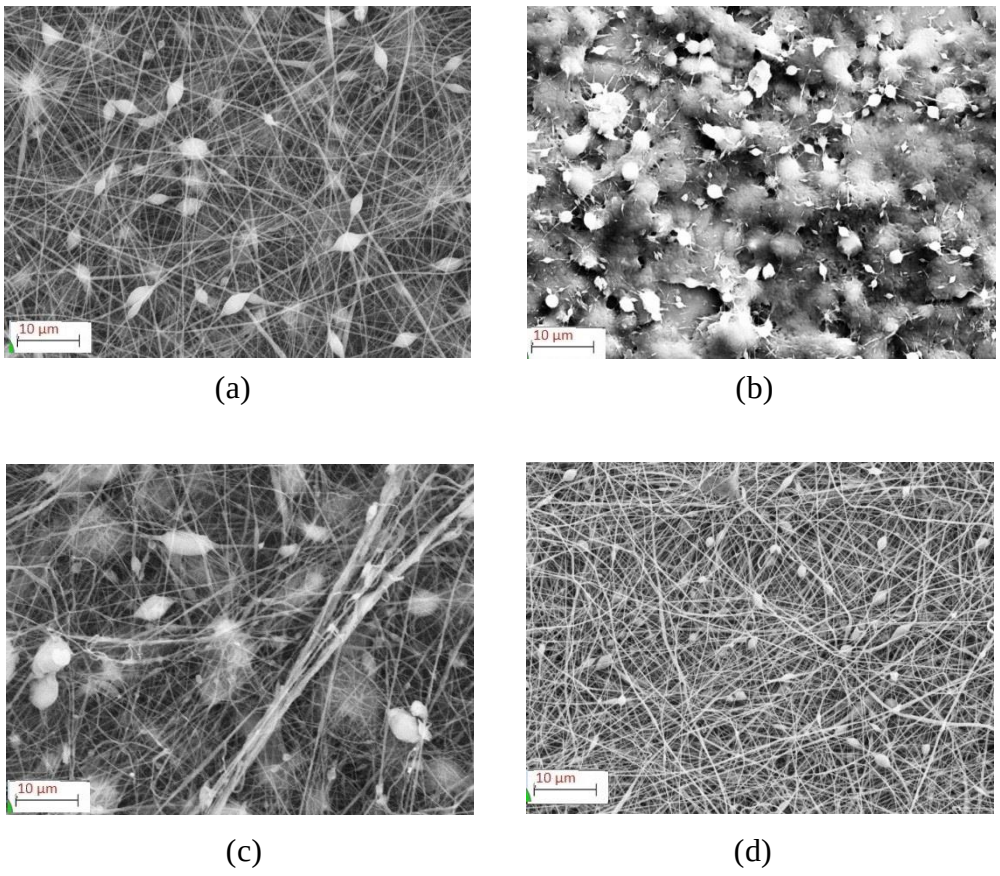

(a) (b)

(c) (d)

Figure 4.10: SEM microscopy of a) Bentonite-2.0%; b) Bentonite-4.9%; c) Bentonite-9.3% and d) Bentonite-13.3% electrospun membranes.

4.4. Crystalline properties

4.4.1. Total PVDF crystallinity analysis

PVDF total crystallinity is a measure of degree of crystallisation in PVDF. It refers to the sum of mass percentage of all types of crystalline phase in the PVDF matrix and can be obtained by using DSC method and calculated using Equation 1:

$$X_c = \Delta H_m / \Delta H_m^0 \times 100\% \qquad (4.1)$$

Where X_c is the degree of crystallinity in mass percentage, ΔH_m is heat of fusion (J/g) for the crystalline phases in PVDF and ΔH_m^0 is heat of fusion for an imaginary case of 100% crystallinity which was found to be 104.6 J/g from literature (Nakagawa & Ishida, 1973).

ΔH_m can be obtained from DSC which measures the heat of fusion (J/g) for the crystalline phases in the composite, $\Delta H_{m,s}$ ad thus need to be converted to ΔH_m using mass of the PVDF. This can be done using ω_P, $wt\%$ of PVDF in the composites on dry mass, which can be found in Table 5 using Equation 2.

$$\Delta H_m = \Delta H_{m,s} / \omega_p \qquad (4.2)$$

ΔH_m was calculated from the DSC curves using a TA Universal Analysis software. As it requires manual identification of the onset and finish points of the melting peaks from the DSC curves for automatic numeric integration, each value of ΔH_m was obtained as a mean of three repetitions of calculation to mitigate the human error in the manual inputs. Each DSC test is composed of four "cycles" (in sequence of: heating-cooling-heating-cooling) and curve of the third cycle (the second heating) was used to calculate ΔHm, since the first heating was used to eliminate thermal history of sample.

Table 4.1: $\Delta H_{m,s}$, ω_P and X_c of PVDF in the electrospun membranes and cast films

Sample ID	$\Delta H_{m,s}$ (J/g)	ω_P (%)	X_c of PVDF (%)
Neat PVDF (casting)	29.4	100.0	28.1
Neat PVDF	33.3	100.0	31.9
BT-12.5% (casting)	20.9	66.7	29.9
BT-12.5%	17.8	66.7	25.5
BT-17.6% (casting)	17.1	57.2	28.5
BT-17.6%	15.3	57.2	25.6
BT-22.2% (casting)	13.7	50.1	26.1
BT-22.2%	8.1	50.1	15.6
ZnO-13.4% (casting)	16.9	66.7	24.3
ZnO-13.4%	10.7	66.7	15.4
ZnO- 9 % (casting)	12.0	50.1	22.9
ZnO- 9 %	12.5	50.1	23.9
ZnO-31.7% (casting)	8.7	40.1	20.7
ZnO-31.7%	9.9	40.1	23.6
Halloysite-1.4% (casting)	29.8	98.0	29.0
Halloysite-1.4%	21.9	98.0	21.3
Halloysite-3.3% (casting)	26.5	95.3	26.6
Halloysite-3.3%	25.9	95.3	26.0
Halloysite-6.4% (casting)	29.9	90.9	31.4
Halloysite-6.4%	25.7	90.9	27.1
Halloysite-9.3% (casting)	25.0	87.0	27.5
Halloysite-9.3%	27.1	87.0	29.8
Bentonite-2.0% (casting)	27.6	98.0	26.9
Bentonite-2.0%	24.2	98.0	23.6
Bentonite-4.9% (casting)	25.5	95.3	25.6
Bentonite-4.9%	20.3	95.3	20.4
Bentonite-9.3% (casting)	27.8	90.9	29.2

Bentonite-9.3%	**21.8**	**90.9**	**22.9**
Bentonite-13.3% (casting)	**22.9**	**87.0**	**25.1**
Bentonite-13.3%	**20.9**	**87.0**	**23.0**

The PVDF total crystallinity in samples prepared by film casting and electrospinning are plotted in Figure 4.11.

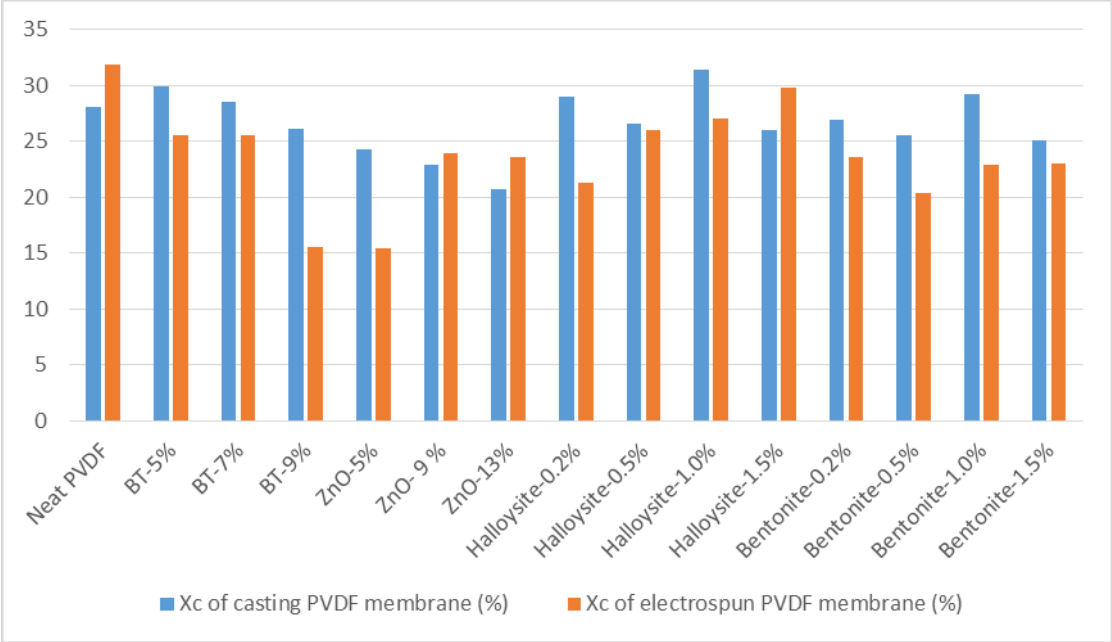

Figure 4.11: PVDF total crystallinity in the neat PVDF and PVDF/ceramic composites prepared by film casting and electrospinning.

PVDF total crystallinity is a measure of degree of crystallisation in PVDF. It varies with the raw material used, the compositions if combined with others and processing history. In comparison with 36.7% for the as-received PVDF powder, it reduced to 31.9% and 28.1% for the electrospun membrane and casting membrane, respectively. Ribeiro et al. (2010) argued that solidification of PVDF molecular chains under high elongation rate during electrospinning process might enhance development of PVDF crystallinity. And this seems to be the case when compare that of the electrospun membrane with the casting membrane, both from the neat PVDF solution (Table 4.1), but it is not supported when compare with that of the as-received powder. Subbiah et al. (2005) observed that electrospun Poly-L-lactide (PLLA) fibre have lower crystallinity than the as-received semicrystalline PLLA resins. This reduction of crystallinity was attributed to the high evaporation rate followed by rapid

solidification at final stages of electrospinning. In support of the observations, comparison of crystallinity of the casting membranes and electrospun membranes in Table 4.1 for the PVDF/ceramic composites also show that the PVDF total crystallinity for a majority of the electrospun membranes are relatively lower than that of the casting membranes or comparable, indicating that the membrane casting process provide more favourable crystallisation conditions in PVDF than that of the electrospinning process, due probably to the lower rates of solvent evaporation and solidification of PVDF in the casting process as the membranes have much higher specific surface area.

Looking into each electrospun composite system in more details in Table 4.1 and Figure 4.10 in comparison with the electrospun neat PVDF, the influence of different ceramic fillers (and their loading) on the total PVDF crystallinity (X_c) can be revealed. Overall, the inclusion of all types of ceramic fillers had resulted in a reduction in X_c compared with that of the neat PVDF. In terms of effect of loading on X_c, different trends are observed: X_c decreased with the BT loading in the PVDF/BT system but the opposite trend was noticed for the PVDF/ZnO and PVDF/halloysite systems while X_c was found to decrease initially and increase with loading in the PVDF/bentonite system.

The influence of fillers on the degree of crystallinity of electrospun PVDF/ceramic composites, in comparison with that of neat PVDF electrospun membrane, reported in literature and the proposed mechanisms are mixed. Bafqi et al. (2015) observed a small increase (3.1%) in crystallinity for PVDF electrospun nanocomposite containing 15 wt% ZnO. This can be attributable to the usual heterogeneous nucleation effect by fillers. However Yu and Cebe (2009) reported that the inclusion of Lucentite™ SWN and STN nanoclay fillers decreased crystallinity of PVDF in the nanocomposites. It was argued that nanoclay could constraint chain mobility and impede crystal growth and that nanoclay bond with PVDF chains, causing greater orientation of chains along the fibre axis and impeding chain folding during electrospinning. Neppalli et al. (2013) reported that crystallinity of PVDF increased with loading of Cloisite 20A (an organically modified montmorillonite nanoclay), the crystallinities of PVDF nanocomposites with 3 and 5 wt% nanoclay were lower and higher than that of neat PVDF respectively, in agreement with the observation in this work for the PVDF/ZnO, PVDF/halloysite and PVDF/bentonite systems.

Ceramic fillers are considered to play a double role in crystallisation of PVDF (Neppalli et al., 2013) as a nucleating agent and a hindrance to growth of crystalline phase. Both roles of a filler depends on factors such as interfacial physical and chemical properties (e.g. type of ceramics, surface energy, chemical modification and specific surface area of the fillers) for a given polymer matrix. It is likely that as loading increase, initial hindrance is dominated by the enhancement of nucleation at higher loading. For PVDF/BT system, it was dominated by filler role of hindrance therefore the crystallinity dropped with loading of BT, but with possibility for the crystallinity to increase after loading of BT exceeding 10 wt% when filler role of nucleation dominates; For PVDF/ZnO system, filler role of hindrance dominated first, then nucleation and then both roles were played by ZnO at the same time; For PVDF/halloysite system, filler role of hindrance dominated first and then nucleation thus the crystallinity dropped when halloysite was first added but then increased with loading of halloysite; And for PVDF/bentonite system, the crystallinity was first decreased and then increased with loading of bentonite indicating that both of the filler roles dominated.

4.4.2. Analysis for relative fraction of β phase, F_β, in crystalline PVDF

PVDF is commonly crystallised in non-polar crystalline α phase, and it is the β phase that possesses piezoelectric property (Sencadas et al., 2006), this work was focused on studying transformation between α and β phases, meanwhile FTIR data confirmed that only α and β phases were predominantly present (Rajesh et al., 2014), therefore it was assumed that PVDF crystalline phase was composed of α and β phases. Relative fraction of β phase, F_β, in the total crystalline phases of PVDF was obtained from FTIR spectra of the as-received PVDF powder, the electrospun membranes and cast films (see Table 1-3) based on Equation 4.3.

$$F_\beta = A_\alpha / (1.26\, A_\alpha + A_\beta) \ \% \qquad (4.3)$$

Where A_α is the absorbency by α phase at 766 cm^{-1} and A_β is the absorbency by β phase at 840 cm^{-1}. Equation 4.3 was based on assumptions that infrared absorption follows the Lambert-Beer law (Sencadas et al., 2006). Repeatability of F_β calculation was assessed using multiple FTIR scans for a given sample and the discrepancy was found negligible (standard deviation in F_β was found to be 0.014%), and thus a single scan was considered sufficient for calculation of F_β for each sample.

A_α and A_β data are recorded in Appendix I. F_β for the neat PVDF electrospun membrane and electrospun PVDF and carbon based filler composites is listed in Table 4.2 and plotted in Figure 4.11. F_β for the as-received PVDF powder and the electrospun neat PVDF are 55.1% and 72.0%, respectively, indicating that the electrospinning process promoted formation of β crystalline phase, as reported elsewhere (Pu et al., 2010; Ribeiro et al., 2010; Sundaray et al., 2013).

Table 4.2: F_β of casting and electrospun membranes

Sample ID	F_β of casting membranes (%)	F_β of electrospun membranes (%)
Neat PVDF	**N/A**	**72.0**
BT-12.5%	**59.9**	**62.6**
BT-17.6%	**67.7**	**61.7**
BT-22.2%	**62.0**	**63.3**
ZnO-13.4%	**70.8**	**64.1**
ZnO-23.6%	**72.1**	**67.0**
ZnO-31.7%	**68.3**	**61.1**
Halloysite-1.4%	**66.7**	**80.2**
Halloysite-3.3%	**62.4**	**79.6**
Halloysite-6.4%	**65.6**	**75.8**
Halloysite-9.3%	**70.7**	**76.8**
Bentonite-2.0%	**74.3**	**82.0**
Bentonite-4.9%	**71.0**	**71.6**
Bentonite-9.3%	**63.8**	**79.1**
Bentonite-13.3%	**70.4**	**73.8**

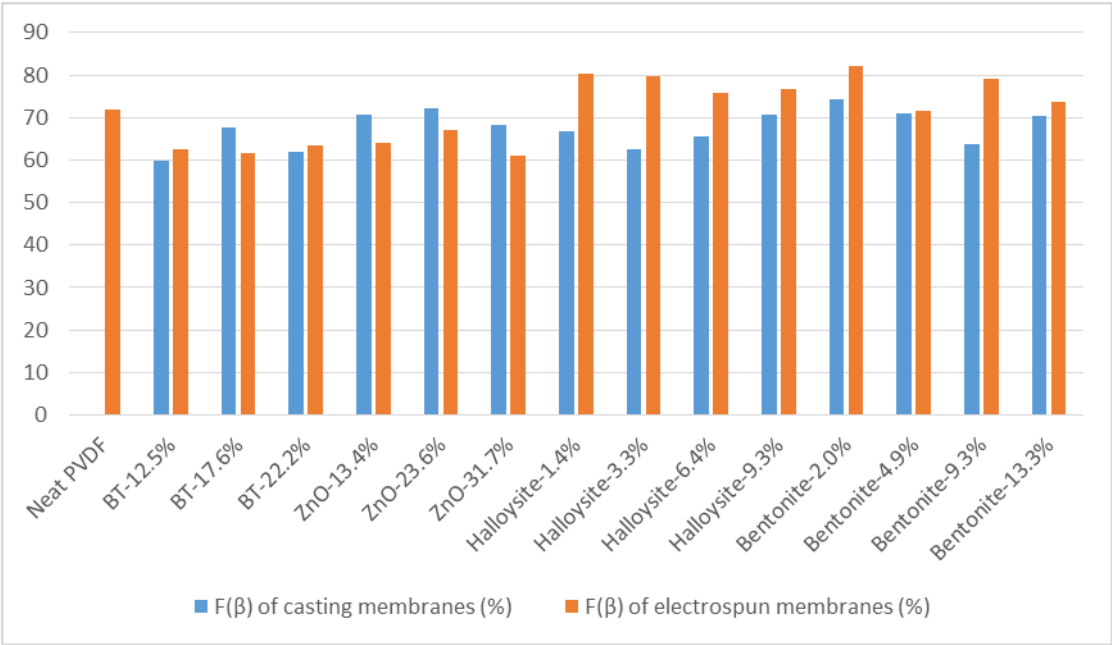

Figure 4.12: F_β of cast films and electrospun membranes

With exception of the PVDF/ZnO system, F_β of the electrospun membranes are higher than that of the casting membranes. The enhancement of β phase formation in electrospinning process was attributed to stretching of jet (or straining of the fibrils) by large elongational strains by high electrostatic potential (Ribeiro et al., 2010).

The influence of loading on F_β in Table 4.2 or Figure 4.11 vary with ceramic types. For the PVDF/BT system, addition of BT had reduced F_β in comparison with the neat PVDF. As loading of BT increase however, F_β did not change much. Chanmal and Jog (2011) reported different trend showing that in electrospun PVDF/BT nanocomposite, addition of BT lead to an increase of F_β from 62% to 80% at loading from 0 to 5 wt%, while F_β dropped from 72% to 63% in the same loading range in this work. For the PVDF/ZnO system, addition of ZnO resulted in overall reduction in F_β. There appear to be a peak value of F_β at ZnO loading of 9 wt%. In a similar study by Bafqi et al. (2015), it was observed that F_β increased from 80% to 87% at loading from 0 to 15 wt% while F_β dropped from 72% to 61% at loading from 0 to 13 wt% in this work.

The addition of halloysite in the PVDF/halloysite system had resulted in an overall increase in F_β in comparison with the neat PVDF (Table 4.2 and Figure 4.11). High F_β was achieved at low concentration of halloysite as low as 1.4 vol% but further increase in halloysite loading gave rise to reduction in F_β. With an exception at 4.9 vol%, inclusion of bentonite in the

PVDF/bentonite system also increased the F_β in comparison with the neat PVDF showing also a trend of decrease in F_β with loading of bentonite. The observations are in good agreement with study of Yoon and Kelarakis (2014) in PVDF/nanoclay systems that organically modified Lucentite nanoclay preferentially stabilises all-trans polymer chain conformation, promoting an α to β crystalline phase transformation (enhancing β-phase crystallisation at expense of α-phase crystallisation). It was attributed to constrained nature of the polymer crystallisation or to the matching between the lattices of the β crystals and the filler or to the development of ion-dipole interactions between the negatively charged clay surface and the PVDF dipoles.

4.4.3. Volume fraction of β phase in the PVDF and PVDF/ceramic composites

Some researchers (Gregorio et al., 1995; Hartono et al., 2013; Li et al., 2014; Ourry et al., 2015) speculated improvement in piezoelectric property of PVDF composites simply based on the increase of relative β fraction, F_β. It seems more reasonable that since it is the β phase that possesses piezoelectric property in PVDF, piezoelectric performance of PVDF composite should depend on the volume fraction of β phase in the composites, rather than the relative fraction F_β in the crystalline PVDF. The β phase fraction, v_β, can be calculated using Equation 4.4 based on a unit mass of sample:

$$v_\beta = \omega_P X_c F_\beta / \rho_\beta \times 100\% \qquad (4.4)$$

Where v_β is the volume fraction (*vol%*) of β phase; ω_P is the mass fraction (*wt%*) of PVDF in the samples on dry basis, as shown section 3.2.1 (Tables 3.8-3.10). X_c is the total crystallinity of PVDF (in *wt%*) determined from DSC method as described in section 4.4.1; F_β is the relative fraction of β phase in crystalline PVDF determined using FTIR method, as described in section 4.4.2 and ρ_β is density of the β phase using the value in Table 4.3.

Table 4.3: Densities of different phases in PVDF (Ameduri, 2009)

Phases	Density *(g/ml)*
Amorphous-PVDF	**1.68**
α-PVDF	**1.92**
β-PVDF	**1.97**

The volume fraction of β phase in the samples, v_β, is listed in Table 4.4 and plotted in Figure 4.12.

Table 4.4: Volume fraction of β phase, v_β, in the PVDF and PVDF/ceramic composites

Samples	v_β (vol%)
The as-received PVDF	18.2
neat PVDF	20.5
BT-12.5%	12.4
BT-17.6%	11.5
BT-22.2%	6.7
ZnO-13.4%	7.5
ZnO-23.6%	10.8
ZnO-31.7%	8.7
Halloysite-1.4%	14.8
Halloysite-3.3%	17.7
Halloysite-6.4%	17.0
Halloysite-9.3%	18.5
Bentonite-2.0%	16.4
Bentonite-4.9%	11.6
Bentonite-9.3%	13.2
Bentonite-13.3%	11.5

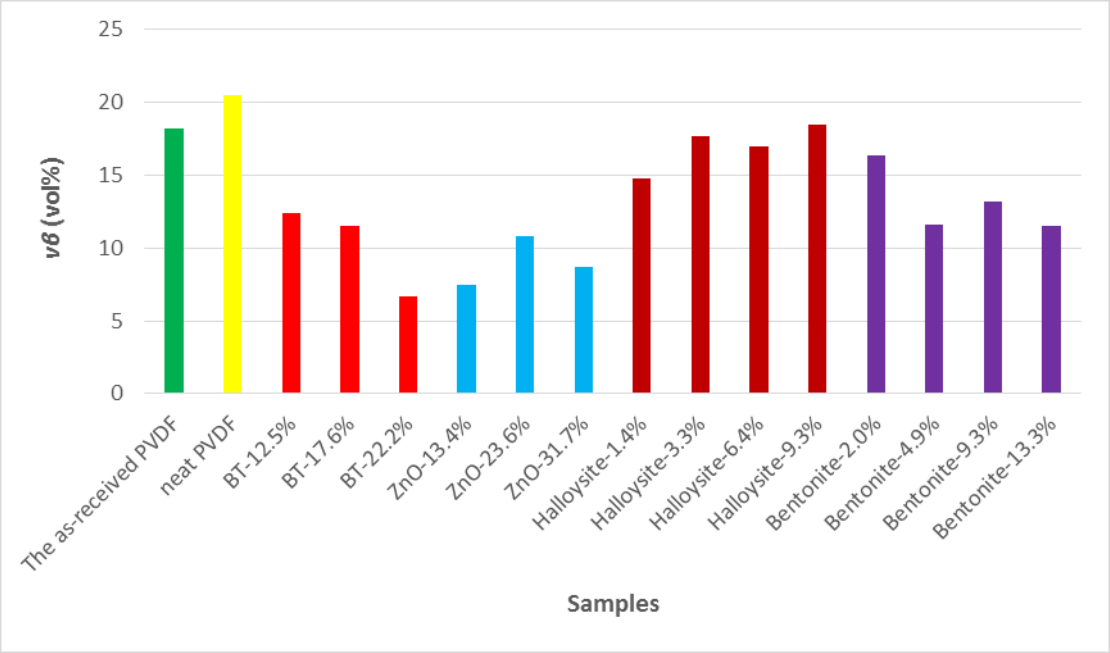

Figure 4.13: Volume fraction of β phase, vβ, in the PVDF and PVDF/Ceramic composites

As shown in Table 4.4 and Figure 4.12, volume fraction of β phase in the samples, v_β for the as-received and electrospun neat PVDF are higher in general compared with the PVDF/ceramic composites. For the PVDF/BT and PVDF/ZnO systems comparing with the neat PVDF electrospun membrane, v_β was reduced by 67.4% and 47.2% for addition of BT and ZnO, respectively, at loading of 10 wt%. It is clear that formation of β phase PVDF is hindered by addition of BT and ZnO. In addition v_β decreased with increased loading of BT while reached a peak value at an intermediate loading of ZnO at 23.6 vol%.

On contrast, much higher v_β was achieved in the PVDF/halloysite and PVDF/bentonite systems. v_β value reached 90.2% of that of the neat PVDF at halloysite loading of 9.3 vol% and 80.0% at bentonite loading of 2.0 vol%. In addition, v_β increased with higher halloysite loading while decreased with higher bentonite loading. It should be noted that calculation of v_β value has taken account the combined influence of fillers on total crystallinity in PVDF and formation of the β phase. Thus despite the significant increase in relative fraction of β phase, F_β, by addition of halloysite and bentonite, as shown in section 4.4.1, had a negative impact on X_c, the total crystallinity of PVDF.

It would be reasonable to expect that the inclusion of ceramic fillers may not be beneficial for enhancement of piezoelectric property. However, it worth noting that although v_β is assumed to be a key factor that determines piezoelectric property, other factors such as orientation of β crystalline and conductivity of the composites can also play parts, as will be assessed further.

4.5. Piezoelectric properties

Piezoelectric coefficient d_{33} is defined as follows:

$$d_{33} = \left(\frac{D_3}{T_3}\right)^E = \left(\frac{S_3}{E_3}\right)^T$$

Where D_3 and E_3 represent charge density (C/m^2) and electric field (V/m), and T_3 and S_3 represent mechanical stress (N/m^2) and strain respectively. For the case at hand the upper equation is simplified to

$$d_{33} = \frac{Q/A}{F/A} = \frac{Q}{F} = \frac{CV}{F}$$

Where A is the area stressed by the force F, the shunt capacitance C connected in parallel with the tested specimen is significantly larger than the capacitance of the tested specimen in order to provide the correct boundary condition (constant electric field) for the measurement of d_{33}.

The influence of distance between the measurement points and the edge and the angle variation from their horizontal position is shown in Table 4.5, where the mean piezoelectric coefficient d_{33} was obtained from averaging of 5 points of the same distance from the edge. As all the selected samples show the same trend, only one is presented here and the others can be found in the Appendix II.

Table 4.5: d_{33} measurement showing the influence of distances to the edge of sample and angle from the horizontal position for BT-22.2%

Distance (mm)	d_{33} (*pC/N*)	SD (*pC/N*)
5	**10.80**	**±0.84**
10	**12.80**	**±0.45**

15	**14.60**	**±1.52**
20	**15.80**	**±1.30**
25	**13.80**	**±1.48**
Angle	**d_{33} (*pC/N*)**	**SD (*pC/N*)**
12°	**10.00**	**±1.73**
24°	**9.40**	**±0.55**
36°	**10.20**	**±2.17**
48°	**10.00**	**±2.24**
60°	**8.60**	**±0.89**

Table 4.5 shows that d_{33} for the same distance are consistent (low standard deviations, SD). No systematic variations can be found as a function of the distance and thus influence of choices of measurement position points can be neglected. A noticeable overall reduction of d_{33} values can be observed when the membranes were deviated from the required horizontal position, due most likely to additional stress generated from the bending, and thus care must be taken to avoid such bending and minimise the measurement errors.

Using the 5×5 d_{33} measurement point matrix, the mean d_{33} was obtained from averaging that of the 25 points. The results are summarised in Table 4.6 and plotted in Figure 4.13.

Table 4.6. Results of d_{33} measurement for electrospun neat PVDF and the PVDF/ceramic composite membranes

Sample ID	d_{33} (*pC/N*)	SD (*pC/N*)
neat PVDF	**10.00**	**±0.71**
BT-12.5%	**8.88**	**±1.84**
BT-17.6%	**11.21**	**±2.24**
BT-22.2%	**12.84**	**±2.52**
ZnO-13.4%	**6.00**	**±1.32**
ZnO-23.6%	**12.26**	**±3.11**
ZnO-31.7%	**8.14**	**±1.12**

Halloysite-1.4%	**11.00**	**±1.66**
Halloysite-3.3%	**12.14**	**±1.64**
Halloysite-6.4%	**12.72**	**±1.20**
Halloysite-9.3%	**14.43**	**±1.76**
Bentonite-2.0%	**13.13**	**±2.26**
Bentonite-4.9%	**10.13**	**±1.90**
Bentonite-9.3%	**10.52**	**±1.30**
Bentonite-13.3%	**11.63**	**±1.65**

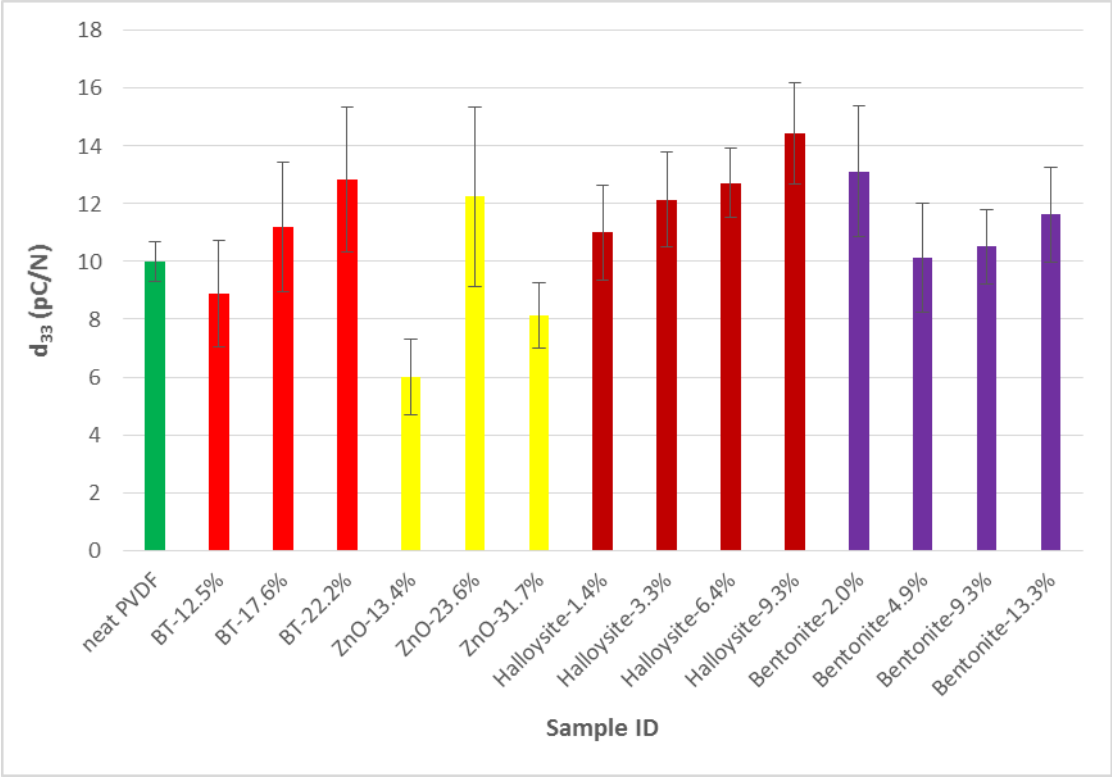

Figure 4.14: Results of d_{33} measurement for electrospun neat PVDF and the PVDF/ceramic composite membranes

From Table 4.6 and Figure 4.13, d_{33} for the electrospun neat PVDF is 10 *pC/N* which can be succeeded by that of all PVDF/ceramic composites at certain loadings.

In the PVDF/BT system, BT loadings higher than 17.6 vol% is sufficient to outperform the neat PVDF and becomes 28% higher than d_{33} of the neat PVDF at 22.2 vol % BT loading. As BT itself possess high piezoelectric property with d_{33} of 190 pC/N (Vijatović et al., 2008), the

combined contributions to piezoelectric behaviour of the composite should be accounted, in addition to that from the β phase in PVDF as suggested by Baji et al. (2011). ZnO, being a relatively lower piezoelectric ceramic with d_{33} of 11.6 pC/N (Luo et al., 2010) can also outperform the neat PVDF by 22.6% at 23.6 vol% ZnO loading, although inferior at the other loading levels. Considering the low β volume fraction of the system (Figure 4.12), the possible combined piezoelectric contributions from both ZnO and β phase cannot be neglected.

In the PVDF/halloysite and PVDF/bentonite systems, d_{33} of the PVDF/halloysite system increases with the concentration of halloysite and are higher than that of neat PVDF at all loading levels and outperform the neat PVDF by 44.3% at 9.3 vol% loading. In comparison, d_{33} of the PVDF/bentonite system outperform the neat PVDF by 31.3% at bentonite loading of 2.0 vol% but no clear benefit at higher level of loadings. This may be attributed, in part, to the lower F_β values at these high loadings (section 4.4.2). Clearly the same argument of "combined contributions" cannot apply to the non-piezoelectric nanoclays. The fact that the PVDF/non-piezoelectric ceramic composites can outperform the neat PVDF indicates that while v_β is considered an important factor influence the piezoelectric performance (d_{33}), other factors (such as piezoelectricity of the filler itself as mentioned earlier) have also to be considered. One additional possible mechanisms contributing to such extraordinary behaviour may be the orientation of β crystalline phase. It is possible while the nanoclays promote formation of β phase (section 4.4.3), they may also promote the orientation of β crystalline phase along the direction of the nanofibres. Despite of the randomness lay-up of fibres, they are layered on a single plane perpendicular to the d_{33} measurement and thus it is possible to create a dominating orientation in the d_{33} direction.

4.6. Summary

Electrospun PVDF/BT, PVDF/ZnO and PVDF/nanoclay (halloysite and bentonite) nanocomposites with different loadings were manufactured by electrospinning process, and influence of fillers on crystalline and piezoelectric properties were studied.

Total PVDF crystallinity X_c for a majority of the electrospun PVDF/ceramic composite membranes are relatively lower than that of the casting membranes or comparable, indicating

that the membrane casting process provide more favourable crystallisation conditions in PVDF than that of the electrospinning process. For the electrospun membranes, the inclusion of all types of ceramic fillers had resulted in a reduction in X_c compared with that of the neat PVDF. X_c decreased with the BT loading but an opposite trend was noticed for the PVDF/ZnO and PVDF/halloysite systems while X_c was found to decrease initially and increase with loading in the PVDF/bentonite system. Ceramic fillers are considered to play a double role in crystallisation of PVDF as a nucleating agent and a hindrance to growth of crystalline phase, and it is likely that as loading of filler increase, initial hindrance is dominated by the enhancement of nucleation at higher loading.

With exception of the PVDF/ZnO system, relative fraction of β phase F_βs of the electrospun membranes are higher than that of the casting membranes. Addition of BT and ZnO had reduced F_β in comparison with the neat PVDF while F_β increased as loading of BT increase and there appear to be a peak value of F_β at ZnO loading of 9 wt%. The addition of halloysite had resulted in an overall increase in F_β in comparison with the neat PVDF. High F_β was achieved at low concentration of halloysite as low as 1.4 vol% but further increase in halloysite loading gave rise to reduction in F_β. With an exception at 4.9 vol%, inclusion of bentonite also increased the F_β showing also a trend of decrease in F_β with loading of bentonite.

Volume fraction of β phase in the samples v_β for the as-received and electrospun neat PVDF are higher in general compared with the PVDF/ceramic composites. For the PVDF/BT and PVDF/ZnO systems comparing with the neat PVDF electrospun membrane, v_β was reduced by 67.4% and 47.2% for addition of BT and ZnO, respectively, at loading of 10 wt%. It is clear that formation of β phase PVDF is hindered by addition of BT and ZnO. In addition v_β decreased with increased loading of BT while reached a peak value at an intermediate loading of ZnO at 23.6 vol%. On contrast, much higher v_β was achieved in the PVDF/halloysite and PVDF/bentonite systems. In addition, v_β increased with higher halloysite loading while decreased with higher bentonite loading.

Piezoelectric coefficient d_{33} for the electrospun neat PVDF can be succeeded by that of all PVDF/ceramic composites at certain loadings. BT loadings higher than 17.6 vol% is sufficient to outperform the neat PVDF and becomes 28% higher than d_{33} of the neat PVDF at 22.2 vol % BT loading. ZnO can outperform the neat PVDF by 22.6% at 23.6 vol% ZnO

loading although inferior at the other loading levels. The combined contributions to piezoelectric behaviour of the PVDF/BT and PVDF/ZnO composites should be accounted. d_{33} of the PVDF/halloysite system increases with the concentration of halloysite and are higher than that of neat PVDF at all loading levels and outperform the neat PVDF by 44.3% at 9.3 vol% loading, d_{33} of the PVDF/bentonite system outperform the neat PVDF by 31.3% at bentonite loading of 2.0 vol% but no clear benefit at higher level of loadings.

While v_β is considered an important factor influence the piezoelectric performance (d_{33}), other factors (such as piezoelectricity of the filler itself and β phase orientation) have also to be considered. It is possible while the nanoclays promote formation of β phase, they may also promote the orientation of β crystalline phase along the direction of the nanofibres, and it is possible to create a dominating orientation in the d_{33} direction.

Chapter 5. Results and discussions – The PVDF/carbon systems

5.1. State of dispersion and sedimentation stability of the suspensions

Optical microscopy showing state of dispersion in the PVDF/CNT suspensions are shown in Figure 5.1. It could be observed that CNT-0.05% suspension (Figure 5.1a) was well dispersed without obvious agglomerate, certain amount of agglomerate residues could be observed in the CNT-0.15% suspension (Figure 5.1b) and CNT-0.25% suspension (Figure 5.1c). This suggests that the ultrasonification method was not sufficiently powerful to completely destruct the agglomerates within the as-received CNT at higher concentrations.

(a) (b) (c)

Figure 5.1: SEM microscopy showing morphology and quality of electrospun membrane from suspensions: a) CNT-0.05%; b) CNT-0.15% and c) CNT-0.25%

Optical microscopy showing state of dispersion in the PVDF/GO suspensions are shown in Figure 5.2a-c. The existence of large number of fine GO in all cases indicate that agglomerates in the as-received GO powder is relatively weak and can be destructed effectively by the ultrasonification. Loose clusters were found to increase in population with the increase in GO loading. These are most likely to have resulted from flocculation of originally dispersed particles, as observed by Song et al. (1994) due to insufficient interparticle repulsion in low-viscosity liquid systems, which can be minimised by absorption of effective surfactants at suitable levels based on loading of fillers (Song et al, 1994), or use of polyacylic acid (PAA) or polyethylene glycol (PEG) as suggested by Chen et al. (2013).

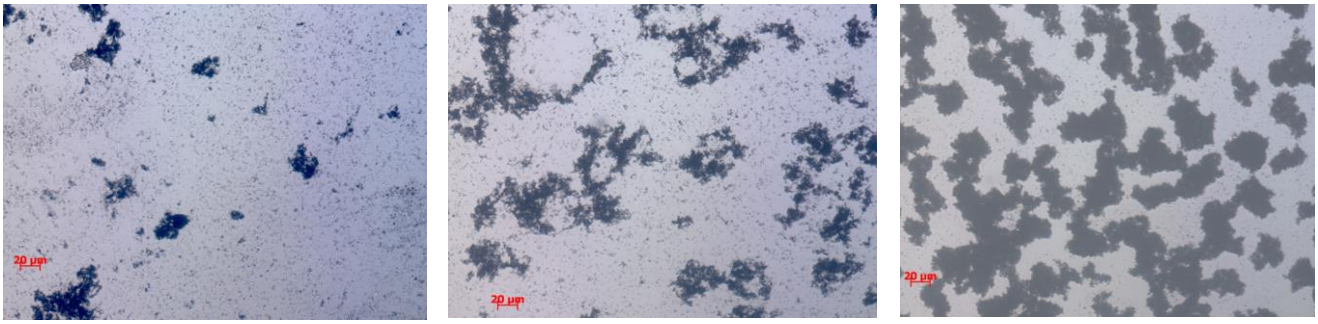

(a) (b) (c)

Figure 5.1: Optical microscopy showing low magnification status of GO dispersion in: a) GO-4.6%; b) GO-12.6% and c) GO-19.4% suspensions showing degrees of flocculation of fine dispersed GO particles and loose clusters of them.

No obvious sedimentation or phase separation was observed for all the suspensions over 6-8 hours after preparation. Although high density agglomerates tend to settle fast under gravitation, the low density carbon fillers and agglomerates make them much more resistance to sedimentation. Loose clusters in the flocculated suspension would have even lower density relative to the polymer solution and thus more stable against sedimentation. The suspensions were found sufficiently stable for the duration of electrospinning process and did not cause any problem such as clogging of the needle or the pipeline.

5.2. Dispersion of particles in the composites

The status of GO filler dispersion in the dried composites was assessed by TEM of microtomed cast films from the suspensions and shown in Figure 5.3 for the GO-12.6% nanocomposites. Although some fine GO sheets (probable of single or a few layer stacks) can be found, most of them are in loosely clustered form. Such loose packing allowed penetration of the PVDF polymer matrix and thus the nanocomposites is dominated by an intercalated structure.

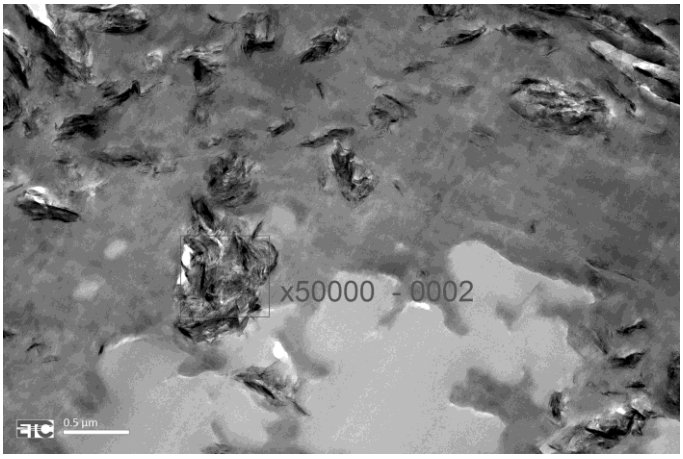

Figure 5.2: TEM image showing domination of intercalation structure in cast film made from the GO-12.6% suspension.

5.3. Morphology of the electrospun membranes

Typical features of electrospun membranes and desirable morphologies have been discussed in section 4.3.

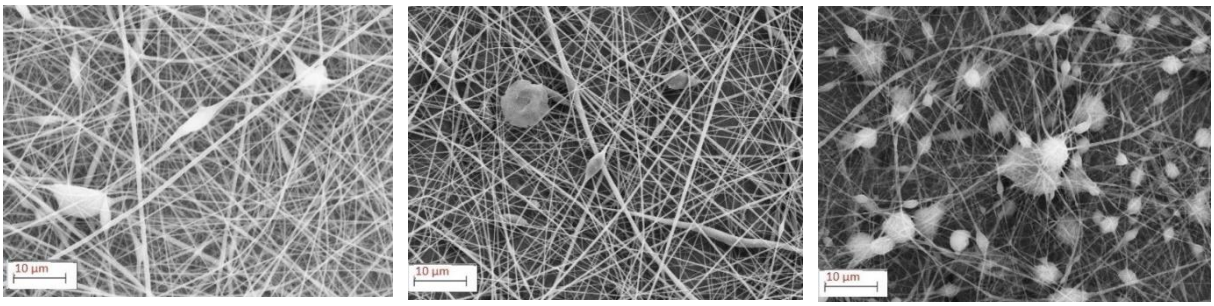

(a) (b) (c)

Figure 5.4: SEM microscopy showing morphology and quality of electrospun membrane from suspensions: a) CNT-0.05%; b) CNT-0.15% and c) CNT-0.25%

For the PVDF/CNT system, as shown in Figure 5.4a-c, as the loading of CNT increases, the population density of beads increases. This can be attributable to the quality of dispersion discussed earlier in section 5.1.

For the PVDF/GO system, as shown in Figure 5.5a-c, a large amount of beads and relatively fewer fibres were observed in GO-4.6% (Figure 5.5a) and GO-12.6% (Figure 5.5b), while a decent non-woven structure with reduced number of beads was produced in GO-19.4% (Figure 5.5c). Unlike the equiaxial particles in ZnO, flocculation (as discussed earlier in section 5.1) of the flack-like filler appeared to have negative effects on jet break-up and formation of beads, although other parameters such as viscosity, surface tension, flow rate and applied voltage etc. may have also contributed to this.

It is interesting to note that the beads are not isolated but connected by very fine fibres. This should be taken into account when consider electric conductivity and connectivity of the membrane by addition of the GO filler.

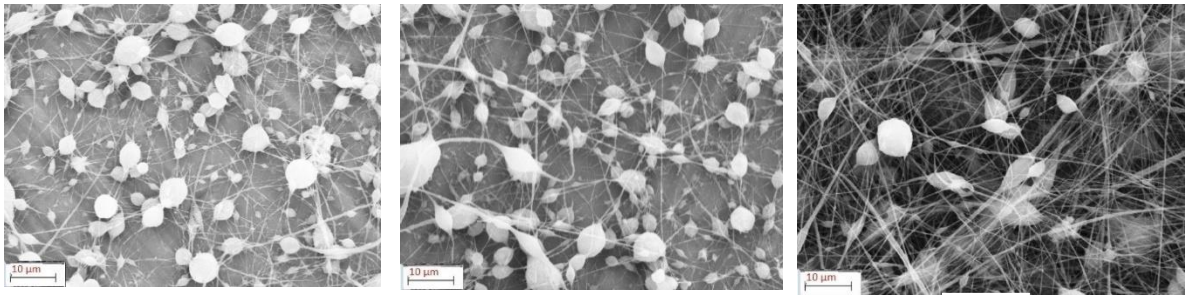

(a) (b) (c)

Figure 5.5: SEM microscopy showing morphology and quality of electrospun membrane from suspensions: a) GO-4.6%; b) GO-12.6% and c) GO-19.4%

5.5. Crystalline properties

5.5.1. Total PVDF crystallinity, X_c

As described in section 4.4.1, total crystallinity, X_c for the PVDF/carbon systems were calculated using Equation (4.1) and shown in Table 5.1.

Table 5.1: Heat of fusion ($\Delta H_{m,s}$), concentration of PVDF in the DSC samples (ω_P) and crystallinity of the PVDF matrix (X_c)

Sample ID	$\Delta H_{m,s}$ (J/g)	ω_P (wt%)	X_c (%)

Neat PVDF	**33.3**	**100.0**	**31.9**
CNT-0.05%	**11.7**	**66.7**	**16.8**
CNT-0.15%	**1.5**	**66.6**	**2.2**
CNT-0.25%	**0.4**	**66.5**	**0.6**
GO-4.6%	**20.5**	**95.3**	**20.5**
GO-12.6%	**19.7**	**87.0**	**21.6**
GO-19.4%	**17.4**	**80.0**	**20.8**

Looking into each electrospun composite system in more details in Table 5.1 in comparison with the electrospun neat PVDF, the influence of different carbon based fillers (and their loading) on the total PVDF crystallinity (X_c) can be revealed. Overall, the inclusion of all types of carbon based fillers had resulted in considerable reduction in X_c compared with that of the neat PVDF. In terms of effect of loading on X_c, different trends are observed: X_c decreased with the CNT loading in the PVDF/CNT system while GO loading did not have much influence on X_c.

The influence of carbon fillers on the degree of crystallinity of electrospun PVDF composites, in comparison with that of neat electrospun PVDF membrane, reported in literature and the proposed mechanisms are mixed. Yee et al. (2008) observed a slight increase in crystallinity for PVDF electrospun nanocomposite containing 0.01 *wt%* functionalised MWCNT. This was attributed to the utilisation of a modified rotating disk and stretching of nanofibers. Similar result to that of Yee et al. was reported by Baji et al. (2013), and it was argued that MWCNT could constrain molecular mobility in amorphous regions of PVDF during electrospinning giving rise to lower X_c.

Li et al. (2013) using different processing method (non-solvent vapour adsorption, ageing, dipping in fresh water and freeze-drying) reported that PVDF chains immobilised on graphene sheets might work as crystallisation nuclei therefore inclusion of graphene enhanced degrees of crystallisation in PVDF. The observation contradict that in this work, it may due partly to the difference in processing methods, but the flocculation of GO particles and the resulted intercalated structure may have restricted nucleation and growth in the confined spaces between the GO layers.

5.5.2. Analysis for relative fraction of β phase, F_β, in crystalline PVDF

As described in 4.4.2, relative fraction of β phase, F_β, in the total crystalline phases of PVDF was obtained from FTIR spectra of the as-received PVDF powder, the electrospun membranes and cast films from the PVDF/carbon suspensions. From intensities of absoptions A_α and A_β listed in Appendix I, repeatability of F_β calculated using Equation 4.2 are shown in Table 5.2 and plotted in Figure 5.6.

Table 5.2: The relative fraction of β phase, F_β for the electrospun neat PVDF and PVDF/carbon composites

Sample ID	F_β (%)
neat PVDF	72.0
CNT-0.05%	58.3
CNT-0.15%	59.6
CNT-0.25%	62.1
GO-4.6%	54.0
GO-12.6%	48.7
GO-19.4%	47.7

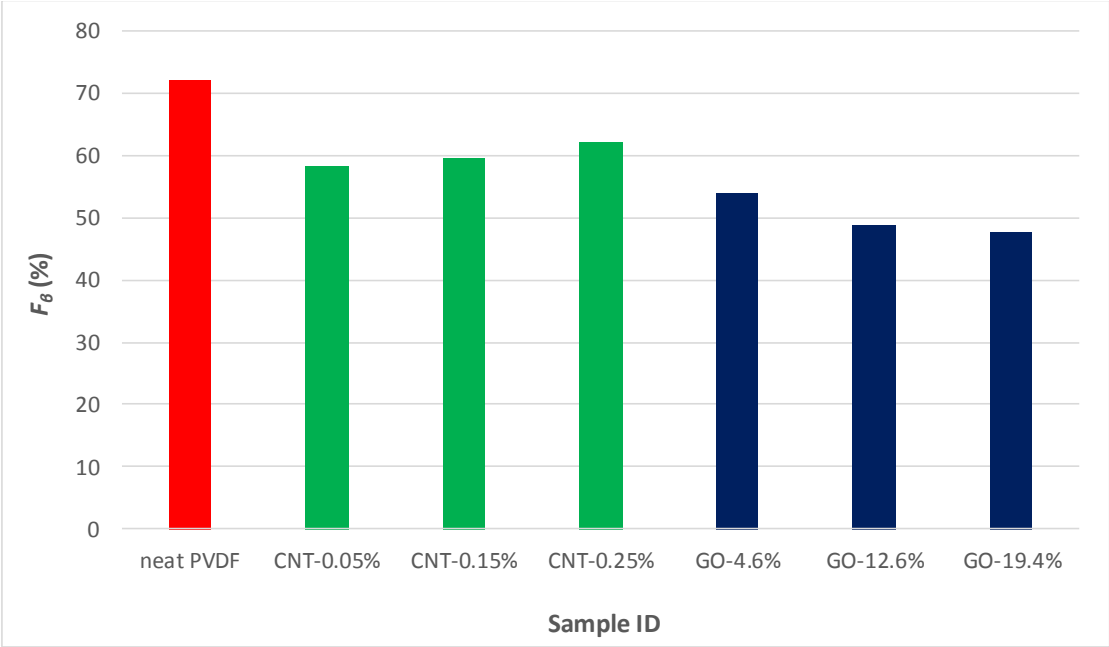

Figure 5.3: The relative fraction of β phase, Fβ for the electrospun neat PVDF and PVDF/carbon composites

The influence of loading on F_β in Table 5.2 or Figure 5.6 vary with filler types. For the PVDF/CNT system, addition of CNT had reduced F_β in comparison with the neat PVDF. As loading of CNT increase however, F_β increased. Wang et al. (2014) reported similar trend showing that addition of CNT lead to a noticeable increase of F_β at loading from 0.6 to 2 *wt%* in electrospun PVDF/CNT nanocomposite. For the PVDF/GO system, addition of GO had reduced F_β in comparison with the neat PVDF. As loading of GO increase, F_β decreased. F_β of the electrospun PVDF/CNT nanocomposites is higher than that of the PVDF/GO nanocomposites, even though loading of GO (4.6-19.4 *vol%*) was much higher than that of CNT (0.05-0.25 *vol%*).

5.5.3. Volume fraction of β phase in PVDF and PVDF/carbon composites, v_β

As described in section 4.4.3 using Equation 4.3 and density of the β phase, ρ_β , in Table 5.3, volume fraction of β phase in PVDF and PVDF/carbon composites, v_β , are calculated as shown in Table 5.4 and plotted in Figure 5.7.

Table 5.3: Densities of different phases in PVDF (Ameduri, 2009)

Phases	Density *(g/ml)*
Amorphous-PVDF	**1.68**
α-PVDF	**1.92**
β-PVDF	**1.97**

Table 5.4: Volume fraction of β phase in the PVDF and PVDF and carbon based filler composites, v_β

Samples	v_β *(vol%)*
The as-received PVDF	**18.2**
neat PVDF	**20.5**
CNT-0.05%	**5.0**

CNT-0.15%	**0.7**
CNT-0.25%	**0.2**
GO-4.6%	**9.3**
GO-12.6%	**8.1**
GO-19.4%	**7.0**

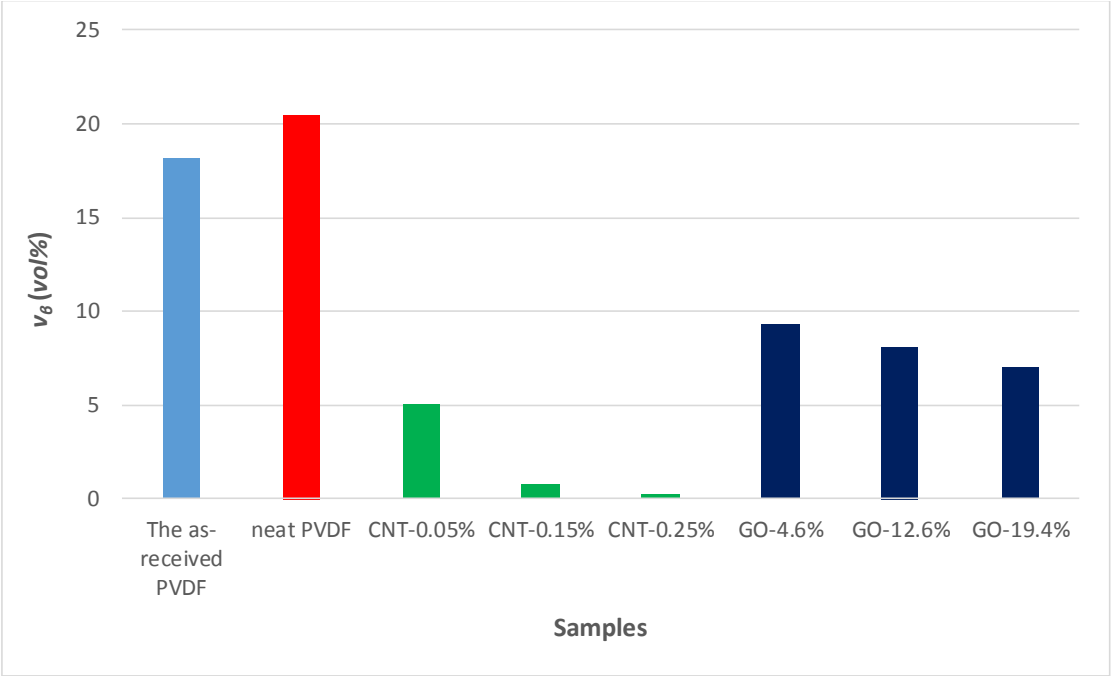

Figure 5.4: Volume fraction of β phase in the PVDF and PVDF and carbon based filler composites, v_β.

As shown in Table 5.4 or Figure 5.7, volume fraction of β phase in the samples, v_β for the as-received and electrospun neat PVDF are much higher in general compared with the PVDF and carbon based filler composites. It is clear that formation of β phase PVDF is significantly hindered by addition of CNT and GO. In addition v_β decreased with increased loading of CNT and GO. It should be noted that calculation of v_β value has taken account the combined influence of fillers on total crystallinity in PVDF and formation of the β phase. Both PVDF total crystallinity X_c (as shown in section 5.5.1) and relative fraction of β phase F_β (as shown in section 5.5.2) of the composites were reduced by incorporation of CNT and GO therefore v_β value was expected to be decreased. In addition, v_β of the PVDF/GO composites is higher than that of the PVDF/CNT composites.

It would be logical to expect from the foregoing discussions that the inclusion of carbon based filler is not beneficial for the enhancement of piezoelectric property. However, it worth noting that although v_β is assumed to be a key factor that determines piezoelectric property, other factors such as orientation of β crystalline and conductivity of the composites can also play parts, as will be assessed further.

5.6. Piezoelectric properties

The influence of distance between the measurement points to the sample edge and the angle variation from their horizontal position (section 3.5.3) is shown in Table 5.5, where the mean piezoelectric coefficient d_{33} was obtained from averaging of 5 points of the same distance from the edge. As all the selected samples show the same trend, only one is presented here and the others can be found in Appendix II.

Table 5.5: Piezoelectric coefficient, d_{33}, showing the influence of distances to the edge of sample and angle from the horizontal position for CNT-0.05%

Distance (mm)	d_{33} (*pC/N*)	SD (*pC/N*)
5	12.00	±1.22
10	14.40	±3.05
15	12.20	±2.17
20	14.00	±2.45
25	14.80	±1.79
Angle	**d_{33} (*pC/N*)**	**SD (*pC/N*)**
12°	11.60	±1.52
24°	10.80	±1.64
36°	11.00	±1.58
48°	10.80	±0.84
60°	11.00	±1.41

Table 5.5 shows that d_{33} for the same distance are consistent (low standard deviations, SD). No systematic variations can be found as a function of the distance and thus influence of choices of measurement position points can be neglected. A noticeable overall reduction of

d_{33} values can be observed when the membranes were deviated from the required horizontal position, due most likely to additional stress generated from the bending, and thus care must be taken to avoid such bending and minimise the measurement errors.

Using the 5×5 d_{33} measurement point matrix (section 3.5.3), the mean d_{33} was obtained from averaging that of the 25 points. The results are summarised in Table 5.6 and plotted in Figure 5.8.

Table 5.6. Results of d_{33} measurement for electrospun neat PVDF and the PVDF/carbon composite membranes

Sample ID	d_{33} (*pC/N*)	SD (*pC/N*)
neat PVDF	10.00	±0.71
CNT-0.05%	13.58	±2.19
CNT-0.15%	15.97	±1.85
CNT-0.25%	13.61	±1.15
GO-4.6%	10.50	±1.52
GO-12.6%	8.67	±0.75
GO-19.4%	7.46	±2.59

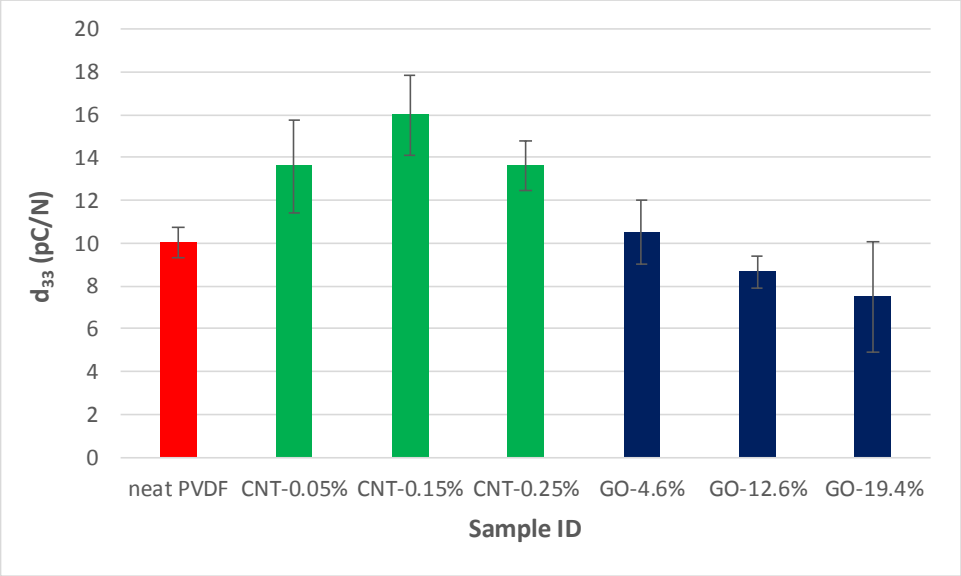

Figure 5.5: Results of d_{33} measurement for electrospun neat PVDF and the PVDF/carbon composite membranes

It is clear from Table 5.6 or Figure 5.8, that d_{33} for the electrospun neat PVDF (10 *pC/N*) can be succeeded by that of both PVDF/CNT and PVDF/GO composites at certain loadings. In the PVDF/CNT system, CNT loadings higher than 0.5 *vol%* is sufficient to outperform the neat PVDF and becomes 59.7% higher than d_{33} of the neat PVDF at 1.6 *vol%* CNT loading. Similar results has been reported by Pu et al. (2010). Considering the low β volume fraction of the system v_β (section 5.5.3), this was not expected. Conductivity of PVDF increases rapidly with loading of MWCNT due to its high electric conductivity (Wang et al., 2014). CNT can also reach percolation threshold at a very low concentration (Bauhofer & Kovacs, 2009), resulting surge in electric conductivity of polymer composites. The d_{33} increase in the PVDF/CNT system might have been caused by the increased electric conductivity by CNT and by possibly enhanced orientation of β crystals. The former would conduct the charge of polycrystalline β phases to the surface of the membrane and the latter enhance the coordinated response from the β phases polycrystalline in the d_{33} direction. The orientation of the β crystals can be promoted by increased electrostatic force during electrospinning owing to the enhanced electric conductivity by CNT (Chang et al., 2009).

In the PVDF/GO system, only GO loadings of 4.6 *vol%* achieved d_{33} comparable to that of the neat PVDF. Further increase in GO loading had resulted in a declined d_{33}. In general, d_{33} of the PVDF/CNT composites is higher than that of the PVDF/GO composites. This may due to the influence of flocculation in GO (section 5.1), the lower aspect ratio as compared with CNT as they can result lower electric connection and orientation of the β phases polycrystalline.

5.7. Summary

Electrospun PVDF/CNT and PVDF/GO nanocomposites with different loadings were manufactured by electrospinning process, and influence of fillers on crystalline and piezoelectric properties were studied. The inclusion of all types of carbon fillers had resulted in a reduction in total PVDF crystallinity (X_c) compared with that of the neat PVDF, and X_c decreased with the CNT loading while GO loading did not have much influence on X_c, the flocculation of GO particles and the resulted intercalated structure may have restricted nucleation and growth in the confined spaces between the GO layers.

In comparison with the neat PVDF, addition of CNT had reduced Relative fraction of β phase in total crystalline of PVDF (F_β) but F_β increased as loading of CNT increase, while addition of GO reduced F_β while F_β decreased as loading of GO increase. F_β of the electrospun PVDF/CNT nanocomposites is higher than that of the PVDF/GO nanocomposites, even though loading of GO (4.6-19.4 *vol%*) was much higher than that of CNT (0.05-0.25 *vol%*).

Volume fraction of β phase in the samples (v_β) for the as-received and electrospun neat PVDF are much higher in general compared with the PVDF/carbon composites. It is clear that formation of β phase PVDF is significantly hindered by addition of CNT and GO. In addition v_β decreased with increased loading of CNT and GO. Since calculation of v_β value has taken account the combined influence of fillers on total crystallinity in PVDF and formation of the β phase, both X_c and F_β of the composites were reduced by incorporation of CNT and GO therefore v_β value was expected to be decreased. In addition, v_β of the PVDF/GO composites is higher than that of the PVDF/CNT composites.

Piezoelectric coefficient d_{33} for the electrospun neat PVDF is 10 *pC/N* which can be succeeded by that of both PVDF/CNT and PVDF/GO composites at certain loadings. CNT loadings higher than 0.5 *vol%* is sufficient to outperform the neat PVDF and becomes 59.7% higher than d_{33} of the neat PVDF at 1.6 *vol%* CNT loading. Considering the low β volume fraction of the system v_β, this was not expected, the d_{33} increase in the PVDF/CNT system might have been caused by the increased electric conductivity by CNT and by possibly enhanced orientation (a dominating orientation in the d_{33} direction, which may be promoted by increased electrostatic force during electrospinning due to the enhanced electric conductivity by the CNT) of β crystals. In the PVDF/GO system, only GO loadings of 4.6 *vol%* achieved d_{33} comparable to the neat PVDF. Further increase in GO loading had resulted decline in d_{33}. In general, d_{33} of the PVDF/CNT composites is higher than that of the PVDF/GO composites.

Chapter 6. Results and discussions – The PVDF/cellulose systems

6.1. State of dispersion and sedimentation stability of the suspensions

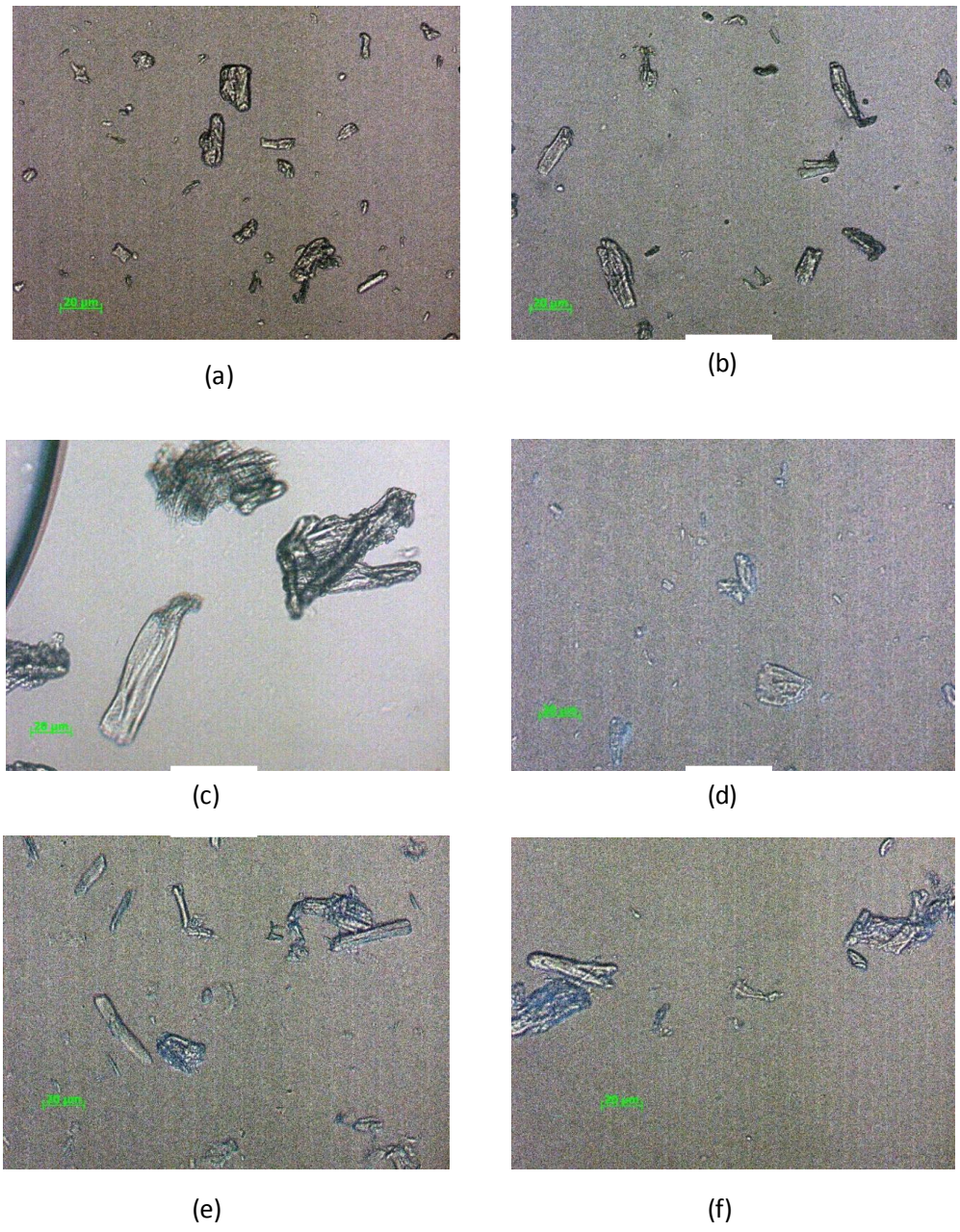

(a) (b) (c) (d) (e) (f)

Figure 6.1. Optical microscopic microscopy showing dispersion of cellulose particles in suspensions: a) MCC20-10.2%; b) MCC50-10.2%; c) MCC90-10.2%; d) MCC20-9.2% (PEG); e) MCC50-9.2% (PEG) and f) MCC90-9.2% (PEG).

Figure 6.1 are optical microscopy showing states of dispersion in the PVDF/MCC suspensions. The particles in the as-received MCCs (section 3.1.4) were well separated, as expected for such large particle sizes and no apparent difference in dispersion could be observed for those with or without PEG.

Optical microscopy showing state of dispersion in the PVDF/NCC suspensions are shown in Figure 6.2. In comparison with MCC suspensions, particle size of NCCs are by far much finer, confirming the effectiveness size reduction in the hydrolysis treatment. Due to resolution limitation, nano- to submicron- metre sized particles in the NCCs could not be revealed and it is difficult to tell if there is systematic increase in the mean particle size of the NCCs made from MCCs with different original particle sizes. However it could potentially be case that coarser MCC may have resulted in relatively coarser NCC for the same intensity of acid hydrolysis power to break up the chemical bonds. The particles in the NCC were also well dispersed and free from agglomeration (as expected for the particles had been kept suspended in the hydro-gels to prevent agglomeration), or flocculation.

No obvious sedimentation or phase separation was observed for all the suspensions over 6-8 hours after preparation. Although high density agglomerates tend to settle fast under gravitation, the low density carbon fillers and agglomerates make them much more resistance to sedimentation. Loose clusters in the flocculated suspension would have even lower density relative to the polymer solution and thus more stable against sedimentation. The suspensions were found sufficiently stable for the duration of electrospinning process and did not cause any problem such as clogging of the needle or the pipeline.

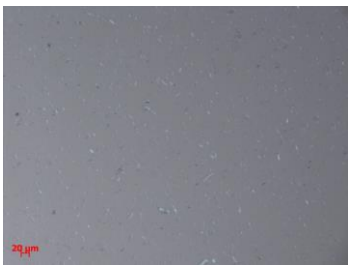

(a)

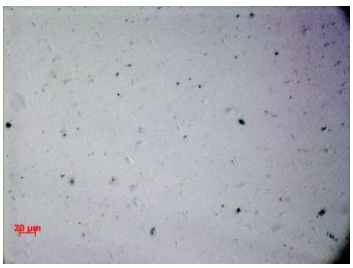

(b)

(c)

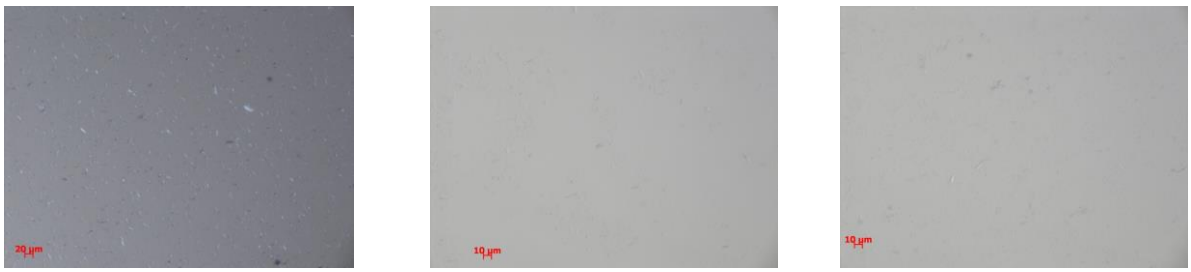

(d) (e) (f)

Figure 6.2: Optical microscopic microscopy showing dispersion of particles in suspensions: a) NCC20-1.1%; b) NCC50-1.1%; c) NCC90-1.1%; d) NCC20-5.4%; e) NCC50-5.4% and f) NCC90-5.4%

6.2. Morphology of the electrospun membranes

Typical features of electrospun membranes and desirable morphologies have been discussed in section 4.3.

For the PVDF/MCC20 system, as shown in Figure 6.3a-c, nano- to micro-meter fibres form quite uniform non-woven structure for all the MCC20 concentrations. The beads sizes (~20 μm) and their shape bare resemblance to that in the as-received MCC powder. This indicate that the MCC particles have resulted jet breakup as they exit from the needle forming the beads.

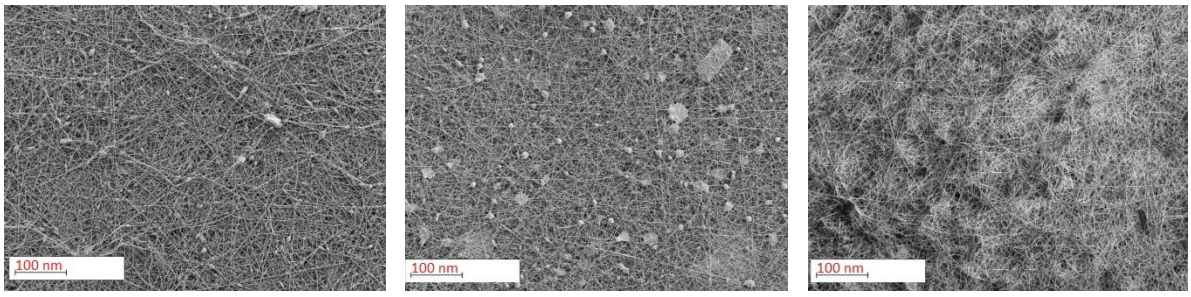

(a) (b) (c)

Figure 6.3: SEM microscopy showing morphologies of nanofibre membranes electrospun from the MCC20 suspensions: a) MCC20-1.1%; b) MCC20-9.2% (PEG) and c) MCC20-37.3%

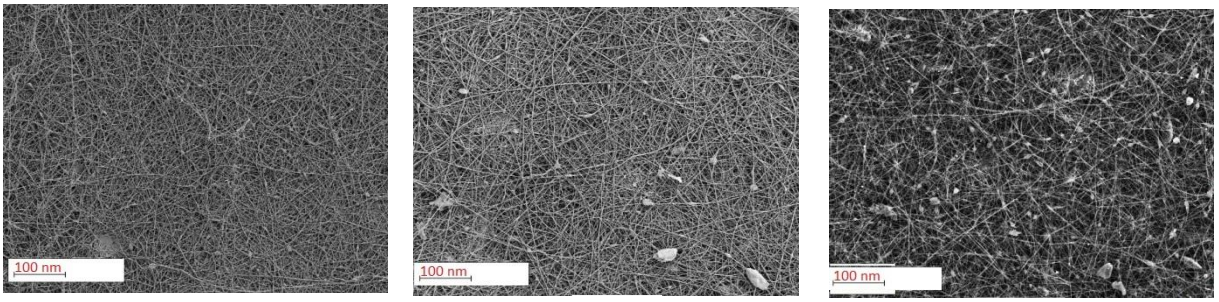

(a) (b) (c)

Figure 6.4: SEM microscopy showing morphologies of nanofibre membranes electrospun from the MCC50 suspensions: a) MCC50-10.2%; b) MCC50-9.2% (PEG) and c) MCC50-37.3%

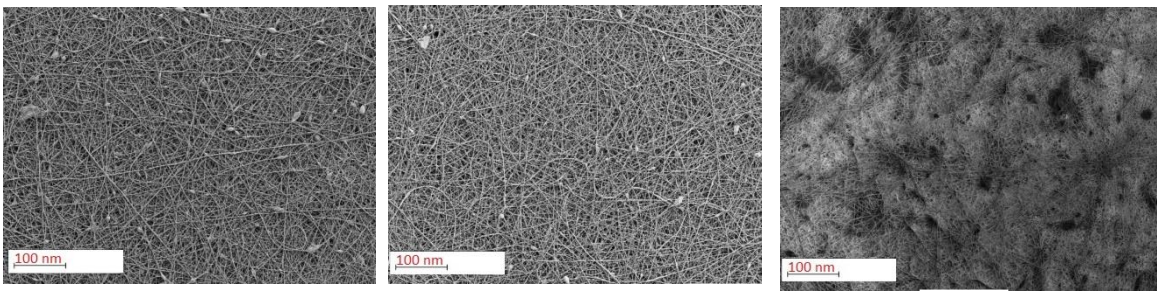

(a) (b) (c)

Figure 6.5: SEM microscopy showing morphologies of nanofibre membranes electrospun from the MCC90 suspensions: a) MCC90-10.2%; b) MCC90-9.2% (PEG) and c) MCC90-37.3%.

Similar morphologies were observed in the PVDF/MCC50 and PVDF/MCC90 systems, as shown in Figure 6.4 and Figure 6.5. The correlation of bead size with particle size in the as-received MCCs can also be observed.

For PVDF/NCC systems, as shown in Figure 6.6, better overall quality non-woven structure can be observed in comparison with those of the PVDF/MCC systems (Figures 6.3-6.5) in term of the size of the beads: they are much finer (up to ~ 5 μm) rather than ~20-90μm. This fine beads may have been also produced as a result of disturbance of the jet by the relatively

larger cellulose particles within the PVDF/NCC systems. This is supported by an observation that as the concentration of NCC increases, the beads population density seemed also increased (comparing Figures 6.6 between a_1 and a_2, b_1 and b_2, c_1 and c_2). The fact that there was no apparent difference in bead size of different NCCs (comparing Figures 10 between groups a_1, b_1 and c_1) also support this argument since particle size in NCCs was insensitive to change in that of the original MCC powders, as discussed earlier.

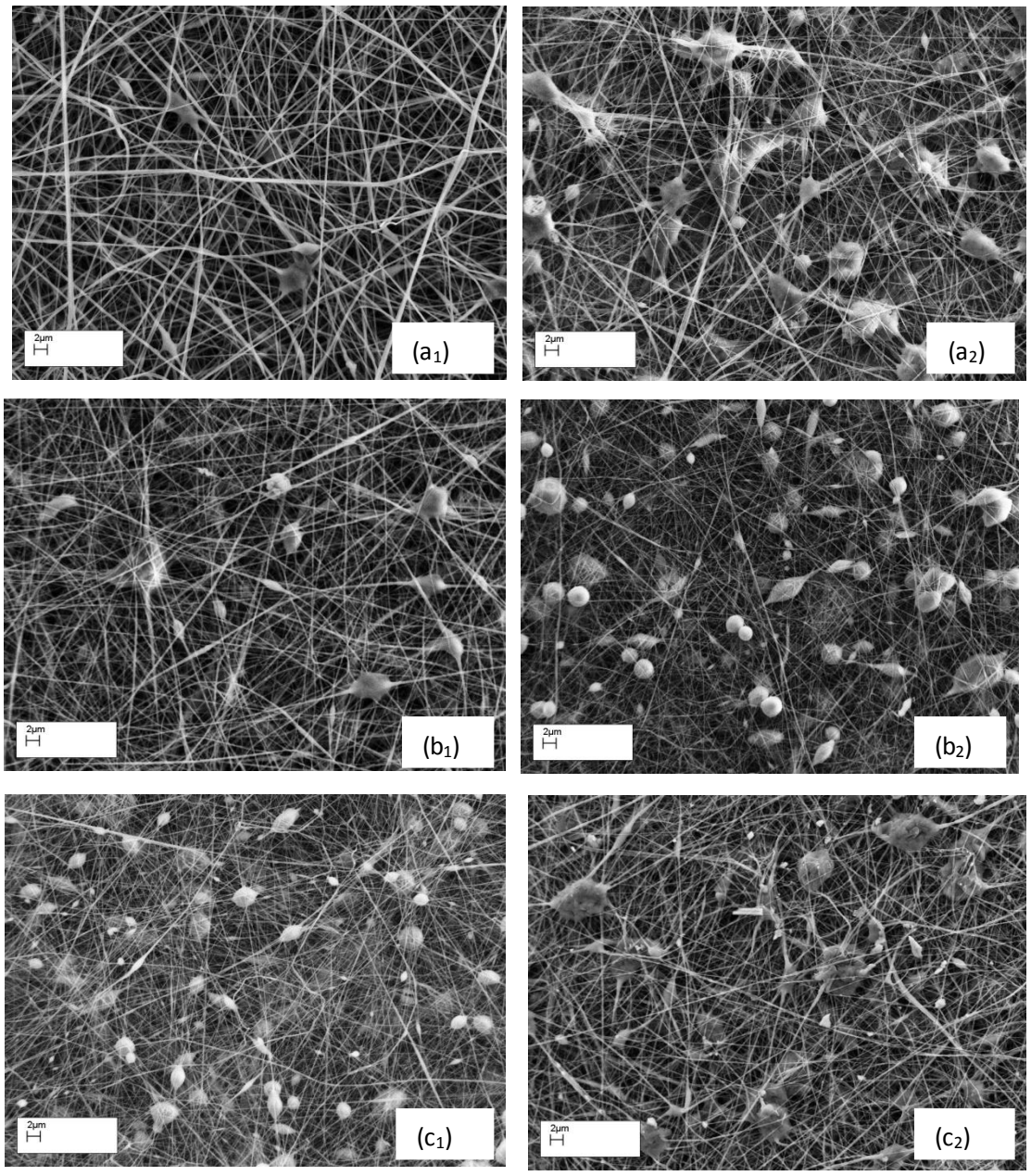

Figure 6.6: SEM microscopy showing morphologies of nanofibre membranes electrospun from the NCC suspensions: a_1) NCC20-1.1%; a_2) NCC20-5.4%; b_1) NCC50-1.1%; b_2) NCC50-5.4%; c_1) NCC90-1.1%; c_2) NCC90-5.4%.

6.3. Crystalline properties

6.3.1. Total PVDF crystallinity analysis, X_c

As described in section 4.4.1, total crystallinity, X_c for the PVDF/cellulose systems were calculated using Equation (4.1) and shown in Table 6.1.

Table 6.1: Heat of fusion ($\Delta H_{m,s}$), concentration of PVDF in the DSC samples (ω_P) and crystallinity of the PVDF matrix (X_c)

Sample ID	$\Delta H_{m,s}$ (J/g)	ω_P ($wt\%$)	X_c (%)
Neat PVDF	33.3	100.0	31.9
MCC20-10.2%	20.8	91.0	21.8
MCC50-10.2%	35.1	91.0	36.8
MCC90-10.2%	27.8	91.0	29.2
MCC20-9.2% (PEG)	19.0	83.4	21.7
MCC50-9.2% (PEG)	24.0	83.4	27.5
MCC90-9.2% (PEG)	20.2	83.4	23.1
NCC20-1.1%	21.7	99.0	21.0
NCC20-5.4%	19.9	95.3	19.9
NCC50-1.1%	24.8	99.0	23.9
NCC50-5.4%	26.1	95.3	26.2
NCC90-1.1%	29.4	99.0	28.4
NCC90-5.4%	28.5	95.3	28.6

Looking into each electrospun composite system in more details in Table 6.1 in comparison with the electrospun neat PVDF, the inclusion of MCC and NCC fillers had resulted in a significant reduction in X_c. In terms of effect of loading on X_c in the PVDF/NCC systems, no

significant influence could be concluded. Meanwhile addition of PEG in the systems reduced X_c.

6.3.2. Analysis for relative fraction of β phase, F_β, in total crystalline PVDF

As described in 4.4.2, relative fraction of β phase, F_β, in the total crystalline phases of PVDF was obtained from FTIR spectra of the as-received PVDF powder, the electrospun membranes and cast films from the PVDF/cellulose suspensions. From intensities of absoptions A_α and A_β listed in Appendix I, repeatability of F_β calculated using Equation 4.2 are shown in Table 6.2 and plotted in Figure 6.7.

The influence of loading on F_β in Table 6.2 or Figure 6.7 vary with filler types. For the PVDF/MCC system, addition of MCC had, in general, significantly increased F_β (by a maximum 17.5%) in comparison with that of neat PVDF suggesting that the MCCs have played a role in promoting of β phase formation (possibly more by heterogeneity induction of β phase than nucleation, considering the lowered *Xc* discussed earlier). However, F_β decreased as loading of MCCs increased and hence high loadings impeded β phase formation possibly due to higher absorption of PVDF molecules that reduced chain mobility. At the same concentration, inclusion of PEG resulted in drops of F_β in all three groups (containing MCC20, MCC50 and MCC90). And hence in addition to the lack of contribution to dispersion stability (mentioned earlier), PEG also had negative impacts on β phase formation.

Table 6.2: Relative fraction of β phase, F_β for the neat PVDF electrospun membrane and electrospun PVDF/cellulose composites

Sample ID	F_β (%)
Neat PVDF	**72.0**
MCC20-1.1%	**84.6**
MCC20-10.2%	**81.8**
MCC20-9.2% (PEG)	**75.3**
MCC20-37.3%	**71.5**
MCC50-1.1%	**81.4**
MCC50-10.2%	**83.6**
MCC50-9.2% (PEG)	**79.5**

MCC50-37.3%	**74.0**
MCC90-10.2%	**83.5**
MCC90-9.2% (PEG)	**80.5**
MCC90-37.3%	**76.7**
NCC20-1.1%	**82.0**
NCC20-5.4%	**83.8**
NCC50-1.1%	**82.6**
NCC50-5.4%	**79.6**
NCC90-1.1%	**72.0**
NCC90-5.4%	**78.0**

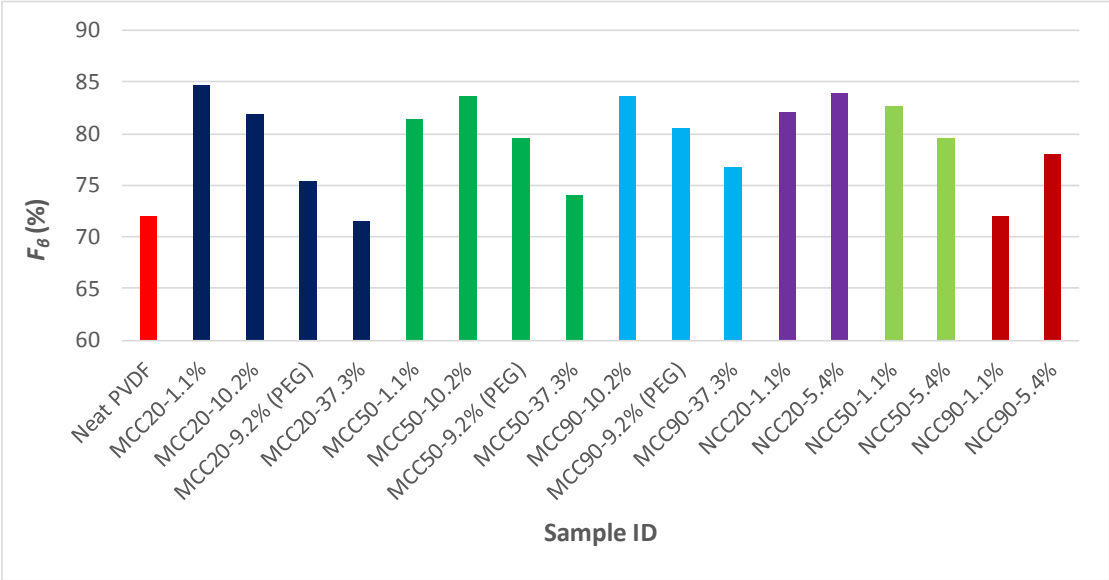

Figure 6.7: Relative fraction of β phase, F_β for the neat PVDF electrospun membrane and electrospun PVDF/cellulose composites

Similar to PVDF/MCC system, addition of NCCs has also increased F_β compared with that of neat PVDF suggesting that NCCs have played a role in promoting β phase formation. Inclusion of NCCs at the same loading of 0.1 *wt*% produced less degrees of increases in F_β in comparison with that of MCCs. This indicate lack of benefit in promotion of β phase formation by the extra effort of particle size refinement from MCC to NCCs. For 5 folds of increase in loading from 0.1 to 0.5 wt%, F_β hardly changed for PVDF/NCC20 and PVDF/NCC50. This may be attractable to the insensitivity of the driving force for promoting β phase formation in such fine fillers.

6.3.3. Volume fraction of β phase in the PVDF and PVDF/cellulose composites, v_β

As described in section 4.4.3 using Equation 4.3 and density of the β phase, ρ_β , in Table 6.3, volume fraction of β phase in PVDF and PVDF/cellulose composites, v_β, are calculated as shown in Table 6.4 and plotted in Figure 6.8.

Table 6.3: Density of the PVDF and cellulosic fillers

Materials	Density* (*g/ml*)
Amorphous-PVDF	**1.68**
α-PVDF	**1.92**
β-PVDF	**1.97**

* (Ameduri, 2009)

Table 6.4: Volume fraction of β phase in the PVDF and PVDF/cellulose composites, v_β

Samples	v_β (*vol%*)
The as-received PVDF	**18.2**
neat PVDF	**20.5**
MCC20-10.2%	**11.7**
MCC20-9.2% (PEG)	**9.6**
MCC50-10.2%	**21.5**
MCC50-9.2% (PEG)	**13.4**
MCC90-10.2%	**16.9**
MCC90-9.2% (PEG)	**11.4**
NCC20-1.1%	**15.0**
NCC20-5.4%	**13.9**
NCC50-1.1%	**17.2**
NCC50-5.4%	**17.5**
NCC90-1.1%	**18.0**
NCC90-5.4%	**18.8**

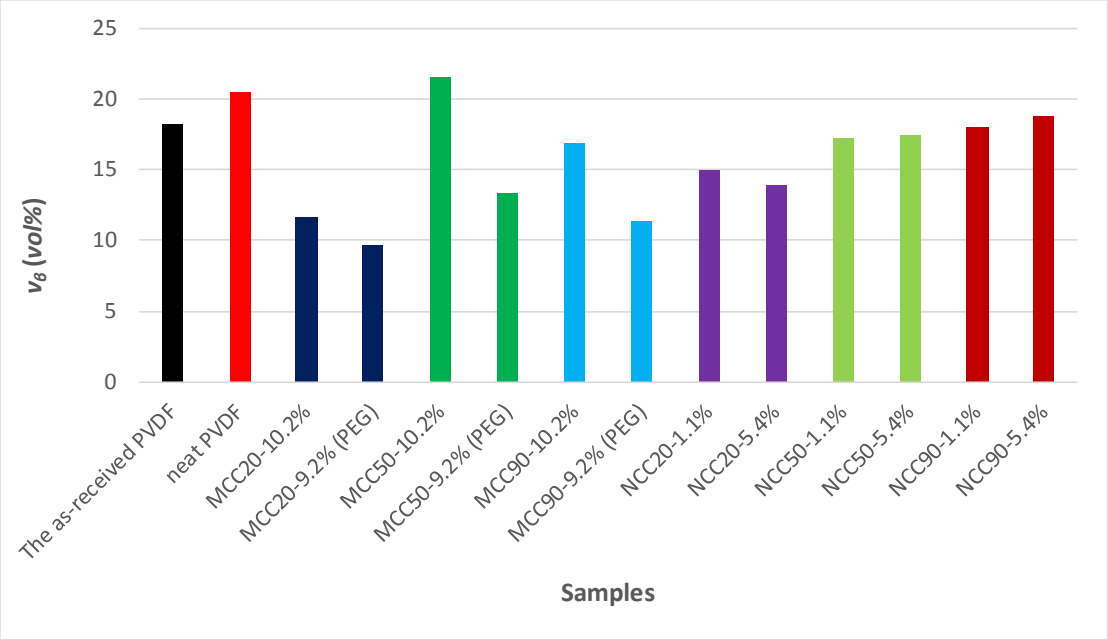

Figure 6.8: Volume fraction of β phase in the PVDF and PVDF/cellulose composites

As shown in Table 6.4 or Figure 6.8, volume fraction of β phase in the samples, v_β for electrospun neat PVDF are higher in general compared with the PVDF/cellulose composites (except for MCC50-10.2%). At the same MCC loading of 1 *wt%* within the PVDF/MCC system, particle size 50 μm appeared to give a relatively high v_β. The inclusion of PEG, as the influence on X_c and F_β discussed previously, gave rise to reduction in v_β and hence, once again had no benefit at all.

For the PVDF/NCC system, no significant influence could be found from the three NCCs and the 5-fold difference in loading (0.1 to 0.5 *wt%*). This is somewhat expected as no apparent difference in particle sizes between them and the lack of promotion of β phase formation by such fine particles.

6.4. Piezoelectric properties

The influence of distance between the measurement points to the sample edge and the angle variation from their horizontal position is shown in Table 6.5, where the mean piezoelectric coefficient d_{33} was obtained from averaging of 5 points of the same distance from the edge. As all the selected samples show the same trend, only one is presented here and the others can be found in Appendix II.

Table 6.5. Piezoelectric coefficient, d_{33} results showing the influence of distances to the edge of sample and angle from the horizontal position for NCC20-1.1%

Distance (*mm*)	d_{33} (*pC/N*)	SD (*pC/N*)
5	14.20	±0.45
10	14.40	±0.89
15	14.00	±0.71
20	13.20	±0.45
25	12.80	±0.45
Angle	**d_{33} (*pC/N*)**	**SD (*pC/N*)**
12°	9.60	±0.55
24°	10.80	±1.64
36°	11.40	±1.82
48°	12.60	±1.52
60°	11.80	±1.64

Table 6.5 shows that d_{33} for the same distance are consistent (low standard deviations, SD). No systematic variations can be found as a function of the distance and thus influence of choices of measurement position points can be neglected. A noticeable overall reduction of d_{33} values can be observed when the membranes were deviated from the required horizontal position, due most likely to additional stress generated from the bending, and thus care must be taken to avoid such bending and minimise the measurement errors.

Using the 5×5 d_{33} measurement point matrix, the mean d_{33} was obtained from averaging that of the 25 points. The results are summarised in Table 6.6 and plotted in Figure 6.9.

Table 6.6: Results of d_{33} measurement for electrospun neat PVDF and the PVDF/cellulose composite membranes

Sample ID	d_{33} (*pC/N*)	SD (*pC/N*)
neat PVDF	10.00	±0.71
MCC20-10.2%	11.80	±0.98
MCC20-9.2% (PEG)	8.83	±2.17

MCC50-10.2%	**11.33**	**±0.95**
MCC50-9.2% (PEG)	**10.40**	**±0.52**
MCC90-10.2%	**11.23**	**±2.71**
MCC90-9.2% (PEG)	**10.17**	**±2.06**
NCC20-1.1%	**8.67**	**±0.52**
NCC20-5.4%	**8.40**	**±1.34**
NCC50-1.1%	**12.20**	**±0.84**
NCC50-5.4%	**12.20**	**±0.45**
NCC90-1.1%	**14.33**	**±0.82**
NCC90-5.4%	**13.50**	**±0.58**

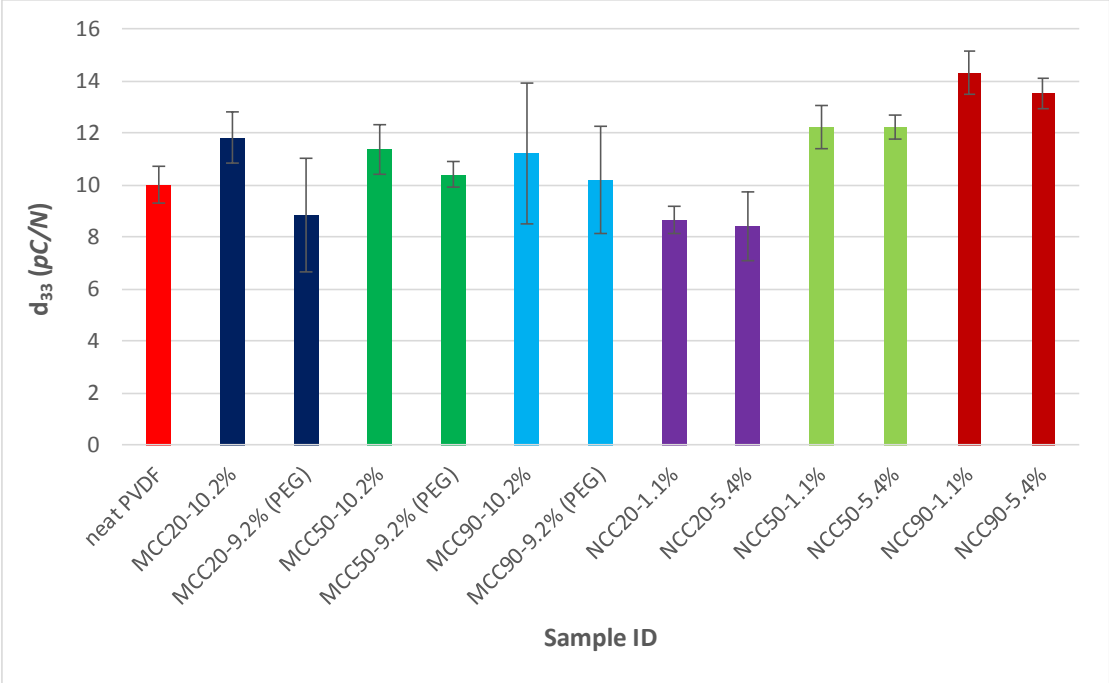

Figure 6.9: Results of d_{33} measurement for electrospun neat PVDF and the PVDF/cellulose composite membranes.

From Table 6.6 or Figure 6.9, at the same 1 *wt*% loading of the MCCs, d_{33} for the electrospun neat PVDF (10 *pC/N*) has been succeeded by PVDF/MMCs without PEG but no apparent influence from particle size could be identified. This can also be attributable to the low particle population density for such large particles at the loading levels. PVDF/MCC

composite and hence PEG had negative impact on all parameters related to piezoelectricity (X_c, F_β, v_β and d_{33}) and hence the incorporation of which had no benefit at all!

In the PVDF/NCC system, d_{33} was insensitive to the 5-fold loading difference but the trend of increasing from NCC20 to NCC90 has been mirrored in d_{33} and thus for this particular system, there is a clear correlation between v_β and d_{33}, as predicted by the proposed hypothesis. In view of the constant increase in both v_β and d_{33} from NCC20 to NCC90 (as shown in Figures 6.8 and 6.9), it seems to be reasonable to suggest that the mean particle size in the NCCs increase in the same order from NCC20 to NCC90 as argued in section 2.2. For particle in the range of nano- to micrometre sizes, too fine particles reduce the site area of nucleation and low heterogeneity and hence poorer β phase formation.

6.5. Summary

Electrospun PVDF/MCC and PVDF/NCC nanocomposites with different loadings were manufactured by electrospinning process, and influence of fillers on crystalline and piezoelectric properties were studied.

No apparent difference in dispersion could be observed for those with or without PEG. The inclusion of MCC and NCC fillers had resulted in a significant reduction in X_c in comparison with the electrospun neat PVDF. In terms of effect of loading on X_c, no significant influence could be concluded in the PVDF/NCC systems. Meanwhile addition of PEG in the systems reduced X_c.

Addition of MCC had significantly increased F_β (by a maximum 17.5%) in comparison with that of neat PVDF for the PVDF/MCC system suggesting that the MCCs have played a role in promoting of β phase formation possibly more by heterogeneity induction of β phase than nucleation. However, F_β decreased as loading of MCCs increased and hence high loadings impeded β phase formation possibly due to higher absorption of PVDF molecules that reduced chain mobility. At the same concentration, inclusion of PEG resulted in drops of F_β in all three groups (containing MCC20, MCC50 and MCC90). And hence in addition to the lack of contribution to dispersion stability, PEG also had negative impacts on β phase formation. Addition of NCCs has also increased F_β compared with that of neat PVDF suggesting that NCCs have played a role in promoting β phase formation. Inclusion of NCCs

at the same loading of 0.1 *wt*% produced less degrees of increases in F_β in comparison with that of MCCs. This indicate lack of benefit in promotion of β phase formation by the extra effort of particle size refinement from MCC to NCCs. For 5 folds of increase in loading, F_β hardly changed for PVDF/NCC20 and PVDF/NCC50. This may be attractable to the insensitivity of the driving force for promoting β phase formation in such fine fillers.

Volume fraction of β phase in the samples, v_β for electrospun neat PVDF are higher in general compared with the PVDF/cellulose composites (except for MCC50-10.2%). At the same MCC loading of 1 wt% within the PVDF/MCC system, particle size 50 μm appeared to give a relatively high v_β. The inclusion of PEG, as the influence on X_c and F_β discussed previously, gave rise to reduction in v_β and hence, once again had no benefit at all.

For the PVDF/NCC system, no significant influence could be found from the three NCCs and the 5-fold difference in loading. This is somewhat expected as no apparent difference in particle sizes between them and the lack of promotion of β phase formation by such fine particles.

At the same 1 *wt*% loading of the MCCs, d_{33} for the electrospun neat PVDF (10 *pC/N*) has been succeeded by PVDF/MCCs without PEG but no apparent influence from particle size could be identified. This can also be attributable to the low particle population density for such large particles at the loading levels. PVDF/MCC composite and hence PEG had negative impact on all parameters related to piezoelectricity (X_c, F_β, v_β and d_{33}) and hence the incorporation of which had no benefit at all. In the PVDF/NCC system, d_{33} was insensitive to the 5-fold loading difference but the trend of increasing from NCC20 to NCC90 has been mirrored in d_{33} and thus there is a clear correlation between v_β and d_{33} for this system. In view of the constant increase in both v_β and d_{33} from NCC20 to NCC90, it seems to be reasonable to suggest that the mean particle size in the NCCs increase in the same order from NCC20 to NCC90. For particle in the range of nano- to micrometre sizes, too fine particles reduce the site area of nucleation and low heterogeneity and hence poorer β phase formation.

Chapter 7. Comparison across the three systems

In order to compare across the influences of the three class of filler systems on β phase crystallinity and correlate to the piezoelectric property of the PVDF composites, the β phase volume fraction, v_β (*vol%*) in the composites and the piezoelectric coefficient, d_{33} are expressed as a function of *vol%* of fillers in Figure 7.1 and 7.2, respectively. Owning to the large differences in filler density, *vol%* of filler vary across a narrower range (0- 32 *vol%*) in comparison with the *wt%* (0- 60 *wt%*) of the fillers, both on dry basis, and enabled sensible comparison across the composite systems.

The regions in Figure 7.1 can be divided into

a) Effective promoters for β phase formation - those give rise to high v_β values (e.g. >15%) at low volume loading (e.g. < 10 %). These include NCC90, NCC50 and halloysite.
b) Poor promoters for β phase formation- those give rise to low v_β values (e.g. <12%) at high volume loading (e.g. > 10 %). These include ZnO, BT and GO.
c) The highest v_β value achieved is approximately 22% by MCC50 at 10.2 *vol%*.
d) The lowest v_β value is only 0.2% given by CNT at 0.25 *vol%*.

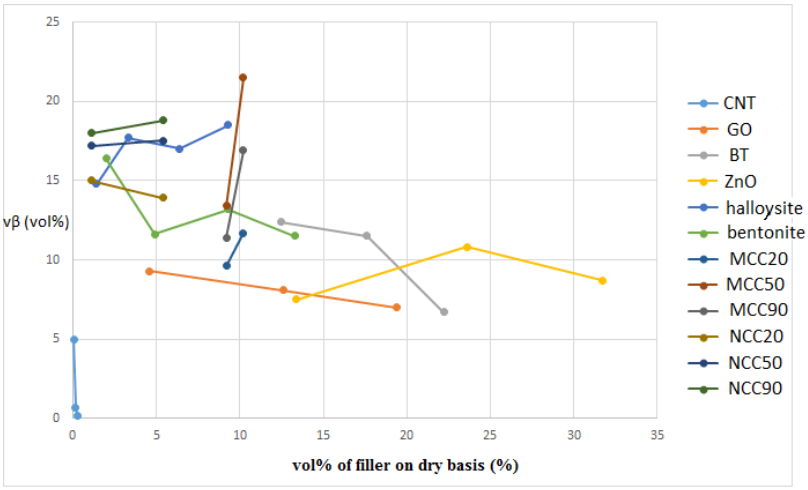

Figure 7.1: β phase volume fraction, v_β (*vol%*) in the composites as function of filler volume loading (vol%) showing their effectiveness in β phase promotion.

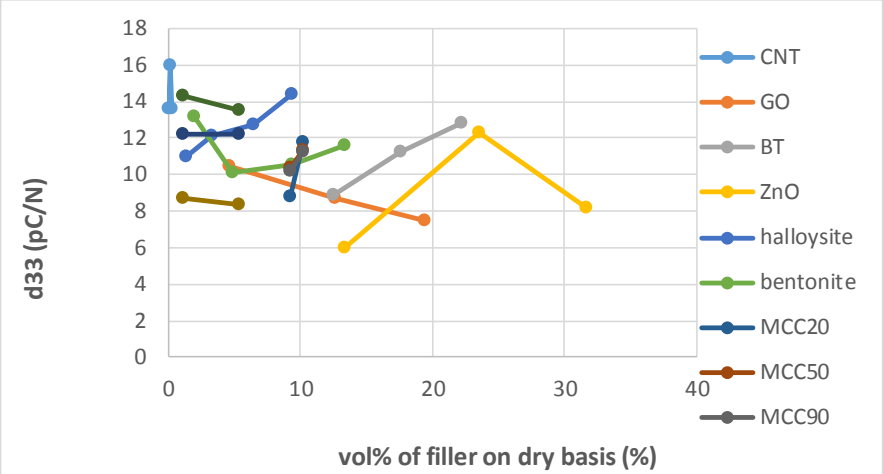

Figure 7.2: piezoelectric coefficient, d_{33} of composites as function of filler volume loading (vol%) showing their effectiveness in the enhancement of piezoelectric property.

Similarly, regions in Figure 7.2 can be divided into

a) Effective promoters for d_{33} - those give rise to high d_{33} values (e.g. >12 *pC/N*) at low volume loading (e.g. < 10 %). These include CNT, NCC90, NCC50 and halloysite.
b) Poor promoters for d_{33} - those give rise to low d_{33} values (e.g. <12 *pC/N*) at high volume loading (e.g. > 10 %). These include ZnO, BT and GO.
c) The highest d_{33} value achieved is approximately 16 *pC/N* by CNT at 0.15 *vol%* .
d) The lowest d_{33} value is 6 *pC/N* given by ZnO at 13.4 *vol%*.

In terms of correlation between the value of v_β and $d_{33,}$ NCC90, NCC50 and Halloysite showed good correlation. These are fillers without piezoelectricity.

On contrary, CNT displayed unexpected correlation, indicating that v_β is not the only factor that affect d_{33} value for the PVDF/CNT composites. Electric conductivity resulted from CNT and potential promotion of β polycrystalline orientation might have played a vital part. GO was expected to give similar performance as CNT. The flocculated low aspect ratio of flakes may have led to low electric connectivity and poorer β polycrystalline orientation.

Judged from low efficiency in promotion of β phase formation, BT and ZnO with piezoelectricity give rise to moderate to high d_{33} values and this discrepancy from the hypothesis can be attributed to the contribution from their intrinsic piezoelectricity.

Chapter 8. Conclusions and proposed further work

Conclusions:

- A comprehensive range of filler systems covering three classes of materials: Ceramics (BT, ZnO and two nanoclays halloysite and bentonite), carbon (CNT and GO), and cellulose (MCCs and NCCs) are studied in electrospun PVDF composite membranes. Influence of filler type and loading on crystalline and piezoelectric properties of the composites were characterised and analysed.

- In terms of correlation between the value of v_β and d_{33}, NCC90, NCC50 and Halloysite showed good correlation. These are fillers without piezoelectricity.

  On contrary, CNT displayed unexpected correlation, indicating that v_β is not the only factor that affect d_{33} value for the PVDF/CNT composites. Electric conductivity resulted from CNT and potential promotion of β polycrystalline orientation might have played a vital part. GO was expected to give similar performance as CNT. The flocculated low aspect ratio of flakes may have led to low electric connectivity and poorer β polycrystalline orientation.

  Judged from low efficiency in promotion of β phase formation, BT and ZnO with piezoelectricity give rise to moderate to high d_{33} values and this discrepancy from the hypothesis can be attributed to the contribution from their intrinsic piezoelectricity.

- The inclusion of PEG, in PVDF/MCCs system did not improve dispersion and imposed negative impact on X_c and F_β and v_β, thus had no benefit at all.

- In comparison with MCCs (20-90 μm), particle size of NCCs are by far much finer (<4μm), confirming the effectiveness size reduction in the hydrolysis treatment.

- Beads formation and population density in electrospun nanofibre membranes was found to be closely related to the sizes of coarse particles as well as undispersed agglomerates and their fractions via breaking-up of the jets.

- All three types of filler had resulted in reduction in total crystallinity X_c to varying degrees, suggesting that they had no contribution to overall crystallisation of PVDF.

- Inclusion of carbon fillers reduced total crystallinity X_c and relative β phase ratio, F_β, leading overall decrease of β volume fraction v_β, indicating that CNT and GO are not promoting formation of β phase.

- Inclusion of ceramic fillers reduced total crystallinity X_c. In comparison with the neat PVDF, the relative β phase ratio F_β is lower for PVDF/BT and PVDF/ZnO composites, and is relatively higher at certain loadings for PVDF/nanoclay composites, but both lead to a decrease in β volume fraction v_β, indicating that influence of ceramic fillers on X_c dominated over that on F_β on the formation of β phase.

- The ceramic fillers gave rise to comparable F_β to the neat PVDF but owing to X_c reduction, v_β values in the PVDF/ceramic composites are still relatively lower than that of neat PVDF.

- The inclusion of PEG in PVDF/MCC system, reduced both X_c and F_β, and therefore gave rise to a reduction in v_β and hence, in addition to lack of promotion for suspension dispersion, it had no benefit at all.

- Piezoelectric coefficient d_{33} for the electrospun neat PVDF can be succeeded by that of all the PVDF composites at certain filler loadings.

Proposed further work:

- Surfactant/dispersant/stabiliser can be used to reduce agglomerates/flocculations in electrospinning suspensions in order to improve filler dispersion.

- Rotating drum/disk collector can be used to produce membrane with much improved fibre alignment and potential enhanced piezoelectric properties.

- Maximum voltage output measurement can be conducted to assess practical performance of the membranes.

- Filler effect on crystal orientation can be examined for β polycrystalline.

- Mechanical properties of the membranes can be checked.

List of references

Abdulkhani, A., Marvast, E.H., Ashori, A., Hamzeh, Y. and Karimi, A.N. (2013) 'Preparation of cellulose/polyvinyl alcohol biocomposite films using 1-n-butyl-3-methylimidazolium chloride', International journal of biological macromolecules, 62, pp. 379-386.

Abraham, E., Deepa, B., Pothan, L., Jacob, M., Thomas, S., Cvelbar, U. and Anandjiwala, R. (2011) 'Extraction of nanocellulose fibrils from lignocellulosic fibres: a novel approach', Carbohydrate Polymers, 86(4), pp. 1468-1475.

Alamri, H. and Low, I.M. (2012) 'Microstructural, mechanical, and thermal characteristics of recycled cellulose fiber-halloysite-epoxy hybrid nanocomposites', Polymer Composites, 33(4), pp. 589-600.

Al-Saleh, M.H. and Sundararaj, U. (2009) 'Electromagnetic interference shielding mechanisms of CNT/polymer composites', Carbon, 47(7), pp. 1738-1746.

Ameduri, B. (2009) 'From vinylidene fluoride (VDF) to the applications of VDF-containing polymers and copolymers: recent developments and future trends†', Chem.Rev, 109(12), pp. 6632-6686.

Arnau, A. (2008) 'Piezoelectric transducers and applications'. Springer.

Atabani, A.E., Silitonga, A.S., Badruddin, I.A., Mahlia, T., Masjuki, H. and Mekhilef, S. (2012) 'A comprehensive review on biodiesel as an alternative energy resource and its characteristics', Renewable and sustainable energy reviews, 16(4), pp. 2070-2093.

Azizi Samir, My Ahmed Said, Alloin, F. and Dufresne, A. (2005) 'Review of recent research into cellulosic whiskers, their properties and their application in nanocomposite field', Biomacromolecules, 6(2), pp. 612-626.

Bafqi, M.S.S., Bagherzadeh, R. and Latifi, M. (2015) 'Fabrication of composite PVDF-ZnO nanofiber mats by electrospinning for energy scavenging application with enhanced efficiency', Journal of Polymer Research, 22(7), pp. 1-9.

Bai, W. and Li, K. (2009) 'Partial replacement of silica with microcrystalline cellulose in rubber composites', Composites Part A: Applied Science and Manufacturing, 40(10), pp. 1597-1605.

Baji, A., Mai, Y., Abtahi, M., Wong, S., Liu, Y. and Li, Q. (2013) 'Microstructure development in electrospun carbon nanotube reinforced polyvinylidene fluoride fibers and its influence on tensile strength and dielectric permittivity', Composites Science and Technology, 88, pp. 1-8.

Baji, A., Mai, Y., Li, Q. and Liu, Y. (2011) 'Nanoscale investigation of ferroelectric properties in electrospun barium titanate/polyvinylidene fluoride composite fibers using piezoresponse force microscopy', Composites Science and Technology, 71(11), pp. 1435-1440.

Bakshi, S., Lahiri, D. and Agarwal, A. (2010) 'Carbon nanotube reinforced metal matrix composites-a review', International Materials Reviews, 55(1), pp. 41-64.

Banerjee, M., Sain, S., Mukhopadhyay, A., Sengupta, S., Kar, T. and Ray, D. (2014) 'Surface treatment of cellulose fibers with methylmethacrylate for enhanced properties of in situ polymerized PMMA/cellulose composites', Journal of Applied Polymer Science, 131(2).

Banerjee, S., Singh, S., Bhattacharya, S.S. and Chattopadhyay, P. (2013) 'Trivalent ion cross-linked pH sensitive alginate-methyl cellulose blend hydrogel beads from aqueous template', International journal of biological macromolecules, 57, pp. 297-307.

Barud, H.S., Souza, J.L., Santos, D.B., Crespi, M.S., Ribeiro, C.A., Messaddeq, Y. and Ribeiro, S.J. (2011) 'Bacterial cellulose/poly (3-hydroxybutyrate) composite membranes', Carbohydrate Polymers, 83(3), pp. 1279-1284.

Bendi, R. and Imae, T. (2013) 'Renewable catalyst with Cu nanoparticles embedded into cellulose nano-fiber film', RSC Adv., 3(37), pp. 16279-16282.

Benenson, W. and Stöcker, H. (2002) Handbook of physics. Springer Science & Business Media.

Bentchikou, M., Guidoum, A., Scrivener, K., Silhadi, K. and Hanini, S. (2004) 'Effect of cellulose fibre on the thermal and mechanical properties of cement paste', Proc. International Conference RILEM. , 724-730.

Bodaghi, H. and Sinangil, M. (2009) Meltblown nonwoven webs including nanofibers and apparatus and method for forming such meltblown nonwoven webs.

Bondeson, D., Mathew, A. and Oksman, K. (2006) 'Optimization of the isolation of nanocrystals from microcrystalline cellulose by acid hydrolysis', Cellulose, 13(2), pp. 171-180.

Borg, K. (2014) 'Energy Harvesting in Wireless Applications', CODEN: LUTEDX/TEIE.

Boukai, A.I., Bunimovich, Y., Tahir-Kheli, J., Yu, J., Goddard Iii, W.A. and Heath, J.R. (2008) 'Silicon nanowires as efficient thermoelectric materials', Nature, 451(7175), pp. 168-171.

Breuer, O. and Sundararaj, U. (2004) 'Big returns from small fibers: a review of polymer/carbon nanotube composites', Polymer composites, 25(6), pp. 630-645.

Buzea, C., Pacheco, I.I. and Robbie, K. (2007) 'Nanomaterials and nanoparticles: sources and toxicity', Biointerphases, 2(4), pp. MR17-MR71.

Cai, J., Yang, S. and Li, T. (2011) 'Logistic distributed activation energy model–Part 2: Application to cellulose pyrolysis', Bioresource technology, 102(3), pp. 3642-3644.

Chang, C., Fuh, Y. and Lin, L. (2009) 'A direct-write piezoelectric PVDF nanogenerator', Solid-State Sensors, Actuators and Microsystems Conference, 2009. TRANSDUCERS 2009. International. IEEE, 1485-1488.

Chanmal, C. and Jog, J. (2008) 'Dielectric relaxations in PVDF/BaTiO3 nanocomposites', Express Polymer Letters, 2(4), pp. 294-301.

Chanmal, C.V. and Jog, J.P. (2011) 'Electrospun PVDF/BaTiO3 nanocomposites: polymorphism and thermal emissivity studies', International Journal of Plastics Technology, 15(1), pp. 1-9.

Chanunpanich, N. and Byun, H. (2007) 'Alignment of electrospun polystyrene with an electric field', Journal of Applied Polymer Science, 106(6), pp. 3648-3652.

Chanunpanich, N., Lee, B. and Byun, H. (2008) 'A study of electrospun PVDF on PET sheet', Macromolecular research, 16(3), pp. 212-217.

Chen, S., Sun, B., Huang, G., Guo, H. and Wang, S. (2013) 'Effects of an (Intumescent flame retardant)-montmorillonite combination on the thermal stability and fire-retardant properties of LDPE/EVA nanocomposites', Journal of Vinyl and Additive Technology, 19(4), pp. 285-292.

Chen, W.D., Jung, H.M., Jang, W.G., Hong, B.P. and Byun, H.S. (2013) 'Preparation and Characterization of Poly (vinylidene fluoride)/Graphene Oxide Composite Nanofiber for MF Application', Advanced Materials Research. Trans Tech Publ, 1715-1719.

Choi, W., Chung, D., Kang, J., Kim, H., Jin, Y., Han, I., Lee, Y., Jung, J., Lee, N. and Park, G. (1999) 'Fully sealed, high-brightness carbon-nanotube field-emission display', Applied Physics Letters, 75(20), pp. 3129-3131.

Cialani, C. and Perman, K. (2014) 'Policy instruments to improve energy efficiency in buildings'.

Corral-Flores, V. and Bueno-Baqués, D. (2011) Flexible Ferroelectric BaTiO3-PVDF Nanocomposites. INTECH Open Access Publisher.

Crabtree, G.W. and Lewis, N.S. (2007) 'Solar energy conversion', Physics Today, 60(3), pp. 37-42.

Dang, Z., Shen, Y. and Nan, C. (2002) 'Dielectric behavior of three-phase percolative Ni–BaTiO3/polyvinylidene fluoride composites', Applied Physics Letters, 81(25), pp. 4814-4816.

Dang, Z., Wang, H., Zhang, Y. and Qi, J. (2005) 'Morphology and dielectric property of homogenous $BaTiO_3$/PVDF nanocomposites prepared via the natural adsorption action of nanosized $BaTiO_3$', Macromolecular rapid communications, 26(14), pp. 1185-1189.

Dreyer, D.R., Park, S., Bielawski, C.W. and Ruoff, R.S. (2010) 'The chemistry of graphene oxide', Chemical Society Reviews, 39(1), pp. 228-240.

Duan, H., Kuang, M. and Wang, Y.A. (2010) 'Quantum dots with multivalent and compact polymer coatings for efficient fluorescence resonance energy transfer and self-assembled biotagging', Chemistry of Materials, 22(15), pp. 4372-4378.

Dufresne, A. (2013) 'Nanocellulose: a new ageless bionanomaterial', Materials Today, 16(6), pp. 220-227.

Eichhorn, S. and Davies, G. (2006) 'Modelling the crystalline deformation of native and regenerated cellulose', Cellulose, 13(3), pp. 291-307.

Eichhorn, S.J. (2011) 'Cellulose nanowhiskers: promising materials for advanced applications', Soft Matter, 7(2), pp. 303-315.

Ellison, C.J., Phatak, A., Giles, D.W., Macosko, C.W. and Bates, F.S. (2007) 'Melt blown nanofibers: fiber diameter distributions and onset of fiber breakup', Polymer, 48(11), pp. 3306-3316.

Emanetoglu, N., Gorla, C., Liu, Y., Liang, S. and Lu, Y. (1999) 'Epitaxial ZnO piezoelectric thin films for saw filters', Materials Science in Semiconductor Processing, 2(3), pp. 247-252.

Enseñat Porcel, J. (2011) 'Developing and testing an amplifier system for piezoelectric sensors'.

Erdtman, E., Satyanarayana, K.C. and Bolton, K. (2012) 'Simulation of α-and β-PVDF melting mechanisms', Polymer, 53(14), pp. 2919-2926.

Fauchais, P., Etchart-Salas, R., Rat, V., Coudert, J., Caron, N. and Wittmann-Ténèze, K. (2008) 'Parameters controlling liquid plasma spraying: Solutions, sols, or suspensions', Journal of Thermal Spray Technology, 17(1), pp. 31-59.

Fernando, K.S., Lin, Y., Wang, W., Kumar, S., Zhou, B., Xie, S., Cureton, L.T. and Sun, Y. (2004) 'Diminished band-gap transitions of single-walled carbon nanotubes in complexation with aromatic molecules', Journal of the American Chemical Society, 126(33), pp. 10234-10235.

Filipe, V., Hawe, A. and Jiskoot, W. (2010) 'Critical evaluation of Nanoparticle Tracking Analysis (NTA) by NanoSight for the measurement of nanoparticles and protein aggregates', Pharmaceutical research,27(5), pp. 796-810.

Frenger, P., Linnell, O. and Moe, J. (2014) Method and arrangement in a communication system.

Frenger, P., Linnell, O. and Moe, J. (2014) Method and arrangement in a communication system.

Fu, J., Hou, Y., Zheng, M., Wei, Q., Zhu, M. and Yan, H. (2015) 'Improving Dielectric Properties of PVDF Composites by Employing Surface Modified Strong Polarized BaTiO3 Particles Derived by Molten Salt Method', ACS applied materials & interfaces, 7(44), pp. 24480-24491.

Gabr, M.H., Phong, N.T., Abdelkareem, M.A., Okubo, K., Uzawa, K., Kimpara, I. and Fujii, T. (2013) 'Mechanical, thermal, and moisture absorption properties of nano-clay reinforced nano-cellulose biocomposites', Cellulose, 20(2), pp. 819-826.

Gandhi, M., Bohra, H., Daniel, V. and Gupta, A. (2010) 'Nanotechnology in blood brain barrier: a review', Int.J.Pharmaceut.Biol.Arch, 1(1), pp. 37-43.

Gilman, J.W. (1999) 'Flammability and thermal stability studies of polymer layered-silicate (clay) nanocomposites', Applied Clay Science, 15(1), pp. 31-49.

Giordani, S., Bergin, S.D., Nicolosi, V., Lebedkin, S., Kappes, M.M., Blau, W.J. and Coleman, J.N. (2006) 'Debundling of single-walled nanotubes by dilution: observation of large populations of individual nanotubes in amide solvent dispersions', The Journal of Physical Chemistry B, 110(32), pp. 15708-15718.

Gojny, F.H., Nastalczyk, J., Roslaniec, Z. and Schulte, K. (2003) 'Surface modified multi-walled carbon nanotubes in CNT/epoxy-composites', Chemical physics letters, 370(5), pp. 820-824.

Gonçalves, R., Martins, P., Caparrós, C., Martins, P., Benelmekki, M., Botelho, G., Lanceros-Mendez, S., Lasheras, A., Gutiérrez, J. and Barandiarán, J. (2013) 'Nucleation of the electroactive β-phase, dielectric and magnetic response of poly (vinylidene fluoride) composites with Fe 2 O 3 nanoparticles', Journal of Non-Crystalline Solids, 361, pp. 93-99.

Gong, H., Hu, J., Wang, J., Ong, C. and Zhu, F. (2006) 'Nano-crystalline Cu-doped ZnO thin film gas sensor for CO', Sensors and Actuators B: Chemical, 115(1), pp. 247-251.

Gregorio Jr, R. and Cestari, M. (1994) 'Effect of crystallization temperature on the crystalline phase content and morphology of poly (vinylidene fluoride)', Journal of Polymer Science Part B: Polymer Physics, 32(5), pp. 859-870.

Gregorio Jr, R. and de Souza Nociti, N Chaves Pereira (1995) 'Effect of PMMA addition on the solution crystallization of the alpha and beta phases of poly (vinylidene fluoride) (PVDF)', Journal of Physics D: Applied Physics, 28(2), pp. 432.

Gregorio Jr, R., Cestari, M. and Bernardino, F. (1996) 'Dielectric behaviour of thin films of β-PVDF/PZT and β-PVDF/BaTiO3 composites', Journal of Materials Science, 31(11), pp. 2925-2930.

Grunlan, J.C., Mehrabi, A.R., Bannon, M.V. and Bahr, J.L. (2004) 'Water-Based Single-Walled-Nanotube-Filled Polymer Composite with an Exceptionally Low Percolation Threshold', Advanced Materials, 16(2), pp. 150-153.

Habibi, Y., Lucia, L.A. and Rojas, O.J. (2010) 'Cellulose nanocrystals: chemistry, self-assembly, and applications', Chemical reviews, 110(6), pp. 3479-3500.

Hahn, H. (1997) 'Gas phase synthesis of nanocrystalline materials', Nanostructured Materials, 9(1), pp. 3-12.

Hartono, A., Djamal, M. and Satira, S. (2013) 'Preparation of PVDF film using deep coating method for biosensor transducer applied', Instrumentation, Communications, Information Technology, and Biomedical Engineering (ICICI-BME), 2013 3rd International Conference on. IEEE, 408-411.

He, L., Xia, G., Sun, J., Zhao, Q., Song, R. and Ma, Z. (2013) 'Unzipped multiwalled carbon nanotubes-incorporated poly (vinylidene fluoride) nanocomposites with enhanced interface and piezoelectric β phase', Journal of colloid and interface science, 393, pp. 97-103.

Hermans, J. (1963) 'Flow of gels of cellulose microcrystals. I. Random and liquid crystalline gels', Journal of Polymer Science Part C: Polymer Symposia. Wiley Online Library, 129-144.

Hong, J., Winberg, P., Schadler, L. and Siegel, R. (2005) 'Dielectric properties of zinc oxide/low density polyethylene nanocomposites', Materials Letters, 59(4), pp. 473-476.

Hsu, D.P. and Viscio, D.B. (1997) 'Polyethylene glycol is a stabilizer for calcium peroxide/sodium bicarbonate mixtures'.

Hu, Y., Hsu, W., Wang, Y., Ho, C. and Chang, P. (2014) 'Enhance the pyroelectricity of polyvinylidene fluoride by graphene-oxide doping', Sensors, 14(4), pp. 6877-6890.

Hua, L., Kai, W. and Inoue, Y. (2007) 'Synthesis and characterization of poly (ϵ-caprolactone)–graphite oxide composites', Journal of Applied Polymer Science, 106(3), pp. 1880-1884.

Hua, L., Wu, W., Liu, Y., McBride, M.B. and Chen, Y. (2009) 'Reduction of nitrogen loss and Cu and Zn mobility during sludge composting with bamboo charcoal amendment', Environmental Science and Pollution Research, 16(1), pp. 1-9.

Hudson, M.S.L., Raghubanshi, H., Awasthi, S., Sadhasivam, T., Bhatnager, A., Simizu, S., Sankar, S. and Srivastava, O. (2014) 'Hydrogen uptake of reduced graphene oxide and

graphene sheets decorated with Fe nanoclusters', International Journal of Hydrogen Energy, 39(16), pp. 8311-8320.

Hussain, A., Kumar, A., Singh, F. and Avasthi, D. (2006) 'Effects of 160 MeV Ni12 ion irradiation on HCl doped polyaniline electrode', Journal of Physics D: Applied Physics, 39(4), pp. 750.

Jung, H.M., Kang, J., Yang, S.Y., Won, J.C. and Kim, Y.S. (2009) 'Barium titanate nanoparticles with diblock copolymer shielding layers for high-energy density nanocomposites', Chemistry of Materials, 22(2), pp. 450-456.

Kalidindi, S., Ounaies, Z. and Kaddami, H. (2010) 'Toward the preparation of nanocomposites with oriented fillers: electric field-manipulation of cellulose whiskers in silicone oil', Smart Materials and Structures, 19(9), pp. 094002.

Kalidindi, S.V., Ounaies, Z. and Kaddami, H. (2010) 'Electric Field Manipulation of Cellulose Whiskers in Polyvinyl Acetate', ASME 2010 Conference on Smart Materials, Adaptive Structures and Intelligent Systems. American Society of Mechanical Engineers, 233-238.

Kalogirou, S.A. (2013) Solar energy engineering: processes and systems. Academic Press.

Kawai, H. (1969) 'The piezoelectricity of poly (vinylidene fluoride)', Japanese Journal of Applied Physics, 8(7), pp. 975.

Khalil, H.A., Bhat, A. and Yusra, A.I. (2012) 'Green composites from sustainable cellulose nanofibrils: a review', Carbohydrate Polymers, 87(2), pp. 963-979.

Klemm, D., Heublein, B., Fink, H. and Bohn, A. (2005) 'Cellulose: fascinating biopolymer and sustainable raw material', Angewandte Chemie International Edition, 44(22), pp. 3358-3393.

Klemm, D., Philipp, B., Heinze, T., Heinze, U., Wagenknecht, W. and Mischnick, P. (1999) 'Comprehensive Cellulose Chemistry. Vol. 1 2', Angewandte Chemie-German Edition, 111(12), pp. 1942-1942.

Koczkur, K.M., Mourdikoudis, S., Polavarapu, L. and Skrabalak, S.E. (2015) 'Polyvinylpyrrolidone (PVP) in nanoparticle synthesis', Dalton Transactions, 44(41), pp. 17883-17905.

Kuilla, T., Bhadra, S., Yao, D., Kim, N.H., Bose, S. and Lee, J.H. (2010) 'Recent advances in graphene based polymer composites', Progress in polymer science, 35(11), pp. 1350-1375.

KumaráThakur, V., JináTan, E. and SeeáLee, P. (2011) 'Surface functionalization of $BaTiO_3$ nanoparticles and improved electrical properties of $BaTiO_3$/polyvinylidene fluoride composite', RSC Advances, 1(4), pp. 576-578.

Lalia, B.S., Guillen, E., Arafat, H.A. and Hashaikeh, R. (2014) 'Nanocrystalline cellulose reinforced PVDF-HFP membranes for membrane distillation application', Desalination, 332(1), pp. 134-141.

Lee, J.H., Park, S.H. and Kim, S.H. (2013) 'Preparation of cellulose nanowhiskers and their reinforcing effect in polylactide', Macromolecular Research, 21(11), pp. 1218-1225.

Lee, M., Chen, C., Wang, S., Cha, S.N., Park, Y.J., Kim, J.M., Chou, L. and Wang, Z.L. (2012) 'A hybrid piezoelectric structure for wearable nanogenerators', Advanced Materials, 24(13), pp. 1759-1764.

Lehman, J.H., Terrones, M., Mansfield, E., Hurst, K.E. and Meunier, V. (2011) 'Evaluating the characteristics of multiwall carbon nanotubes', Carbon, 49(8), pp. 2581-2602.

Levi, N., Czerw, R., Xing, S., Iyer, P. and Carroll, D.L. (2004) 'Properties of polyvinylidene difluoride-carbon nanotube blends', Nano Letters, 4(7), pp. 1267-1271.

Li, J., Wu, X. and Liu, Z. (2013) 'Non-isothermal crystallization of poly (vinylidene fluoride)/multiwalled carbon nanotube composites', International Journal of Polymer Analysis and Characterization, 18(2), pp. 83-92.

Li, L., Zhang, M., Rong, M. and Ruan, W. (2014) 'Studies on the transformation process of PVDF from α to β phase by stretching', RSC Advances, 4(8), pp. 3938-3943.

Li, X., Zhou, C., Du, R., Li, N., Han, X., Zhang, Y., An, S. and Xiao, C. (2013) 'Evolution of Polyvinylidene Fluoride (PVDF) Hierarchical Morphology during Slow Gelation Process and Its Superhydrophobicity', ACS applied materials & interfaces, 5(12), pp. 5430-5435.

Li, Y.C., Li, R.K.Y. and Tjong, S.C. (2010) 'Electrical transport properties of graphite sheets doped polyvinylidene fluoride nanocomposites', Journal of Materials Research, 25(08), pp. 1645-1648.

Liu, H., Wang, G., Mai, Y. and Zeng, Y. (2011) 'On fracture toughness of nano-particle modified epoxy', Composites Part B: Engineering, 42(8), pp. 2170-2175.

Liu, Z., Pan, C., Lin, L. and Lai, H. (2013) 'Piezoelectric properties of PVDF/MWCNT nanofiber using near-field electrospinning', Sensors and Actuators A: Physical, 193, pp. 13-24.

Liu, Z., Pan, C., Ou, Z. and Wang, W. (2013) 'Piezoelectricity of Well-Aligned Electrospun Fiber Composites', Sensors Journal, IEEE, 13(10), pp. 4098-4103.

Lund, P. (2012) 'The European Union challenge: integration of energy, climate, and economic policy', Wiley Interdisciplinary Reviews: Energy and Environment, 1(1), pp. 60-68.

Luo, J., Yang, Y., Zhu, X., Chen, G., Zeng, F. and Pan, F. (2010) 'Enhanced electromechanical response of Fe-doped ZnO films by modulating the chemical state and ionic size of the Fe dopant', Physical Review B, 82(1), pp. 014116.

Lusiola, T. (2012) 'Synthesis and processing of KNN powders and thick films for MEMS devices'.

Mago, G., Fisher, F.T. and Kalyon, D.M. (2008) 'Effects of multiwalled carbon nanotubes on the shear-induced crystallization behavior of poly (butylene terephthalate)', Macromolecules, 41(21), pp. 8103-8113.

Maksimenko, S., Rodionova, V., Slepyan, G.Y., Karpovich, V., Shenderova, O., Walsh, J., Kuznetsov, V., Mazov, I., Moseenkov, S. and Okotrub, A. (2007) 'Attenuation of electromagnetic waves in onion-like carbon composites', Diamond and related materials, 16(4), pp. 1231-1235.

Mao, Y., Mao, S., Ye, Z., Xie, Z. and Zheng, L. (2010) 'Size-dependences of the dielectric and ferroelectric properties of BaTiO3/polyvinylidene fluoride nanocomposites', Journal of Applied Physics, 108(1), pp. 4102.

Marchessault, R., Morehead, F. and Walter, N. (1959) 'Liquid crystal systems from fibrillar polysaccharides'.

Martel, R., Schmidt, T., Shea, H., Hertel, T. and Avouris, P. (1998) 'Single-and multi-wall carbon nanotube field-effect transistors', Applied Physics Letters, 73(17), pp. 2447-2449.

Mathur, R., Pande, S., Singh, B. and Dhami, T. (2008) 'Electrical and mechanical properties of multi-walled carbon nanotubes reinforced PMMA and PS composites', Polymer Composites, 29(7), pp. 717-727.

Meyabadi, T.F., Sadeghi, G.M.M., Dadashian, F. and Asl, H.E.Z. (2013) 'From cellulosic waste to nanocomposites. Part 2: synthesis and characterization of polyurethane/cellulose nanocomposites', Journal of Materials Science, 48(20), pp. 7283-7293.

Mitcheson, P.D., Green, T.C., Yeatman, E.M. and Holmes, A.S. (2004) 'Architectures for vibration-driven micropower generators', Microelectromechanical Systems, Journal of, 13(3), pp. 429-440.

Mohamed, A.M., Jafari, R. and Farzaneh, M. (2014) 'An optimization of superhydrophobic polyvinylidene fluoride/zinc oxide materials using Taguchi method', Applied Surface Science, 288, pp. 229-237.

Moon, R.J., Martini, A., Nairn, J., Simonsen, J. and Youngblood, J. (2011) 'Cellulose nanomaterials review: structure, properties and nanocomposites', Chemical Society Reviews, 40(7), pp. 3941-3994.

Müller, C.M., Laurindo, J.B. and Yamashita, F. (2009) 'Effect of cellulose fibers addition on the mechanical properties and water vapor barrier of starch-based films', Food Hydrocolloids, 23(5), pp. 1328-1333.

Nakagawa, K. and Ishida, Y. (1973) 'Annealing effects in poly (vinylidene fluoride) as revealed by specific volume measurements, differential scanning calorimetry, and electron microscopy', Journal of Polymer Science: Polymer Physics Edition, 11(11), pp. 2153-2171.

Nalwa, H.S. (1995) Ferroelectric Polymers: Chemistry: Physics, and Applications. CRC Press.

Neppalli, R., Wanjale, S., Birajdar, M. and Causin, V. (2013) 'The effect of clay and of electrospinning on the polymorphism, structure and morphology of poly (vinylidene fluoride)', European Polymer Journal, 49(1), pp. 90-99.

Niedermeyer, W.H. (2016) COMPOSITION CONTAINING SPHERICAL AND CORAL-SHAPED NANOPARTICLES AND METHOD OF MAKING SAME.

Nishino, T., Matsuda, I. and Hirao, K. (2004) 'All-cellulose composite', Macromolecules, 37(20), pp. 7683-7687.

Olivo, J., Carrara, S. and De Micheli, G. (2011) 'Energy harvesting and remote powering for implantable biosensors', IEEE Sensors Journal, 11(EPFL-ARTICLE-152140), pp. 1573-1586.

Olmos, D., Montero, F., González-Gaitano, G. and González-Benito, J. (2013) 'Structure and morphology of composites based on polyvinylidene fluoride filled with BaTiO3 submicrometer particles: Effect of processing and filler content', Polymer Composites, 34(12), pp. 2094-2104.

Orts, W.J., Shey, J., Imam, S.H., Glenn, G.M., Guttman, M.E. and Revol, J. (2005) 'Application of cellulose microfibrils in polymer nanocomposites', Journal of Polymers and the Environment, 13(4), pp. 301-306.

Ourry, L., Marchesini, S., Bibani, M., Mercone, S., Ammar, S. and Mammeri, F. (2015) 'Influence of nanoparticle size and concentration on the electroactive phase content of PVDF in PVDF–CoFe2O4-based hybrid films', physica status solidi (a), 212(2), pp. 252-258.

Pande, S., Singh, B., Mathur, R., Dhami, T., Saini, P. and Dhawan, S. (2009) 'Improved electromagnetic interference shielding properties of MWCNT–PMMA composites using layered structures', Nanoscale research letters, 4(4), pp. 327-334.

Panwar, V., Kang, B., Park, J., Park, S. and Mehra, R. (2009) 'Study of dielectric properties of styrene-acrylonitrile graphite sheets composites in low and high frequency region', European Polymer Journal, 45(6), pp. 1777-1784.

Paredes, J., Villar-Rodil, S., Martinez-Alonso, A. and Tascon, J. (2008) 'Graphene oxide dispersions in organic solvents', Langmuir, 24(19), pp. 10560-10564.

Park, K., Lee, S., Kim, C. and Han, J. (2006) 'Fabrication and electromagnetic characteristics of electromagnetic wave absorbing sandwich structures', Composites Science and Technology, 66(3), pp. 576-584.

Percy, S., Knight, C., Cooray, F. and Smart, K. (2012) 'Supplying the power requirements to a sensor network using radio frequency power transfer', Sensors, 12(7), pp. 8571-8585.

Pirani, S., Abushammala, H. and Hashaikeh, R. (2013) 'Preparation and characterization of electrospun PLA/nanocrystalline cellulose-based composites', Journal of Applied Polymer Science, 130(5), pp. 3345-3354.

Potts, J.R., Dreyer, D.R., Bielawski, C.W. and Ruoff, R.S. (2011) 'Graphene-based polymer nanocomposites', Polymer, 52(1), pp. 5-25.

Prasad, D. and Snow, M. (2014) Designing with solar power: a source book for building integrated photovoltaics (BiPV). Routledge.

Pu, J., Yan, X., Jiang, Y., Chang, C. and Lin, L. (2010) 'Piezoelectric actuation of direct-write electrospun fibers', Sensors and Actuators A: Physical, 164(1), pp. 131-136.

Purica, M., Budianu, E. and Rusu, E. (2000) 'Heterojunction with ZnO polycrystalline thin films for optoelectronic devices applications', Microelectronic Engineering, 51, pp. 425-431.

Qian, D., Dickey, E.C., Andrews, R. and Rantell, T. (2000) 'Load transfer and deformation mechanisms in carbon nanotube-polystyrene composites', Applied Physics Letters, 76(20), pp. 2868-2870.

Rahmani, P., Dadbin, S. and Frounchi, M. (2014) 'Electron beam induced modifications in crystalline structure of polyvinylidene fluoride/nanoclay composites', Radiation Measurements, 60, pp. 1-6.

Rajesh, P., Bodkhe, S., Kamle, S. and Verma, V. (2014) 'Enhancing beta-phase in PVDF through physicochemical modification of cellulose', Electronic Materials Letters, 10(1), pp. 315-319.

Ramanathan, T., Abdala, A., Stankovich, S., Dikin, D., Herrera-Alonso, M., Piner, R., Adamson, D., Schniepp, H., Chen, X. and Ruoff, R. (2008) 'Functionalized graphene sheets for polymer nanocomposites', Nature nanotechnology, 3(6), pp. 327-331.

Ramola, R., Chandra, S., Rana, J., Sonkawade, R., Kulriya, P., Singh, F., Avasthi, D. and Annapoorni, S. (2008) 'A comparative study of the effect of O 7ion beam on polypyrrole and CR-39 (DOP) polymers', Journal of Physics D: Applied Physics, 41(11), pp. 115411.

Ranby, B. (1951) 'Cellulose and muscle-the colloidal properties of cellulose micelles', Discussions of the Faraday Society, (11), pp. 158-&.

Rattaz, A., Mishra, S.P., Chabot, B. and Daneault, C. (2011) 'Cellulose nanofibres by sonocatalysed-TEMPO-oxidation', Cellulose, 18(3), pp. 585-593.

Revol, J., Bradford, H., Giasson, J., Marchessault, R. and Gray, D. (1992) 'Helicoidal self-ordering of cellulose microfibrils in aqueous suspension', International journal of biological macromolecules, 14(3), pp. 170-172.

Ribeiro, C., Sencadas, V., Ribelles, J.L.G. and Lanceros-Méndez, S. (2010) 'Influence of processing conditions on polymorphism and nanofiber morphology of electroactive poly (vinylidene fluoride) electrospun membranes', Soft Materials, 8(3), pp. 274-287.

Righter, R.W. (1996) Wind energy in America: A history. University of Oklahoma Press.

Roduner, E. (2006) 'Size matters: why nanomaterials are different', Chemical Society Reviews, 35(7), pp. 583-592.

Rusli, R. and Eichhorn, S.J. (2008) 'Determination of the stiffness of cellulose nanowhiskers and the fiber-matrix interface in a nanocomposite using Raman spectroscopy', Applied Physics Letters, 93(3), pp. 033111.

Ryan, W.L. (1980) 'Method for preparing a platelet reference control'.

Sadeghi, F. and Ajji, A. (2009) 'Study of crystal structure of (polyvinylidene fluoride/clay) nanocomposite films: Effect of process conditions and clay type', Polymer Engineering & Science, 49(1), pp. 200-207.

Schropp, R. and Madan, A. (1989) 'Properties of conductive zinc oxide films for transparent electrode applications prepared by rf magnetron sputtering', Journal of Applied Physics, 66(5), pp. 2027-2031.

Sencadas, V., Moreira, M.V., Lanceros-Méndez, S., Pouzada, A.S. and Gregório Filho, R. (2006) 'α-to β Transformation on PVDF films obtained by uniaxial stretch', Materials science forum. Trans Tech Publ, 872-876.

Song, H. and Zheng, L. (2013) 'Nanocomposite films based on cellulose reinforced with nano-SiO2: microstructure, hydrophilicity, thermal stability, and mechanical properties', Cellulose, 20(4), pp. 1737-1746.

Song, J. and Evans, J. (1993) 'The assessment of dispersion of fine ceramic powders for injection moulding and related processes', Journal of the European Ceramic Society, 12(6), pp. 467-478.

Song, J. and Evans, J. (1994) 'Flocculation after injection molding in ceramic suspensions', Journal of Materials Research, 9(09), pp. 2386-2397.

Song, Y., Shen, Y., Liu, H., Lin, Y., Li, M. and Nan, C. (2012) 'Improving the dielectric constants and breakdown strength of polymer composites: effects of the shape of the $BaTiO_3$ nanoinclusions, surface modification and polymer matrix', Journal of Materials Chemistry, 22(32), pp. 16491-16498.

Srinivas, G., Nielsen, S.O., Moore, P.B. and Klein, M.L. (2006) 'Molecular dynamics simulations of surfactant self-organization at a solid-liquid interface', Journal of the American Chemical Society, 128(3), pp. 848-853.

Šturcová, A., Davies, G.R. and Eichhorn, S.J. (2005) 'Elastic modulus and stress-transfer properties of tunicate cellulose whiskers', Biomacromolecules, 6(2), pp. 1055-1061.

Subbiah, T., Bhat, G., Tock, R., Parameswaran, S. and Ramkumar, S. (2005) 'Electrospinning of nanofibers', Journal of Applied Polymer Science, 96(2), pp. 557-569.

Sun, C.C. (2008) 'Mechanism of moisture induced variations in true density and compaction properties of microcrystalline cellulose', International journal of pharmaceutics, 346(1), pp. 93-101.

Sundaray, B., Bossard, F., Latil, P., Orgéas, L., Sanchez, J. and Lepretre, J. (2013) 'Unusual process-induced curl and shrinkage of electrospun PVDF membranes', Polymer, 54(17), pp. 4588-4593.

Tao, M., Liu, F., Ma, B. and Xue, L. (2013) 'Effect of solvent power on PVDF membrane polymorphism during phase inversion', Desalination, 316, pp. 137-145.

Tashiro, K. (1995) 'Crystal structure and phase transition of PVDF and related copolymers', Plastics Engineering, 28, pp. 63-63.

Teo, W. and Ramakrishna, S. (2006) 'A review on electrospinning design and nanofibre assemblies', Nanotechnology, 17(14), pp. R89.

Thangavel, E., Ramasundaram, S., Pitchaimuthu, S., Hong, S.W., Lee, S.Y., Yoo, S., Kim, D., Ito, E. and Kang, Y.S. (2014) 'Structural and tribological characteristics of poly (vinylidene fluoride)/functionalized graphene oxide nanocomposite thin films', Composites Science and Technology, 90, pp. 187-192.

Thibaud, D. (2011) 'Mechanical properties of materials made of nano-cellulose'.

Tjong, S. and Jiang, W. (1999) 'Mechanical and thermal properties of poly (acrylonitrile–butadiene–styrene) copolymer reinforced with potassium titanate whiskers', Journal of Applied Polymer Science, 73(14), pp. 2985-2991.

Ueberschlag, P. (2001) 'PVDF piezoelectric polymer', Sensor Review, 21(2), pp. 118-126.

Upadhyay, R.H. and Deshmukh, R.R. (2013) 'Investigation of dielectric properties of newly prepared β-phase polyvinylidene fluoride–barium titanate nanocomposite films', Journal of Electrostatics, 71(5), pp. 945-950.

Vijatović, M., Bobić, J. and Stojanović, B. (2008) 'History and challenges of barium titanate: Part II', Science of Sintering, 40(3), pp. 235-244.

Wadell, H. (1935) 'Volume, shape, and roundness of quartz particles', The Journal of geology, pp. 250-280.

Wang, Q., Zhu, J., Gleisner, R., Kuster, T., Baxa, U. and McNeil, S. (2012) 'Morphological development of cellulose fibrils of a bleached eucalyptus pulp by mechanical fibrillation', Cellulose, 19(5), pp. 1631-1643.

Wang, S., Wan, Y., Sun, B., Liu, L. and Xu, W. (2014) 'Mechanical and electrical properties of electrospun PVDF/MWCNT ultrafine fibers using rotating collector', Nanoscale research letters, 9(1), pp. 1-7.

Wu, L., Yuan, W., Nakamura, T., Atobe, S., Hu, N., Fukunaga, H., Chang, C., Zemba, Y., Li, Y. and Watanabe, T. (2013) 'Enhancement of PVDF's piezoelectricity by VGCF and MWNT', Advanced Composite Materials, 22(1), pp. 49-63.

Wu, Q., Meng, Y., Concha, K., Wang, S., Li, Y., Ma, L. and Fu, S. (2013) 'Influence of temperature and humidity on nano-mechanical properties of cellulose nanocrystal films made from switchgrass and cotton', Industrial Crops and Products, 48, pp. 28-35.

Xu, X., Yang, Y., Xing, Y., Yang, J. and Wang, S. (2013) 'Properties of novel polyvinyl alcohol/cellulose nanocrystals/silver nanoparticles blend membranes', Carbohydrate Polymers, 98(2), pp. 1573-1577.

Yee, W.A., Kong, J., Zhang, C., Liu, T., Kotaki, M. and Lu, X. (2012) 'Polymorphism of electrospun polyvinylidene difluoride/carbon nanotube (CNT) nanocomposites: Synergistic effects of CNT surface chemistry, extensional force and supercritical carbon dioxide treatment', Polymer, 53(22), pp. 5097-5102.

Yee, W.A., Nguyen, A.C., Lee, P.S., Kotaki, M., Liu, Y., Tan, B.T., Mhaisalkar, S. and Lu, X. (2008) 'Stress-induced structural changes in electrospun polyvinylidene difluoride nanofibers collected using a modified rotating disk', Polymer, 49(19), pp. 4196-4203.

Yoon, K. and Kelarakis, A. (2014) 'Nanoclay-directed structure and morphology in PVDF electrospun membranes', Journal of Nanomaterials, 2014, pp. 14.

Yousefi, H., Faezipour, M., Hedjazi, S., Mousavi, M.M., Azusa, Y. and Heidari, A.H. (2013) 'Comparative study of paper and nanopaper properties prepared from bacterial cellulose

nanofibers and fibers/ground cellulose nanofibers of canola straw', Industrial Crops and Products, 43, pp. 732-737.

Yu, K., Wang, H., Zhou, Y., Bai, Y. and Niu, Y. (2013) 'Enhanced dielectric properties of BaTiO3/poly (vinylidene fluoride) nanocomposites for energy storage applications', Journal of Applied Physics, 113(3), pp. 034105.

Yu, L. and Cebe, P. (2009) 'Crystal polymorphism in electrospun composite nanofibers of poly (vinylidene fluoride) with nanoclay', Polymer, 50(9), pp. 2133-2141.

Yuen, S., Ma, C.M., Chiang, C., Chang, J., Huang, S., Chen, S., Chuang, C., Yang, C. and Wei, M. (2007) 'Silane-modified MWCNT/PMMA composites–Preparation, electrical resistivity, thermal conductivity and thermal stability', Composites Part A: Applied Science and Manufacturing, 38(12), pp. 2527-2535.

Yusoh, K., Jin, J. and Song, M. (2010) 'Subsurface mechanical properties of polyurethane/organoclay nanocomposite thin films studied by nanoindentation', Progress in Organic Coatings, 67(2), pp. 220-224.

Zeng, S., Baillargeat, D., Ho, H. and Yong, K. (2014) 'Nanomaterials enhanced surface plasmon resonance for biological and chemical sensing applications', Chemical Society Reviews, 43(10), pp. 3426-3452.

Zhang, L., Gu, F., Chan, J., Wang, A., Langer, R. and Farokhzad, O. (2008) 'Nanoparticles in medicine: therapeutic applications and developments', Clinical pharmacology and therapeutics, 83(5), pp. 761-769.

Zhang, R., Zhu, C., Shan, X., Xia, J., Zhu, Q. and Hu, Y. (2013) 'Study on the poly (3-hydroxybutyrate-co-4-hydroxybutyrate)-based nanocomposites reinforced by surface modified nanocrystalline cellulose', Journal of Applied Polymer Science, 130(3), pp. 2015-2022.

Zhijiang, C. and Guang, Y. (2011) 'Optical nanocomposites prepared by incorporating bacterial cellulose nanofibrils into poly (3-hydroxybutyrate)', Materials Letters, 65(2), pp. 182-184.

Zhou, F. and Gong, R. (2008) 'Manufacturing technologies of polymeric nanofibres and nanofibre yarns', Polymer International, 57(6), pp. 837-845.

Zimmermann, T., Bordeanu, N. and Strub, E. (2010) 'Properties of nanofibrillated cellulose from different raw materials and its reinforcement potential', Carbohydrate Polymers, 79(4), pp. 1086-1093.

Appendix I.

Absorbency of α-PVDF (A_α) and β-PVDF (A_β), and relative fraction of β phase PVDF-F_β of as-received, electrospun and cast PVDF samples are shown in Table 1 below.

Table 1: Absorbency of α-PVDF (A_α) and β-PVDF (A_β), and relative fraction of β phase PVDF-F_β of as-received, electrospun and cast PVDF samples

Sample ID	A_α	A_β	F_β (%)
PVDF powder	0.182	0.281	55.122
neat PVDF spun film	0.067	0.218	72.029
CNT-0.5%	0.018	0.031	58.341
CNT-1.6%	0.146	0.273	59.646
CNT-2.6%	0.046	0.094	62.063
GO-4.6%	0.048	0.071	54.013
GO-12.6%	0.110	0.131	48.709
GO-19.4%	0.119	0.137	47.678
BT-12.5%	0.014	0.030	62.612
BT-17.6%	0.012	0.024	61.685
BT-22.2%	0.015	0.033	63.269
ZnO-13.4%	0.007	0.015	64.128
ZnO-23.6%	0.017	0.044	66.968
ZnO-31.7%	0.106	0.210	61.097
Halloysite-1.4%	0.060	0.305	80.176
Halloysite-3.3%	0.090	0.444	79.612
Halloysite-6.4%	0.041	0.161	75.801
Halloysite-9.3%	0.084	0.350	76.784
Bentonite-2.0%	0.014	0.078	81.950
Bentonite-4.9%	0.020	0.063	71.636
Bentonite-9.3%	0.025	0.120	79.057
Bentonite-13.3%	0.036	0.128	73.798
GO-4.6% (casting)	0.280	0.344	49.390
GO-12.6% (casting)	0.358	0.395	46.687
GO-19.4% (casting)	0.413	0.569	52.235

BT-12.5% (casting)	**0.089**	**0.169**	**59.934**
BT-17.6% (casting)	**0.075**	**0.198**	**67.710**
BT-22.2% (casting)	**0.095**	**0.195**	**61.993**
ZnO-13.4% (casting)	**0.092**	**0.281**	**70.783**
ZnO-23.6% (casting)	**0.062**	**0.202**	**72.133**
ZnO-31.7% (casting)	**0.084**	**0.228**	**68.325**
Halloysite-1.4% (casting)	**0.133**	**0.335**	**66.673**
Halloysite-3.3% (casting)	**0.138**	**0.289**	**62.447**
Halloysite-6.4% (casting)	**0.099**	**0.237**	**65.568**
Halloysite-9.3% (casting)	**0.095**	**0.290**	**70.718**
Bentonite-2.0% (casting)	**0.095**	**0.346**	**74.304**
Bentonite-4.9% (casting)	**0.065**	**0.200**	**71.000**
Bentonite-9.3% (casting)	**0.107**	**0.238**	**63.832**
Bentonite-13.3% (casting)	**0.106**	**0.317**	**70.365**

Appendix II

Table 2-6 listed d_{33} measurement results showing the influence of distances to the edge of sample and angle from the horizontal position for GO-4.6%, ZnO-23.6%, Halloysite-6.4%, Bentonite-9.3% and NCC50-1.1%.

Table 2. d_{33} measurement showing the influence of distances to the edge of sample and angle from the horizontal position for GO-4.6%

Distance (*mm*)	d_{33} (*pC/N*)	SD (*pC/N*)
5	11.20	0.45
10	9.80	2.05
15	10.80	0.84
20	10.80	1.30
25	10.60	0.89
Angle	d_{33} (*pC/N*)	SD (*pC/N*)
12°	9.60	0.55
24°	10.00	1.41
36°	10.20	1.10
48°	10.00	0.71
60°	9.80	0.45

Table 3. d_{33} measurement showing the influence of distances to the edge of sample and angle from the horizontal position for ZnO-23.6%

Distance (*mm*)	d_{33} (*pC/N*)	SD (*pC/N*)
5	12.60	0.89
10	14.20	0.84
15	13.20	0.84
20	12.20	0.45
25	12.80	1.30
Angle	d_{33} (*pC/N*)	SD (*pC/N*)
12°	11.00	2.00
24°	11.80	1.79
36°	10.80	1.10
48°	12.60	1.14

60°	**10.40**	**0.55**

Table 4. d_{33} measurement showing the influence of distances to the edge of sample and angle from the horizontal position for Halloysite-6.4%

Distance (*mm*)	**d_{33} (*pC/N*)**	**SD (*pC/N*)**
5	**12.60**	**0.89**
10	**14.20**	**0.84**
15	**13.20**	**0.84**
20	**12.20**	**0.45**
25	**12.80**	**1.30**
Angle	**d_{33} (*pC/N*)**	**SD (*pC/N*)**
12°	**11.00**	**2.00**
24°	**11.80**	**1.79**
36°	**10.80**	**1.10**
48°	**12.60**	**1.14**
60°	**10.40**	**0.55**

Table 5. d_{33} measurement showing the influence of distances to the edge of sample and angle from the horizontal position for Bentonite-9.3%

Distance (*mm*)	**d_{33} (*pC/N*)**	**SD (*pC/N*)**
5	**11.00**	**1.00**
10	**11.20**	**0.45**
15	**10.40**	**0.55**
20	**10.20**	**0.45**
25	**9.40**	**0.55**
Angle	**d_{33} (*pC/N*)**	**SD (*pC/N*)**
12°	**8.40**	**1.34**
24°	**8.20**	**0.84**
36°	**8.20**	**0.84**
48°	**8.00**	**1.00**
60°	**8.60**	**0.89**

Table 6. d_{33} measurement showing the influence of distances to the edge of sample and angle from the horizontal position for NCC50-1.1%.

Distance (*mm*)	d_{33} (*pC/N*)	SD (*pC/N*)
5	14.00	0.71
10	14.20	0.45
15	14.80	1.30
20	14.00	1.22
25	14.60	0.89
Angle	d_{33} (*pC/N*)	SD (*pC/N*)
12°	10.20	0.84
24°	10.40	0.89
36°	10.60	1.52
48°	11.00	1.22
60°	9.60	0.55